ABSTRACT

Title of dissertation: AN INVESTIGATION OF FLAMES,
DEFLAGRATIONS, AND DETONATIONS
IN HIGH-SPEED FLOWS

Gabriel B. Goodwin
Doctor of Philosophy, 2018

Dissertation directed by: Professor Elaine S. Oran
Department of Aerospace Engineering

A comprehensive understanding of the fundamental physics underlying combustion and detonations in turbulent and high-speed flows is crucial to the design of robust ramjet, scramjet, and detonation engines. This work uses high-fidelity, multidimensional numerical simulations to investigate flame stability and deflagration-to-detonation transition (DDT) mechanisms in supersonic reactive flows. The study consists of four major sections.

The first section discusses the acceleration of a flame in a channel with obstacles and its transition from a laminar, expanding flame to a turbulent deflagration and eventual detonation. As the flame accelerates, a highly dynamic, shock-heated region forms ahead of the flame. Shock collisions and reflections focus energy in localized volumes of unburned gas at timescales that are small relative to the acoustic timescale of the unburned gas. The rapid deposition of energy causes the unburned gas to detonate through an energy-focusing mechanism that has elements of both direct initiation and detonation in a gradient of reactivity.

The second section describes how the blockage of a channel with regularly spaced obstacles, analogous to the igniter in a detonation engine, affects flame acceleration

and turbulence in the region ahead of the accelerating flame. The rate of flame acceleration, time and distance to DDT, and detonation mechanism are compared for channels with high, medium, and low blockage ratios. Stochasticity and uncertainty in the numerical solutions are discussed.

In the third section, the stability of premixed flames at high supersonic speeds in a constant-area combustor is investigated. After autoignition of the fuel-oxidizer mixture in the boundary layer at the combustor walls, the flame front eventually becomes unstable due to a Rayleigh-Taylor (RT) instability at the interface between burned and unburned gas. The turbulent flame front transitions to a detonation through the energy-focusing mechanism when a shock passes through the flame and amplifies its energy release.

The final section discusses the effect of inflow Mach number in the supersonic combustor on ignition, flame stability, and transition to detonation of a premixed flame. Timescales for growth of the RT instability and detonation initiation increase rapidly with flow speed, but, qualitatively, flame evolution is independent of Mach number.

AN INVESTIGATION OF FLAMES, DEFLAGRATIONS, AND DETONATIONS IN HIGH-SPEED FLOWS

by

Gabriel B. Goodwin

Dissertation submitted to the Faculty of the Graduate School of the
University of Maryland, College Park, in partial fulfillment
of the requirements for the degree of
Doctor of Philosophy
2018

Advisory Committee:
Professor Elaine Oran, Chair/Advisor
Professor Michael Gollner, Dean's Representative
Professor Carolyn Kaplan
Professor Johan Larsson
Professor Kenneth Yu

Acknowledgments

First and foremost, I would like to acknowledge the support of my advisor, Professor Oran. Thank you for your guidance and mentorship, without which none of this would have been possible. I am very fortunate to have had the opportunity to work with you. Thanks to my parents, Robert and Luanne, and brother, Aaron, for your unending encouragement. Had you not fostered my pursuit of science and engineering from an early age, I never would have attempted this undertaking. Last, but certainly not least, thank you, Tess, for your endless support and understanding through the long nights and weekends.

Dedicated to my grandfather, James L. Keirsey,

an aeronautical engineer and pioneer.

Contents

List of Figures

1 Introduction & Background

1.1 Reactive Flow

The overarching goal of combustion research is to understand the behavior of reactive flows under a wide variety of environmental conditions so that the processes may be controlled and the energy released by combustion may be efficiently harnessed for propulsion, power generation, heating, and other applications. On a more fundamental level, reactive flow has been a major research interest for decades due to the complexity of the interactions between fluid dynamics, chemistry, and diffusive transport.

There are several regimes of reactive flow that are considered in this work: laminar flames, deflagrations, and detonations. One characteristic difference between these three regimes is the speed at which the reaction front propagates. Laminar flames travel subsonically, consuming reactant at a speed much lower than the local speed of sound. The laminar flame speed is primarily dependent on the chemical reaction rates for the fuel-oxidizer mixture. Combustion in a laminar flame is typically a constant-pressure process. Deflagrations are flame fronts that propagate considerably faster than laminar flames and can reach speeds nearing the local sonic velocity. Deflagration fronts are often accelerated by turbulence at the reaction front stretching the flame surface and increasing the rate of energy released by combustion. This increase in energy release rate, in turn, drives the acceleration of the deflagration. A detonation may be thought of as a flame coupled to a shock wave; it is a reaction front that travels supersonically, where the propagation of the shock is sustained by the energy released by combustion and the combustion is initiated by the shock compression.

Deflagrations and detonations are used as propulsion mechanisms for aircraft. In the case of a supersonic combustion ramjet (scramjet), the energy released by combustion of fuel in a supersonic air flow is used to produce thrust. Stable combustion

1

and efficient thrust generation requires the ability to predict the behavior of flames in high-speed flows. The high flow speed results in small timescales for mixing of fuel in the air, ignition of the mixture, and complete combustion. Additionally, the flow through an airbreathing engine is often turbulent, particularly in the mixing and combustion regions. These phenomena lead to one of the predominant challenges in design of a robust supersonic airbreathing engine: maintaining flame stability across a wide range of inflow conditions [1, 2]. Considerable research emphasis has been placed on understanding flame stability and the flame-turbulence interaction in both subsonic and supersonic regimes. This research is performed experimentally, as well as numerically, by modeling a wide range of physical systems and length scales.

Experiments and simulations at full-size engine scale allow researchers to investigate macroscopic features of the system that play a major role in engine performance, such as fuel-air mixing efficiency and combustion completeness in a scramjet combustor. Simulation of turbulent combustion in a full-size engine is particularly challenging due to the need to model the effect of turbulence accurately at scales many orders of magnitude smaller than the length scale of the engine. Resolving all of these scales in the computational grid by direct numerical simulation (DNS) is currently an untenable problem, due to the limitations of computational speed and power. Large eddy simulation (LES) calculations have recently been used to model the flow through a full-size scramjet combustor [3] with reasonable agreement to experimental data. LES calculations resolve turbulence at large scales and model the effect of turbulence below the sub-grid scale using filters calibrated from available DNS or experimental data. Larsson et al. used this method to simulate the flow through the HyShot II scramjet combustor [4]. The calculated pressure rise through the engine agreed with the HyShot II flight data and the changes in flow structure with different fuel equivalence ratios agreed with experimental observations. Performing simulations such as these for which there is flight and experimental data available for comparison is

necessary for assessing the accuracy of turbulence and chemical models such that the simulations may be relied upon for design of flight vehicles.

1.2 Flame Stability

In addition to performing full-size engine simulations, flame stability and flame-turbulence interactions are also studied at a fundamental level using canonical geometries and flow conditions that allow researchers to focus on particular physics of interest. Efforts to understand the effect of subsonic and supersonic turbulence on burning rate, energy release, and flame structure are ongoing. Poludnenko et al. studied the dynamics of premixed flames when perturbed by homogeneous, isotropic turbulence [5], finding that the effect of turbulence at scales smaller than the laminar flame thickness was limited to wrinkling of the flame surface. The evolution of the turbulent flame was completely determined by large-scale fluid motions greater than the laminar flame speed. The authors also determined that turbulence resulted in unstable burning, which created pressure gradients near the flame and the formation of shocks [6]. The interaction of the pressure gradients and shocks with the flames amplified the turbulence within the flames, in some cases resulting in initiation of detonations.

Pressure waves were found to have a profound effect on flame evolution in simulations performed by Xiao et al. [7]. Interaction of the pressure waves with curved flame fronts was found to destabilize the flame due to a Rayleigh-Taylor (RT) instability at the flame surface, resulting in wrinkling and perturbations to the flame shape. The RT instability forms at an interface between two fluids of different densities when the light fluid pushes the heavy fluid and the fluids are accelerated in a direction transverse to their interface [8]. In supersonic flow, the interaction of shocks with flames causes the flames to accelerate and become more turbulent primarily through a Richtmeyer-Meshkov (RM) instability, which occurs when a shock passes through a

fluid interface and accelerates fluids of different densities relative to one another. This interaction generates high levels of vorticity in the turbulent flame brush and can lead to initiation of a detonation [9]. Understanding detonation initiation mechanisms is an active area of analytical, computational, and experimental research.

1.3   Deflagration-to-Detonation Transition

Detonations occur in many physical systems, from micro-thruster engines with length scales of microns to supernovae spanning thousands of kilometers. In some cases detonation initiation must be predicted and prevented, such as in a diesel engine, or stabilized and controlled to produce thrust, as in pulse and rotating detonation engines. Detonations may be initiated by direct initiation or through deflagration-to-detonation transition (DDT). Sufficiently large external energy addition into a fuel-oxidizer mixture at a timescale that is small relative to the acoustic timescale of the explosive mixture can result in a direct initiation of a detonation without first creating a measurable deflagration [10]. Detonations may also arise through the slower process of DDT. In DDT, the fuel-oxidizer mixture is ignited with a flame or a weak spark with much less energy deposition than in the case of a direct initiation. The initially laminar flame accelerates and eventually becomes turbulent. Detonations may initiate on the turbulent flame front or in the unburned gas near the flame.

In nature, DDT can occur with disastrous consequences. In 2011, a tsunami disabled the cooling pumps for the nuclear reactors at the Fukushima Daiichi Nuclear Power Plant. Three reactors experienced meltdowns once the coolant stopped circulating, allowing hydrogen gas to leak from the reactors and accumulate in the facility. The hydrogen mixed with the air, forming a cloud of detonable gas. Contact with a spark or a hot equipment surface ignited the gas and the deflagration transitioned to a detonation that caused significant damage to the plant and release of radiation into the surrounding areas at a level unprecedented since the Chernobyl disaster [11].

Conversely, DDT is desirable and necessary for the generation of thrust in detonation engines; DDT occurs at frequencies on the order of 100 Hz in pulse detonation engines [12, 13].

1.4   Numerical Simulation of DDT

Zeldovich et al. were the first researchers to simulate DDT [14] by computing the one-dimensional propagation of a chemical reaction in a detonable mixture with an initial gradient in temperature. They found that the reaction front would transition to a detonation wave only for a certain range of temperature gradients; if the gradient was too large or small, the shock and flame would decouple or in, some cases, a shock would not form at all. Detonation initiation through this ignition-gradient DDT mechanism was later observed in experiments conducted by Lee et al. [15]. Detonable mixtures were ignited photochemically and it was discovered that detonation initiation required a minimum concentration of free radicals as well as a concentration gradient such that the chemical reaction propagated in phase with the initial shock wave. In the cases where these conditions were met, the energy released by the chemical reactions amplified the shock and a detonation formed.

Numerically simulating DDT from first principles presented a computational challenge due to the vast range of relevant length scales involved, spanning many orders of magnitude from the flame thickness to the size of the physical system. This challenge prompted the development of numerical algorithms for solving coupled ordinary and partial differential equations [16] and methods of adaptively refining the computational grid to provide increased resolution based on local gradients in pressure, temperature, or reactant concentration. As these capabilities developed, DDT was studied in two and three-dimensional simulations in systems of larger scales and increasing complexity requiring greater computational resources. Oran and Gamezo summarized much of this theoretical and numerical work in [17], where they analyzed

a series of simulations to gain insight into how, when, and where DDT occurs. The authors discovered that shock-flame interactions drive turbulence in the flame, which creates the conditions for DDT to occur through the ignition-gradient mechanism in the unburned gas near the turbulent flame front. Interaction of the flame with boundary layers, walls, and obstacles also led to amplified turbulence in the flame and increased likelihood of DDT occurring.

Gamezo et al. continued investigating DDT mechanisms, using obstacle-laden channels filled with a stoichiometric hydrogen-air mixture as a canonical system [18]. Obstacles in a confined geometry generate shocks and induce turbulence in the flame to decrease the time and length scales required for DDT to occur following the ignition of an initially laminar flame. With obstacles regularly spaced and half the height of the channel (blockage ratio of 0.5), DDT would always occur through the ignition-gradient mechanism in the unburned gas. Mach stems, formed by diffraction of shocks over obstacles, reflected from the obstacles and hot spots ignited in the unburned gas behind the Mach stem reflection, which transitioned to detonations.

1.5 Current Approach

Prior research has laid a strong foundation for our understanding of flame instability, flame-turbulence interaction, and DDT in compressible reactive flows, but there are still many open questions. This work focuses on the following:

- Can detonation occur in the unburned gas through a mechanism other than the ignition-gradient mechanism previously observed?

- Does detonation initiation always occur in the unburned gas, or can shock-flame interactions cause the flame front to transition to a detonation?

- How does varying the blockage ratio in the canonical obstacle-laden channel affect flame evolution, development of turbulence, and detonation initiation?

Will the mixture detonate for very low blockage ratios?

- Will the fuel-oxidizer mixture autoignite when flowing through a channel without obstacles at supersonic velocities? If so, does the flame remain stable or does it become turbulent? Will detonations occur and, if so, by what mechanism?

- What is the effect of Mach number on ignition, flame stability, and detonation initiation of the mixture flowing at supersonic speeds?

- How do fluid instabilities contribute to turbulence in the flame and detonation initiation?

These questions are explored using multidimensional numerical simulations solving the compressible Navier-Stokes equations for a chemically reacting gas as detailed in Sec. 3.3. The equations are solved using a fifth-order accurate weighted essentially non-oscillatory (WENO) algorithm, described in [19], which was selected due to its robustness and low dissipation; these qualities are essential for accurate simulation of compressible, turbulent flows. The WENO method is a type of monotone-integrated large eddy simulation (MILES) algorithm. Originally used in the 1970s for solving problems with shocks and blast waves, MILES algorithms have been adopted for computing a variety of reacting and non-reacting high-Reynolds-number flows in aerodynamics, combustion, propulsion, atmospheric sciences, and astrophysics.

Simulations using a MILES method resolve the macroscopic scales of a problem and do not require an explicit filter for the sub-grid scale. Turbulent dissipation at the sub-grid scale is instead modeled by the numerical dissipation inherent to the algorithm. This method has been found to provide physically reasonable behavior near the grid-scale cut-off as long as there is sufficient spatial resolution to capture the large-scale turbulence [20]. In other words, MILES may be used to compute turbulent flows and the inherent properties of the algorithm, particularly conservation,

monotonicity, and causality, are relied upon to provide the correct behavior at the grid-scale cut-off.

This method was first postulated in literature by Boris [21] and there have been a number of studies published since that show qualitative and quantitative agreement between MILES calculations and experiments [22–25], LES calculations using a variety of explicit sub-grid scale models [22, 26, 27], and DNS calculations [27]. The MILES method is well suited to the problems considered in this work due to its computational efficiency and accuracy in simulating turbulent, reactive flow. It is important to note that the accuracy of MILES calculations is predicated upon resolving enough of the large scales to capture the bulk of the turbulent kinetic energy of the flow. Grid resolution and solution sensitivity studies were performed to analyze the robustness of the solution and grid-independence of the physics of interest; these studies are detailed in Secs. 3.5.3, 3.8, 4.5, and 5.5.3.

At the time when this work was written, Chapters 2 and 3 were published in [28] and [29], respectively. Chapter 4 was accepted for presentation at the *2018 AIAA Propulsion and Energy Forum and Exposition*. Chapter 5 was under preparation for submission to the *Journal of Combustion and Flame*. The manuscripts are compiled here as they were originally published or submitted, with supplementary material appended as necessary, as they are all part of ongoing work to answer the questions posed above.

2 Shock Transition to Detonation in Channels with Obstacles

Gabriel B. Goodwin, Ryan W. Houim, Elaine S. Oran

Abstract

Multidimensional numerical simulations of an unconfined, homogeneous, chemically reactive gas were used to study interactions leading to deflagration-to-detonation transition (DDT). The configuration studied was a long rectangular channel with regularly spaced obstacles containing a stoichiometric mixture of ethylene and oxygen, initially at atmospheric conditions and ignited in a corner with a small flame. The compressible reactive Navier-Stokes equations were solved by a high-order numerical algorithm on a locally adapting mesh. The initial laminar flame develops into a turbulent flame with the creation of shocks, shock-flame interactions, shock-boundary layer interactions, and a host of fluid and chemical-fluid instabilities. The

final result may be eventual deflagration-to-detonation transition (DDT). Here two types of simulations are described, one with DDT occurring in a gradient of reactivity, which is common in the channels with higher obstacles, and another in which DDT arises from energy focusing as shocks converge. For the latter case, the rate of energy deposition necessary to initiate a detonation in the unburned gas is analyzed using a control volume analysis.

Keywords: DDT; Turbulent flame; Shock interactions; Direct initiation; Numerical simulations

2.1 Introduction

Deflagration-to-detonation transition (DDT) is a complex process involving turbulence, shock-flame interactions, shock collisions and reflections, and interactions of shocks with boundary layers. It is an important topic because DDT must be prevented in many cases [30, 31] and optimized for specific applications [32–34]. DDT may be initiated by a number of different mechanisms that have been seen in both experiments and computations [17, 18, 35–42]. Not all of these mechanisms, or the interplay among them, are fully understood.

Direct initiation of a detonation in a gas has been studied theoretically and experimentally [35–37]. Sufficiently large external energy addition at a timescale that is small relative to the acoustic timescale of the gas can result in a direct initiation of a detonation without first creating a deflagration [10]. Recently, the response of the gas to a localized, transient energy deposition has been studied by asymptotic analysis in an effort to quantify the gas response (deflagration or detonation) [43]. Initiation of a detonation through a gradient of chemical reactivity [14, 15] has been investigated extensively using numerical simulations, as summarized in [17]. DDT in channels with obstacles has been computed for a variety of fuel-oxidizer mixtures [18, 39, 40] and has been the subject of experimentation [44].

The effect of obstacles, often characterized by a blockage ratio (br, or the obstacle height divided by the channel height), on flame acceleration and DDT has been investigated experimentally [41, 42] and numerically [45]. Gamezo et al. [45] noted the competing effects of high blockage ratios: larger obstacles promote non-uniform flow, which leads to fast flame acceleration and they also weaken shocks diffracting over large obstacles. These authors also observed that the location in the channel where DDT occurs does not vary significantly for $br = 0.31 - 0.56$ range, but it increases sharply outside of this interval for both higher and lower br.

As a background to this paper, a series of simulations was performed with $br = 0.05 - 0.8$ in order to identify how the mechanism of DDT changes as blockage ratio decreases. The detailed results of these simulations, and some unusual trends noted, will be presented in a subsequent paper. In several of these simulations, however, shocks and fluid instabilities evolved that caused flame acceleration and transition to detonation due to energy focusing as opposed to the more predictable detonations that occur in Mach reflections against obstacles in systems with high br. Maeda et al. [46] saw similar phenomena in their experiments in channels with $br = 0.083$ and 0.25. The purpose of this paper is to extract results for low br and compare the mechanism of DDT with those seen for the relatively high $br = 0.5$.

2.2 Numerical and Physical Model

The numerical model solves the full set of Navier-Stokes equations in unsteady, fully compressible, chemically reacting gas, as described in [17]. The reaction of a stoichiometric mixture of ethylene and oxygen, with specific ethylene-oxygen parameters courtesy of Alp Ozgen, is modeled using a simplified, calibrated chemical-diffusive model of the form,

$$\frac{dY}{dt} \equiv \dot{w} = -A\rho Y \exp(-E_{\mathrm{a}}/RT) \tag{1}$$

where ρ, T, Y, and $\dot{w}$ are the mass density, temperature, mass fraction of reactant, and reaction rate, respectively. A is the pre-exponential factor, and E_a is the activation energy. Thermal conductivity, κ, viscosity, ν, and mass diffusivity, D, were modeled using values of 1.0×10^{-5} g/s-cm-K$^{0.7}$, 7.0×10^{-6} g/s-cm-K$^{0.7}$, and 1.0×10^{-5} g/s-cm-K$^{0.7}$, respectively. A Godunov algorithm, fifth-order accurate in space and third-order accurate in time [19], is used to solve the equations on a dynamically adapting grid [47]. The simulations described below used grids with minimum size $dx_\mathrm{min} = 3.3$ μm and coarsest size ranging from $dx_\mathrm{max} = 26.7$ to 53.3 μm. The largest grid had 60 cells across the channel height and the smallest had 960 cells. This choice of grids was tested and shown to resolve the flames, shocks, boundary layers, and other important flow and chemical structures.

The input parameters in Table 1 were chosen to reproduce the flame and detonation properties of the ethylene-oxygen mixture initially at 298 K and 1 atm. Using the input parameters in one-dimensional (1D) and two-dimensional (2D) solutions of the Navier-Stokes equations produces the output flame and detonation properties listed. To estimate the detonation cell height, λ, for this model, a 2D detonation was computed and an average was taken of cell sizes after an initially overdriven detonation had decayed to the Chapman-Jouguet velocity. The value $\lambda = 0.2$ mm agrees surprisingly well with reported experimental results, which range from 0.1 mm to 2 mm [48].

The geometrical setup is shown in Fig. 1. Obstacles are uniformly spaced along the wall. The obstacle width and height are constant through the channel. The *br* for the simulations discussed here are 0.5 and 0.1. The channel is open at the right, with symmetry planes at the left and top boundaries. The bottom wall and all obstacle surfaces are no-slip adiabatic boundaries. To ignite the mixture, a circular region of hot, burned product at 3500 K and 1 atm is placed at the left wall. A channel height of 0.32 cm was chosen for several reasons. Experimental data for DDT in small

Table 1. Input model parameters and output combustion wave properties for stoichiometric ethylene and oxygen initially at 1 atm and 298 K.

	Input	
P_{o}	1 atm	Initial Pressure
T_{o}	298 K	Initial Temperature
ρ_{o}	1.27×10^{-3} g/cm^3	Initial Density
γ	1.2195	Adiabatic Index
M	31 g/mol	Molecular Weight
A	1.05×10^{12} cm^3/(g s)	Pre-Exponential Factor
E_{a}	$39.2RT_{\mathrm{o}}$	Activation Energy
q	$59.7RT_{\mathrm{o}}$/M	Chemical Energy Release
ν_{o}	7.0×10^{-6} g/s-cm-K$^{0.7}$	Viscosity
$\kappa_{\mathrm{o}} = D_{\mathrm{o}}$	1.0×10^{-5} g/s-cm-K$^{0.7}$	Transport Constants
	Output	
S_{L}	413 cm/s	Laminar Flame Speed
T_{b}	$11.7T_{\mathrm{o}}$	Post-Flame Temperature
ρ_{b}	$0.085\rho_{\mathrm{o}}$	Post-Flame Density
x_{l}	8.88×10^{-3} cm	Laminar Flame Thickness
D_{CJ}	2.20×10^5 cm/s	CJ Detonation Velocity
P_{ZND}	$54.5P_{\mathrm{o}}$	Post-Shock Pressure
P_{CJ}	$27.8P_{\mathrm{o}}$	Pressure at CJ Point
T_{ZND}	$6T_{\mathrm{o}}$	Post-Shock Temperature
T_{CJ}	$15.5T_{\mathrm{o}}$	Temperature at CJ Point
ρ_{ZND}	$9.8\rho_{\mathrm{o}}$	Post-Shock Density
ρ_{CJ}	$2\rho_{\mathrm{o}}$	Density at CJ Point
x_{d}	3.2×10^{-4} cm	Half-Reaction Thickness
λ	~ 0.02 cm	Detonation Cell Size

channels with stoichiometric ethylene-oxygen, such as the work by Wu et al. [48], is available for comparison. The small scale detonation properties of this fuel-oxidizer mixture, such as small detonation cell sizes, fast reactions, and energy release, make ethylene-oxygen an ideal fuel-oxidizer mixture for studying DDT in small channels.

2.3 Flame Acceleration and DDT

Previous work [18, 39] has shown that flame acceleration is rapid in channels with $br = 0.5$ for stoichiometric mixtures of hydrogen and air. Figure 2 shows flame acceleration and transition to detonation for the stoichiometric ethylene and oxygen
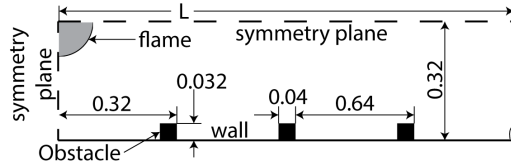
Fig. 1. Computational setup in units of cm. Obstacles evenly spaced along channel length L. Radius of the initial burned region is 0.08 cm. Blockage ratio is 0.1 in this case.
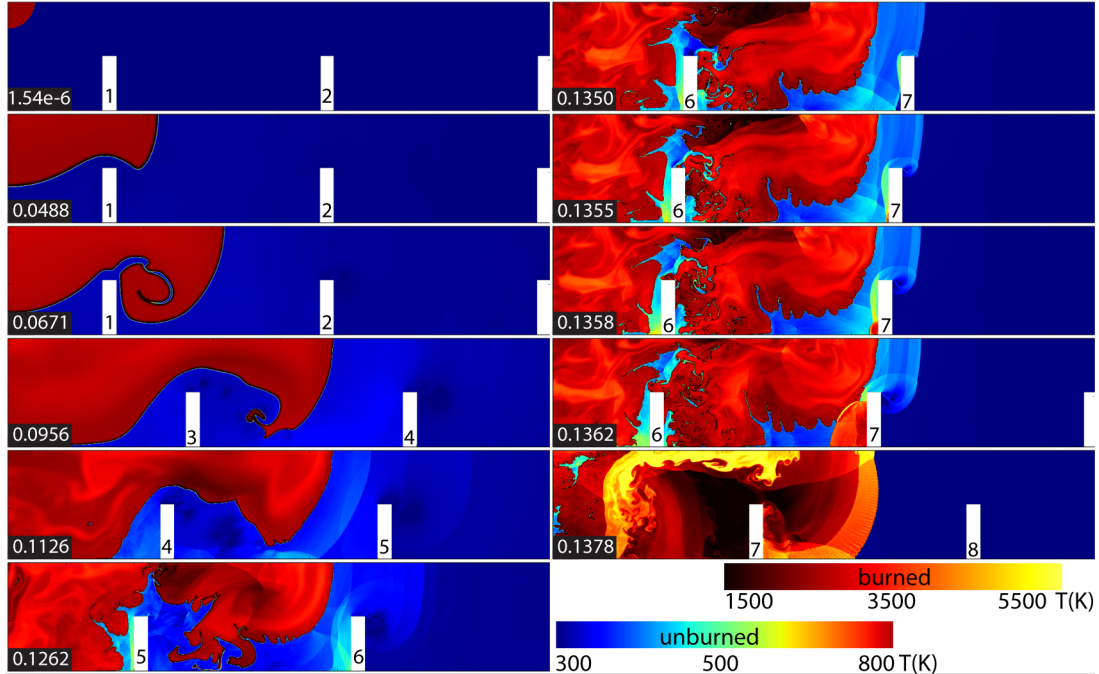
Fig. 2. Accelerating flame and detonation in 2D quarter-channel with $br = 0.5$. Time in milliseconds is shown in the frame corners. Obstacles are numbered.

mixture for $br = 0.5$. As the flame passes over obstacles, its surface area increases due to expansion and fluid instabilities (Rayleigh-Taylor, Richtmyer-Meshkov, and Kelvin-Helmholtz), shocks and all of their interactions. Strong leading shocks propagate into the unburned gas. The leading shock diffracts over obstacles and reflects from the channel floor, eventually forming a Mach stem (0.1126 ms). At 0.1355 ms, detonation occurs in hot, unburned gas as a Mach stem reflects from an obstacle and leaves a hot spot in a gradient of reactivity. In Fig. 2, the unburned material detonates behind a Mach stem reflection from obstacle 7 at 0.1355 ms.

When br is much smaller, 0.1 shown in Fig. 3, the flame accelerates more slowly
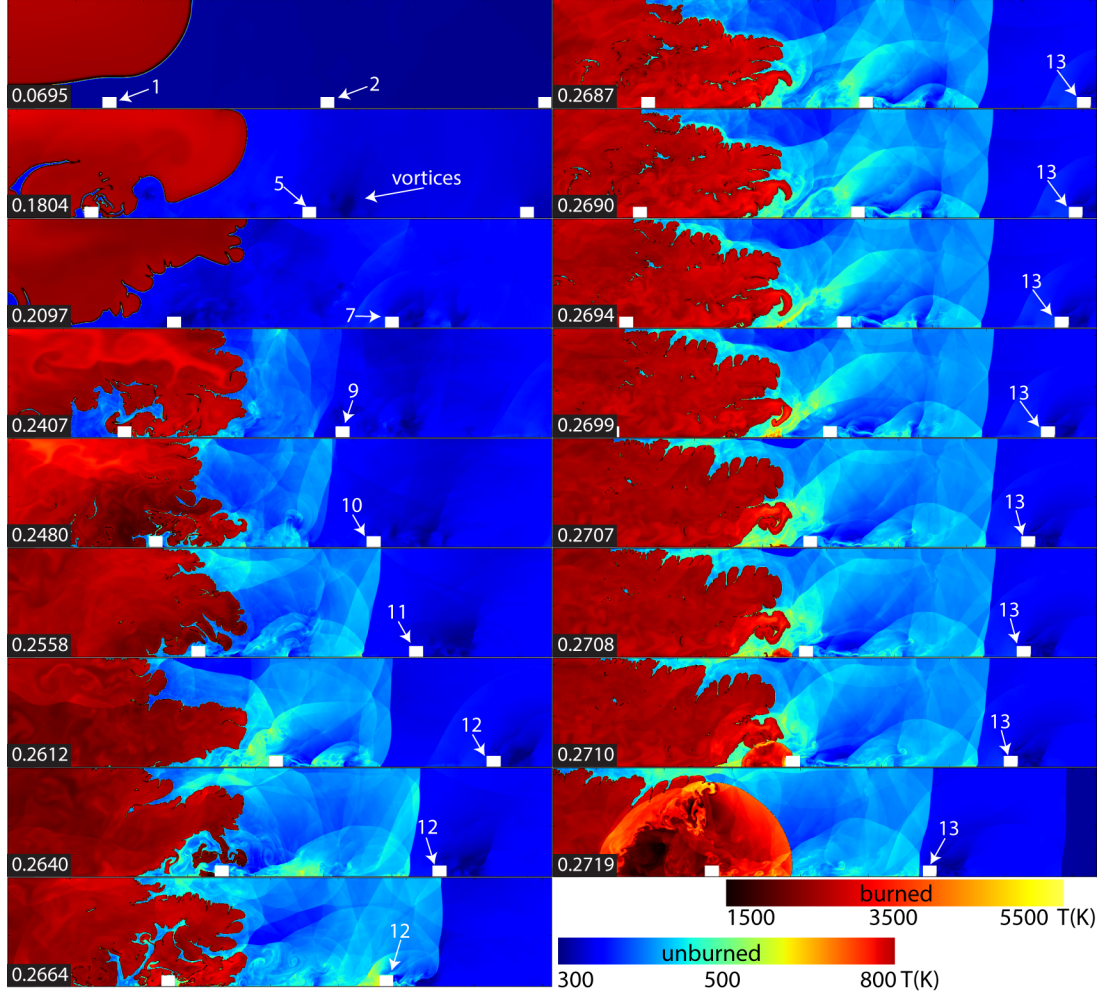
Fig. 3. Full simulation for blockage ratio of 0.10. Time in milliseconds is shown in the frame corners. Obstacles are numbered.

and stays laminar longer as it propagates into the channel. For $br = 0.5$, detonation occurs at 0.136 ms at 3.5 cm from the left edge, having passed six obstacles. When the $br = 0.1$, detonation occurs against the lower wall at 0.271 ms at 7.25 cm, having passed 11 obstacles. Despite the major differences in time and distance to DDT, the flame development is similar in both cases. Unburned gas is driven downstream over obstacles causing vortex shedding from the obstacle's leading edges (seen starting at 0.1804 ms in Fig. 3). Vortices coalesce behind obstacles to form regions of recirculation. The flame surface area increases as it is pulled into the recirculation region and becomes turbulent as the acoustic waves shed by the vortices propagate through

the flame. Shocks form as the flame accelerates, increasing in strength as they reflect off the obstacles, and these shocks collide with one another. Rather than seeing the rapid development of a strong leading shock that is closely coupled with the flame, as seen in Fig. 2, a relatively large unburned, turbulent region filled with shocks and strong vortices now forms between the flame and the leading shock. Figure 4 shows the complexity and dynamic structure in this shock-flame complex.
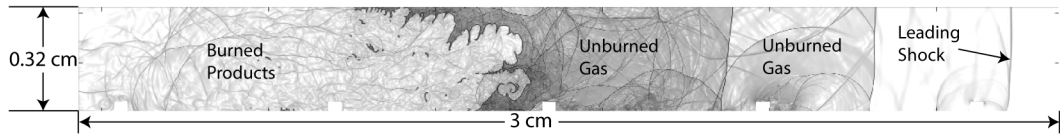
Fig. 4. Numerical schlieren showing the turbulent region.
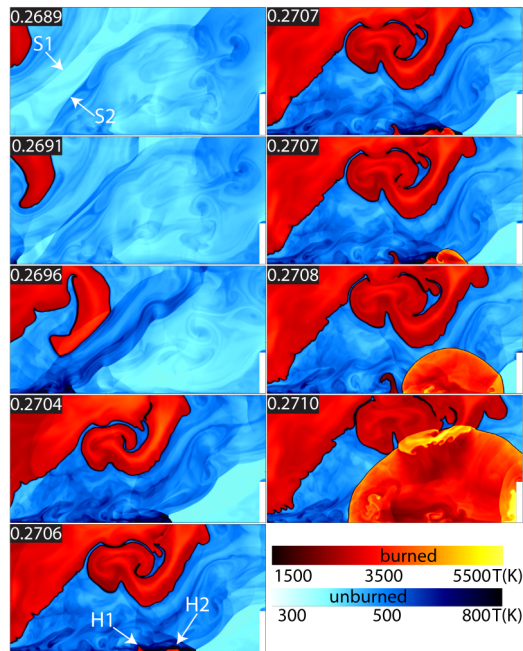
Fig. 5. Multiple shock collision and detonation. Time is shown in ms.

Figure 5 is an enlargement of the detonation that occurs in Fig. 3 for $br = 0.1$. Two shocks, labeled S1 and S2 at 0.2689 ms, collide at 0.2696 ms. Shock S1 is immediately ahead of the flame, traveling to the right, and shock S2 is reflected from the downstream obstacle (shown in white in the lower right corner of Fig. 5) and

16

is traveling to the left. The shock collision ignites two hot spots in the boundary layer, labeled H1 and H2. By 0.2707 ms, H1 evolves into a flame and shock, and H2 evolves into a detonation. The analysis below shows that the confluence of shocks causes transition to detonation in hot unburned gas. This detonation mechanism has elements of both gradient ignition and direct initiation of detonation.

To quantify the change in state of unburned material compressed during the multiple-shock collision, a control volume analysis was performed on a small 33.3 μm $\times$ 33.3 μm region at the location where H2 forms and becomes a detonation. The analysis tracked the change in pressure, temperature, density, and energy release rate over a 0.2 μs period from 270.5 μs to 270.7 μs. This corresponds to a time before the region is compressed by the shock collision to a time after the detonation formed and propagated through the region. Figure 6 shows the trends of the state variables. Shock compression begins at 270.55 μs, and the material begins to react chemically at 270.65 μs. The pressure and density increase dramatically, first from shock compression and then after the detonation. As the detonation propagates out of the region, the pressure and density decrease. The average temperature in the control volume prior to combustion is $\sim$850 K.
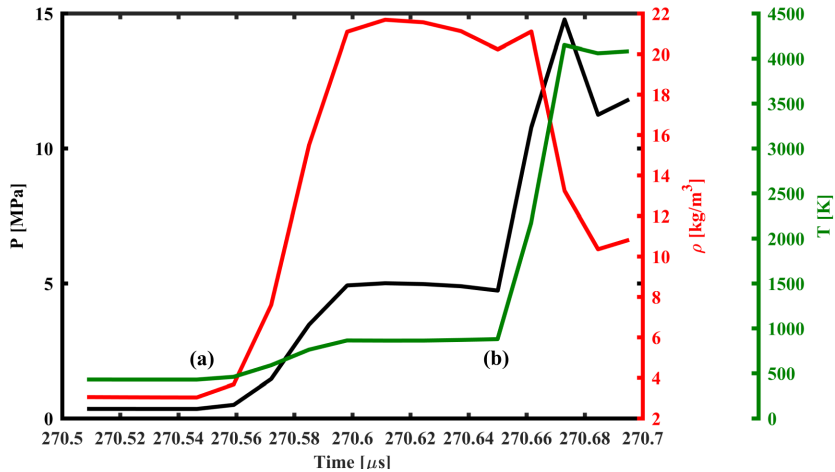
Fig. 6. State variables in the control volume from 270.5 μs to 270.7 μs (a) Shock compression (b) Detonation. The gas begins to react chemically at 270.65 μs.
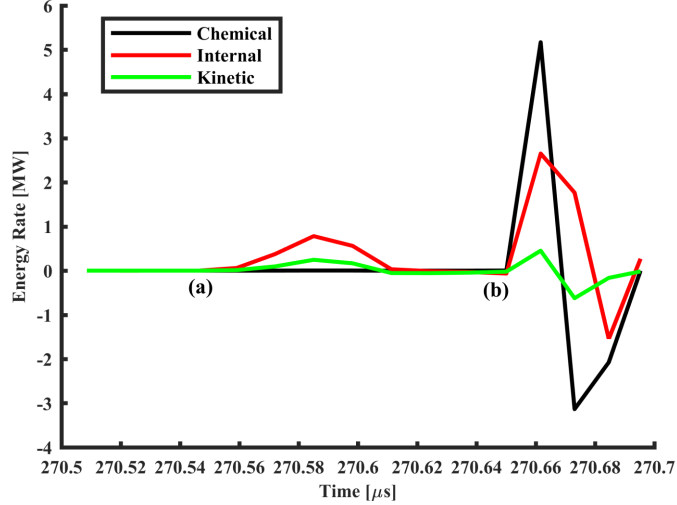
Fig. 7. Rate of energy deposition in control volume during (a) Shock compression (b) Detonation.

Figure 7 shows the rate of energy deposition into the control volume. Chemical energy is defined as heat release per kg of reactant, q, internal energy is $P/(\gamma - 1)$, and kinetic energy is $0.5\rho u^2$, where u is the magnitude of velocity. As the material in the region is compressed, rates of internal and kinetic energy increase, followed by a second peak as the material detonates. The detonation carries energy out of the region as it propagates into the surrounding gas, resulting in the negative energy rates seen after 270.66 μs. The total energy content in the region, defined as the sum of chemical, internal, and kinetic energies, increases by a factor of 15 during shock compression.

Prior work [18] has shown that for hydrogen and air mixtures in channels of different sizes, there were different regimes of DDT. The authors found that in some of these regimes, the detonation mechanism was more sensitive to the turbulence in the flow. The variations in br described in this paper reflect the same phenomenon, that there are different regimes of DDT with varying sensitivity of the detonation mechanism to turbulence. In the $br = 0.1$ regime, the sensitivity of the solution to the turbulence causes the detonation to occur at slightly different times and locations for cases with modified initial conditions.

18
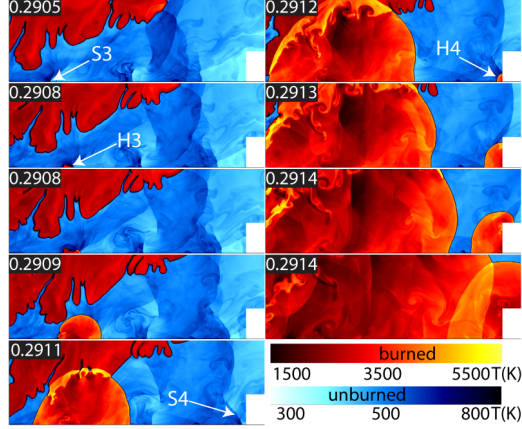
Fig. 8. Shock reflections and collisions result in initiation of two detonations. Time is shown in ms.

Figure 8 shows the detonation in another simulation with $br = 0.1$ with slightly different initial conditions. A smaller coarse mesh size of 26.7 μm was used, as compared to 53.3 μm in the previously described $br = 0.1$ case shown in Fig. 3. The location of the detonation is $\sim$1.2 cm further along the channel boundary than the detonation that occurred in Fig. 5, however, it again appears where shock collisions and reflections are focused. The shock immediately ahead of the flame, labeled S3, reflects off the channel boundary and ignites a hot spot H3 in the boundary layer. The hot spot becomes a detonation while another shock ahead of the flame, labeled S4, reflects off the obstacle shown in the lower right corner of the figure. The reflection of S4 ignites another hot spot, labeled H4, that also becomes a detonation. The two detonations combine and propagate down the channel. Although the time and location of detonation is stochastic due to turbulence in the flow, which is heavily dependent on initial conditions such as grid size, the detonation mechanism in the low br regime is robust. This is consistent with previous work investigating the stochasticity of DDT in flow regimes that are sensitive to turbulence in the flow [18].

A comparison of the simulations with $br = 0.5$ and 0.1 shows that obstacle size plays a major role in the flame acceleration, turbulence in the flame and unburned gas, shock formation, time or distance to detonation, and detonation mechanism.

19
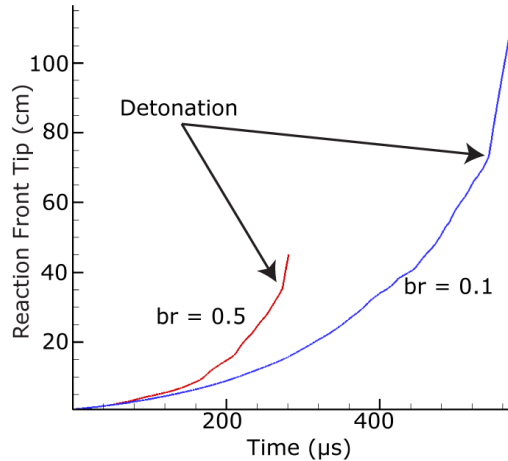
Fig. 9. Forward position of the reaction front within the channel as a function of time for 0.1 and 0.5 blockage ratio cases. Detonations occur at inflection points on the curves.

Figure 9 shows the position of the tip of the reaction front as a function of time for both blockage ratios. Higher values of br result in a more predictable flow as strong leading shocks form very close to the flame. These obstacles consistently produce Mach-stems and detonations that form behind Mach-stem reflections. For this stoichiometric ethylene and oxygen mixture, the flame never falls more than ~ 0.2 cm behind the leading shock. When br decreases, the leading shocks form as far as 1.5 cm ahead of the flame tip, creating a large, unburned turbulent region ahead of the flame. Rather than the detonation always occurring in a Mach reflection against an obstacle, they may occur anywhere that energy is focused sufficiently to initiate the detonation. The actual detonation location is stochastic because the turbulent region is filled with shock collisions and reflections that may focus sufficient energy to detonate the unburned gas anywhere within the turbulent region ahead of the flame.

Turbulence, an essentially stochastic process, dominates this region of shock collisions, shock-boundary layer interactions, and fluid instabilities. This is complicated even further by the nonequilibrium nature of the turbulence itself in these scenarios.

2.4 Conclusions

Multidimensional, unsteady numerical simulations of an initially homogeneous mixture of ethylene and oxygen in partially blocked channels were performed to determine how the mechanism of DDT changes as the blockage ratio (br) is decreased. This paper compared two cases, $br = 0.5$ and 0.1.

For $br = 0.5$, detonation occurs due to the creation of a hot spot in a gradient of reactivity that forms behind a Mach reflection [18, 39, 40]. This was shown for a different fuel-oxidizer mixture than used in previous work. In the case with $br = 0.1$, shock collisions increase the temperature, pressure, and density of the unburned material. These effects and interactions occur frequently due to the complexity of the shock structures and interactions in the unburned turbulent region between the flame and the leading shock. As the flame propagates down the channel, the strength of the shock collisions and reflections increases in this region. Multiple shocks collide and reflect against the channel boundary, focusing energy in a localized region of unburned material and detonating the mixture. These results are consistent with direct initiation theory [10] and with detonations seen in experiments using similar blockage ratios ($br < 0.3$) [46]. Sufficient energy is deposited into a localized region on a timescale that is small relative to the acoustic timescale of the gas, initiating a detonation.

An additional simulation, with $br = 0.1$, investigated the sensitivity of the solution to initial conditions. Modifying the coarse mesh size resulted in a difference in detonation time and location of 0.02 ms and 1.2 cm, respectively, but the detonation mechanism was the same. This phenomenon was also seen in previous work with a different fuel-oxidizer mixture [18], where it was determined that some regimes of DDT are especially sensitive to turbulence in the flow, which is heavily dependent on initial conditions.

It is important to understand the similarities and differences in flame acceleration

and DDT with different fuel-oxidizer mixtures. The small detonation cell size, fast reactions, and rapid energy release in the combustion of ethylene-oxygen result in a smaller length scale than in previous work with other mixtures [18, 39, 40], however, the detonation mechanism for the $br = 0.5$ case in previous work with other mixtures is the same as what is observed for the $br = 0.5$ case for ethylene-oxygen. Future work to directly compare results from different mixtures, such as where and when DDT occur, the flow structures that form ahead of the turbulent flame, and whether the flame is galloping or fast, will be a useful contribution to the study of DDT in channels.

2.5   Acknowledgments

3 Effect of Decreasing Blockage Ratio on DDT in Small Channels with Obstacles

Gabriel B. Goodwin, Ryan W. Houim, Elaine S. Oran

This paper expands upon Chap. 2 by examining the effect of blockage ratio in an obstructed channel on flame evolution and DDT, with the goal of answering the following questions:

- Can detonation occur in the unburned gas through a mechanism other than the ignition-gradient mechanism previously observed?

- Does detonation initiation always occur in the unburned gas, or can shock-flame interactions cause the flame front to transition to a detonation?

- How does varying the blockage-ratio in the canonical obstacle-laden channel affect flame evolution, development of turbulence, and detonation initiation? Will the mixture detonate for very low blockage ratios?

Several simulations with varying blockage ratios are discussed and the energy-focusing detonation mechanism is observed to cause detonations to occur, not only in the unburned gas, but also at the flame front. The rate of energy deposition resulting from the shock collision that initiates the detonation is quantified through a control volume analysis. Two and three-dimensional simulations are compared and the stochastic nature of DDT in this problem is investigated. This paper was originally published [29] in the *Journal of Combustion and Flame.* The manuscript is available at: https://doi.org/10.1016/j.combustflame.2016.07.029

Abstract

Multidimensional numerical simulations of an unconfined, homogeneous, chemically reactive gas were used to catalog interactions leading to the deflagration-to-detonation transition (DDT). The configuration studied was an infinitely long rectangular channel with regularly spaced obstacles containing a stoichiometric mixture of ethylene and oxygen, initially at atmospheric conditions and ignited in a corner with a small flame. The channel height is kept constant at 3200 μm and obstacle heights varied from 2560 μm to 160 μm to decrease the blockage ratio (br) from 0.8 to 0.05. The compressible reactive Navier-Stokes equations were solved by a high-order numerical algorithm on a locally adapting grid. The initially laminar flame develops into a turbulent flame with the creation of shocks, shock-flame interactions, shock-boundary layer interactions, a host of fluid and chemical-fluid instabilities, and DDT. Several different DDT mechanisms are observed as the br is reduced. For br in the range of 0.5 to 0.35, the shocks in the unburned material diffract over the obstacles and reflect against the channel wall, forming Mach stems that increase in strength with every obstacle traversed. Eventually, the Mach stem strength is sufficient for the unburned mixture to detonate after it reflects from an obstacle. For br outside of this range, DDT may occur either through Mach-stem reflection or through direct initiation due to shock focusing. Stochasticity of the turbulence leading to DDT in channels with low br is considered.

Keywords: DDT; Turbulent flame; Shock interactions; Direct initiation; Numerical simulations

3.1 Introduction

Deflagration-to-detonation transition (DDT) is a complex process involving turbulence, shock collisions and reflections, shock-flame interactions, and interactions of shocks with boundary layers. It is an important topic because in many cases DDT

must be prevented [30, 31] and in others its occurence must be controlled in time and space [32–34]. DDT may be initiated by a number of different mechanisms that have been seen in both computations and experiments [17, 18, 35–42]. Because of the complexity of the flow, not all of these mechanisms, or the interplay among them, are completely understood.

Direct initiation of a detonation in a gas has been studied experimentally and theoretically [35–37]. Sufficiently large external energy addition at a timescale that is small relative to the acoustic timescale of the explosive mixture can result in a direct initiation of a detonation without first creating a measurable deflagration [10]. Recently, the response of the inert gas to a localized, transient energy deposition has been studied by asymptotic analysis in an effort to quantify the gas response (deflagration or detonation) [43]. Initiation of a detonation through a gradient of chemical reactivity [14, 15] has been studied extensively using numerical simulations, as summarized in [17]. DDT in channels with obstacles has been simulated for a variety of premixed fuels [18, 39, 40] and has also been the subject of experimentation [44].

The effect of obstacles, often characterized by a blockage ratio (br, or the obstacle height divided by the channel height), on flame acceleration and DDT has been investigated numerically [45] and experimentally [41, 42]. Gamezo et al. [45] noted the competing effects of high blockage ratios: larger obstacles promote nonuniform flow, which leads to rapid flame acceleration, and they also weaken shocks diffracting over large obstacles. These authors also observed that the location in the channel where DDT occurs does not vary significantly for the $br = 0.31 - 0.56$ range, and that distance into the channel where DDT occurs increases sharply outside of this interval for both higher and lower br.

This paper presents a series of simulations covering the range $br = 0.05 - 0.8$ in order to identify how the mechanism of DDT changes as blockage ratio is varied. We

will discuss the transition from an initially laminar flame to a turbulent flame and DDT for several different regimes of flow characterized by br. DDT in the high br regime ($0.35 < br < 0.8$) occured in gradients of reactivity formed behind Mach-stem reflections against obstacles through the gradient mechanism. In the intermediate regime ($0.05 < br < 0.35$), DDT occurred either behind a Mach reflection, at a flame front, or in a volume of unburned gas subjected to shock focusing through a direct initiation mechanism. In the low br regime (0.05), the DDT location was against an obstacle or channel wall. In the case of $br = 0.8$, DDT occurs due to both mechanisms, shock focusing through direct initiation and detonation through a gradient mechanism.

3.2   Background

DDT in channels was first observed in multidimensional simulations when researchers wanted to determine what was required to simulate DDT computationally [17, 18, 39, 40]. The expected result was for the flame front to transition to a detonation as it accelerated down the channel, but researchers were surprised to see the detonation initiate in the unburned mixture between a leading shock and the turbulent flame front. This region between the leading shock and flame was shock-heated, with significantly increased temperature, pressure and density.

DDT ignition in these early simulations was consistent with the DDT mechanism first observed in calculations by Zeldovich et al. [14], who computed the one-dimensional (1D) propagation of a chemical reaction in a detonable mixture, using several different initial temperature gradients. Different regimes of chemical reaction development were observed. For steep initial temperature gradients, a weak shock formed that quickly separated from the reaction front and the reaction proceeded as a normal flame propagation. Conversely, for very small initial temperature gradients, the reaction proceeded throughout the entire mixture uniformly and a shock did not

form. In an intermediate range of temperature gradients, the shock wave coupled with the reaction front. The chemical reaction intensified the shock strength, eventually forming an overdriven detonation wave that gradually decayed to the Chapman-Jouguet velocity, D_{CJ}. This DDT ignition-gradient mechanism was later observed in experiments conducted by Lee et al. [15]. Detonable mixtures were ignited through photochemical initiation and it was determined that detonation initiation required a minimum peak value of free radical concentration as well as an appropriate gradient of the free radical distribution. If the mixture's gradient of reactivity supported propagation of the chemical reaction in phase with the shock propagation, the coherent energy release gave rise to a rapid amplification of the shock, leading to the formation of a detonation. Lee et al. referred to this phenomenon as the "Shock Wave Amplification by Coherent Energy Release" (SWACER) mechanism.

The effect of obstacles in the flow on flame acceleration and DDT in channels has been researched extensively [17, 18, 39]. Using obstacles with a $br = 0.5$ was the predominant method for accelerating the flame and producing strong shocks ahead of the flame in the unburned mixture. The shocks diffracted over the obstacles and formed Mach stems after reflecting from the channel wall, with the strength of the Mach stem increasing with each obstacle traversed. Collision of the Mach stems with the obstacles greatly increased the temperature of the unburned mixture and created a gradient of reactivity. When a correct gradient of reactivity formed such that the temperature reached the autoignition threshold for the mixture, a spontaneous wave would emerge with speed D_{sp} [17],

$$D_{sp} = -\frac{\nabla \tau_c}{|\nabla \tau_c|^2} \tag{2}$$

where τ_c is induction time. This spontaneous wave propagated through the gradient of reactivity and became an overdriven detonation. DDT ignition in channels with obstacles was consistent with the mechanisms observed in earlier work [14, 15].

In channels with smaller br, the diffraction of the shocks over the obstacles does not produce the strong Mach stems seen in the channels with larger br. Recent numerical simulations [28] have shown that the shock heated, unburned mixture may detonate due to shock reflections and collisions rapidly depositing energy into a localized volume at a timescale smaller than the acoustic timescale of the gas. In this regime, DDT does not occur as predictably as it does in the high br regime when it forms in a gradient of reactivity against an obstacle. DDT occurs wherever the rate of energy deposition into a volume of the unburned mixture is sufficient to directly initiate a detonation. This may happen when multiple shocks reflect against the obstacles and channel walls, then collide with one another, or even when shocks intersect in unobstructed space. The collision deposits sufficient energy into the unburned mixture to initiate a detonation. Experimentally, this has been shown to occur against or near the channel wall, just after the flame has traversed an obstacle, likely due to the same energy deposition mechanism [49]. This paper explores these DDT mechanisms observed in a series of two-dimensional (2D) and three-dimensional (3D) calculations with varying br.

3.3   Numerical and Physical Model

The numerical model solves the full set of Navier-Stokes equations for an unsteady, fully compressible, chemically reacting gas, an ideal gas equation of state, and a simplified, calibrated chemical-diffusive model is used to convert fuel to product,

$$\frac{\partial \rho}{\partial t} + \nabla \cdot (\rho \mathbf{U}) = 0 \tag{3}$$

$$\frac{\partial (\rho \mathbf{U})}{\partial t} + \nabla \cdot (\rho \mathbf{U}\mathbf{U}) + \nabla P = \nabla \cdot \hat{\tau} \tag{4}$$

$$\frac{\partial E}{\partial t} + \nabla \cdot ((E + P)\mathbf{U}) = \nabla \cdot (\mathbf{U} \cdot \hat{\tau}) + \nabla \cdot (K\nabla T) - \rho q \dot{w} \tag{5}$$

$$\frac{\partial(\rho Y)}{\partial t} + \nabla \cdot (\rho Y \mathbf{U}) + \nabla \cdot (\rho D \nabla Y) - \rho \dot{w} = 0 \tag{6}$$

$$P = \frac{\rho R T}{M} \tag{7}$$

$$\frac{dY}{dt} \equiv \dot{w} = -A\rho Y \exp(-E_\mathrm{a}/RT) \tag{8}$$

where ρ is the mass density, $\mathbf{U}$ is the velocity, E is the energy density, P is the pressure, T is the temperature, Y is the mass fraction of reactant, $\dot{w}$ is the reaction rate, q is the total chemical energy release, K is the thermal conduction coefficient, D is the mass diffusion coefficient, R is the universal gas constant, M is the molecular weight, A is the pre-exponential factor, and E_a is the activation energy. Thermal conductivity, κ, viscosity, ν, and mass diffusivity, D, were modeled using reference values of 1.0×10^{-5} g/s-cm-K$^{0.7}$, 7.0×10^{-6} g/s-cm-K$^{0.7}$, and 1.0×10^{-5} g/s-cm-K$^{0.7}$, respectively. The viscous stress tensor is defined as

$$\hat{\tau} = \rho\nu((\nabla \mathbf{U}) - (\nabla \mathbf{U})^T - \frac{2}{3}(\nabla \cdot \mathbf{U})\mathbf{I}), \tag{9}$$

where $\mathbf{I}$ is the unit tensor and the superscript T indicates matrix transposition. A Godunov algorithm, fifth-order accurate in space and third-order accurate in time [19], is used to solve the equations on a dynamically adapting mesh [47]. Obstacles were modeled using an immersed boundary method [50]. The simulations described below used meshes with a minimum spacing $dx_\mathrm{min} = 3.3$ μm and coarsest spacing of $dx_\mathrm{max} = 53.3$ μm. The largest grid had 60 cells across the channel height and the smallest had 960 cells. This choice of grids was tested and shown to resolve the flames, boundary layers, shocks, and other important flow and chemical structures.

The input parameters in Table 2 (courtesy of Alp Ozgen) were chosen to reproduce the flame and detonation properties of the ethylene-oxygen mixture initially at 1 atm and 298 K. Using the input parameters in one-dimensional (1D) and two-dimensional (2D) solutions of the Navier-Stokes equations produces the output flame

Table 2. Input model parameters and output combustion wave properties for stoichiometric ethylene and oxygen initially at 1 atm and 298 K.

	Input	
P_o	1 atm	Initial Pressure
T_o	298 K	Initial Temperature
ρ_o	1.27×10^{-3} g/cm^3	Initial Density
γ	1.2195	Adiabatic Index
M	31 g/mol	Molecular Weight
A	1.05×10^{12} cm^3/(g s)	Pre-Exponential Factor
E_a	$39.2RT_o$	Activation Energy
q	$59.7RT_o$/M	Chemical Energy Release
ν_o	7.0×10^{-6} g/s-cm-K$^{0.7}$	Viscosity
$\kappa_o = D_o$	1.0×10^{-5} g/s-cm-K$^{0.7}$	Transport Constants
	Output	
S_L	413 cm/s	Laminar Flame Speed
T_b	$11.7T_o$	Post-Flame Temperature
ρ_b	$0.085\rho_o$	Post-Flame Density
x_l	8.88×10^{-3} cm	Laminar Flame Thickness
D_{CJ}	2.20×10^5 cm/s	CJ Detonation Velocity
P_{ZND}	$54.5P_o$	Post-Shock Pressure
P_{CJ}	$27.8P_o$	Pressure at CJ Point
T_{ZND}	$6T_o$	Post-Shock Temperature
T_{CJ}	$15.5T_o$	Temperature at CJ Point
ρ_{ZND}	$9.8\rho_o$	Post-Shock Density
ρ_{CJ}	$2\rho_o$	Density at CJ Point
x_d	3.2×10^{-4} cm	Half-Reaction Thickness
λ	~ 0.01 cm	Detonation Cell Size

and detonation properties shown. Previous work [17] has shown that it is important to use a chemical-diffusive model for the conversion of reactant to product that accurately reproduces the major characteristics of the system. Such a model is needed because these are complex, multidimensional simulations over length scales of centimeters with reaction scales on the order of micrometers. At a basic minimum, the chemical-diffusive model must reproduce the major features of the system while still being practical computationally. The simulations in this paper used a one-step reaction model described by second-order Arrhenius kinetics (see Eqn. (7)), where the reaction rate $\dot{w}$ is proportional to ρ to account for the binary nature of chemical reac-

tions that take place in typical combustion systems. The effects of viscosity, diffusion, and heat conduction have a similar temperature dependence,

$$\nu = \nu_0 \frac{T^n}{\rho}, D = D_0 \frac{T^n}{\rho}, \frac{K}{\rho C_p} = \kappa_0 \frac{T^n}{\rho}, \tag{10}$$

where ν_0, D_0, and κ_0 are constants, $C_p = \gamma R / M (\gamma - 1)$ is the specific heat at constant pressure, and $n = 0.7$ emulates the typical temperature dependence for the system. To solve Eqs. (2)-(9), we require input values for the chemical and thermophysical parameters for ethylene-oxygen that reproduce ignition, flame, and detonation properties that are similar to those computed using more detailed models or measured in experiments. The model parameters in Table 3 were determined to accurately reproduce induction delay, a 1D laminar flame with correct thickness, laminar flame velocity, adiabatic flame temperature, a 1D detonation with correct thickness, D_{CJ}, and post-shock temperature in a stoichiometric ethylene-oxgen system. To estimate the detonation cell height, λ, for this model, a 2D detonation was computed on a finer mesh with 8.2 grid points per x_{d}. Cell height ranged from 0.08 to 0.12 mm, which is consistent with reported experimental results, which range from 0.1 mm to 2 mm [48].

The computational geometry and setup is shown in Fig. 10. Obstacles are uniformly spaced along the channel wall with a constant obstacle width and height through the channel. The channel is open on the right, with symmetry planes at the top and left boundaries. The bottom wall and all obstacle surfaces are no-slip adiabatic boundaries. To ignite the mixture, a circular region of hot, burned product at 3500 K and 1 atm is placed at the left wall.
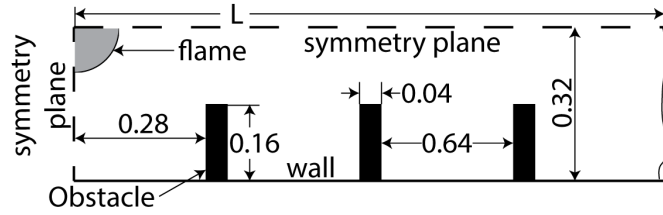
Fig. 10. Computational setup. Units of cm. Obstacles evenly spaced along channel length L. Radius of the initial burned region is 0.08 cm. Blockage ratio is 0.5 in this case.
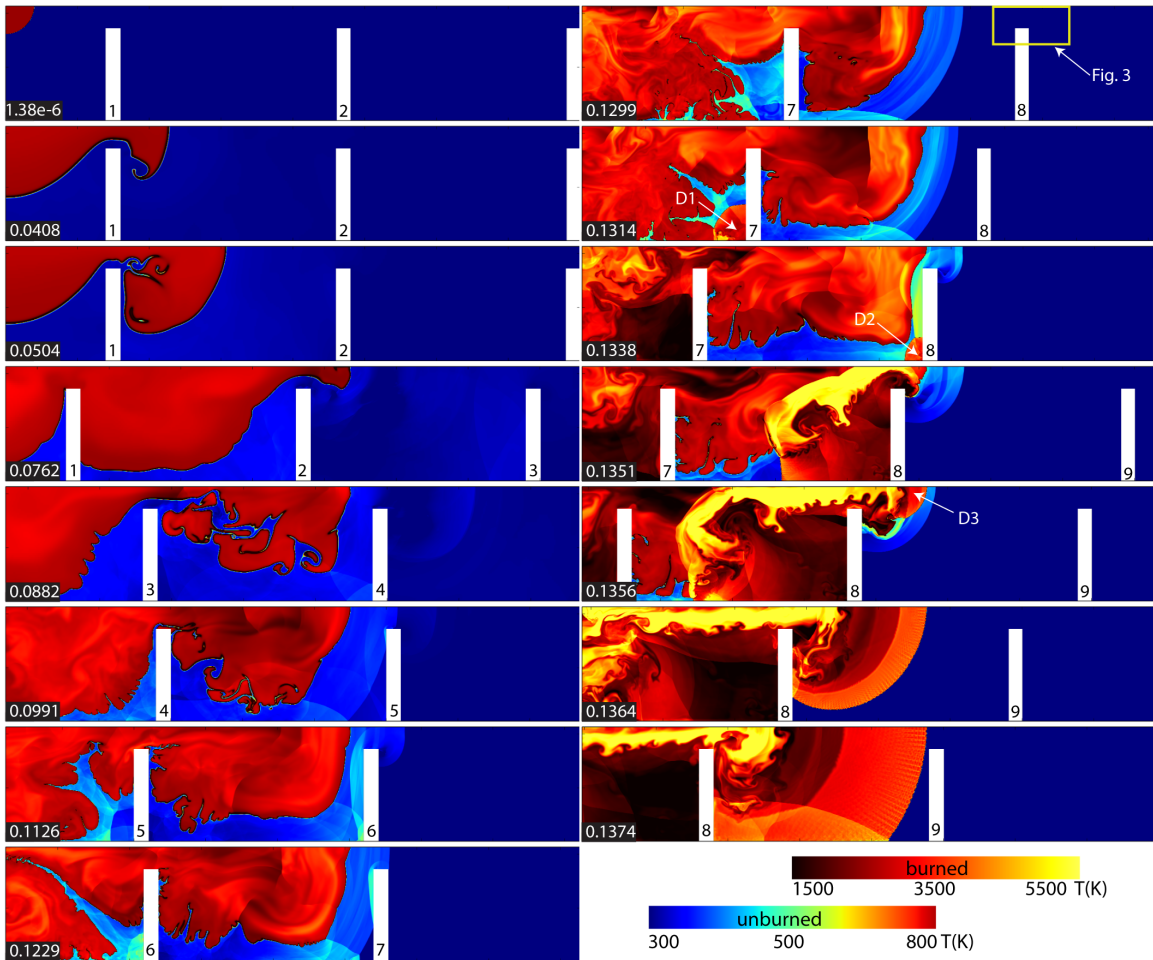
Fig. 11. Accelerating flame and detonation in 2D quarter-channel with $br = 0.8$. Time in milliseconds is shown in the frame corners. Obstacles are numbered. Frame width is 1.6 cm.

3.4 Flame Acceleration and DDT

3.4.1 High Blockage Ratio

In channels with high obstacles, such as the $br = 0.8$ case shown in Fig. 11, the flame accelerates rapidly as it expands over the obstacles and its surface area in-

creases. The flame becomes increasingly turbulent due to fluid instabilities (Rayleigh-Taylor, Richtmyer-Meshkov, and Kelvin-Helmholtz). A strong shock forms immediately ahead of the flame, seen starting at 0.0991 ms in Fig. 11. The leading shock diffracts over obstacles, reflecting from the channel floor and forming a Mach stem behind it (0.1229 ms). As the leading shock traverses the obstacles, the strength of the Mach stem increases. The first detonation, D1, occurs in the corner in front of obstacle 7 when shocks collide and focus energy in a localized region of unburned gas (0.1314 ms). D1 does not survive because there is insufficient reactant available for it to traverse obstacle 7. A second detonation, D2, occurs when the leading Mach stem reflects from obstacle 8 (0.1338 ms). Again, there is not enough reactant available between the top of obstacle 8 and the flame for D2 to survive. The shock created by D2, however, propagates through the back of the flame into the unburned gas, causing it to detonate (D3 at 0.1356 ms). The detonation D3 survives and propagates down the channel length. Figure 12 shows the shock produced by D2 passing through the reaction front and causing the transition to detonation at 0.1353 ms.

Flame acceleration and DDT in channels with $br = 0.5$ has been studied extensively for mixtures of hydrogen and air [18, 39, 40]. Figure 13 shows that the flame development is similar to that for $br = 0.8$. The flame accelerates due to expansion, fluid instabilities, shocks, and all of their interactions. Figure 14 shows that detonation occurs in preheated, unburned gas as a Mach stem reflects from an obstacle and leaves a hot spot in a gradient of reactivity. Pressure and temperature increase behind the Mach reflection, igniting two hot spots at 0.1356 ms. The hot spots become detonations through the gradient mechanism. Detonation occurs 3.5 cm from the left edge after the flame has passed six obstacles.
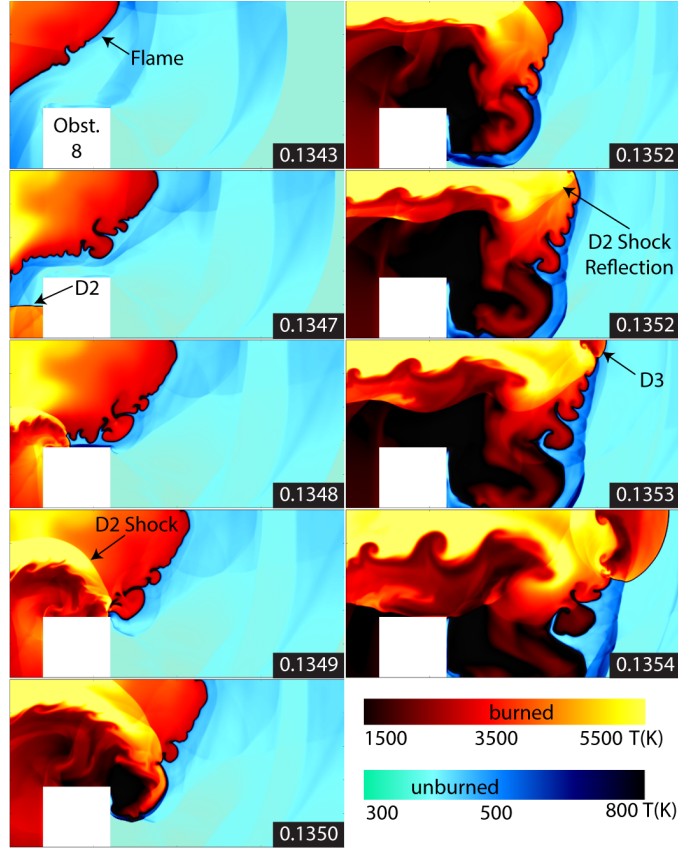
Fig. 12. Detonation with $br = 0.8$. Time in milliseconds is shown in the frame corners. Obstacle 8, detonation D2, the shock formed by D2, and D3 are labeled. Domain is x = [4.1,4.3] cm and y =[0.22,0.32] cm.

3.4.2 Intermediate Blockage Ratio

When $br = 0.1$, detonation occurs at 7.25 cm against the lower wall at 0.271 ms, after the flame has passed 11 obstacles. Unburned gas is pushed downstream over obstacles causing vortex shedding from the obstacle's leading edges (seen starting at 0.1804 ms in Fig. 15). Vortices coalesce behind obstacles to form recirculation regions. The flame surface increases as it is pulled into the recirculation region, and the flame becomes turbulent as the pressure waves created by the compressible vortices propagate through the flame. Shocks form as the flame accelerates, and these shocks increase in strength as they reflect off the obstacles and the channel boundaries. Fluid instability in the unburned region behind the leading shock increases as the
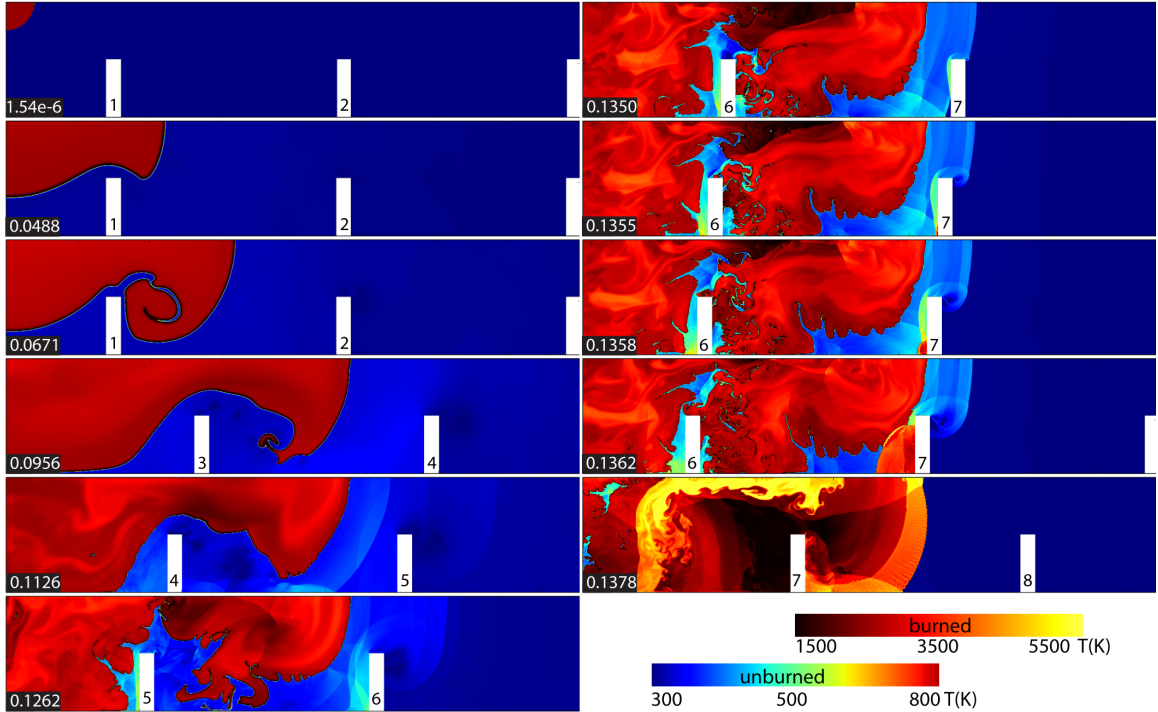
Fig. 13. Accelerating flame and detonation in 2D quarter-channel with $br = 0.5$. Time in milliseconds is shown in the frame corners. Obstacles are numbered. Frame width is 1.6 cm.
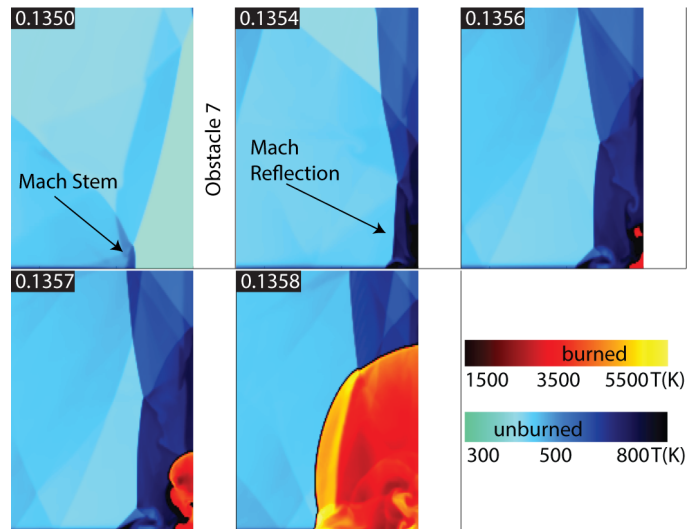
Fig. 14. Detonation with $br = 0.5$. Time in milliseconds is shown in the frame corners. Obstacle 7 shown on right side. Domain is x = [3.4,3.5] cm and y =[0,0.1] cm.

shocks collide and interact with boundary layers and vortices.

Figure 16 is an enlargement of the detonation that occurs in Fig. 15 for $br = 0.1$. Two shocks, labeled S1 and S2 at 0.2689 ms, collide at 0.2696 ms. Shock S1 is
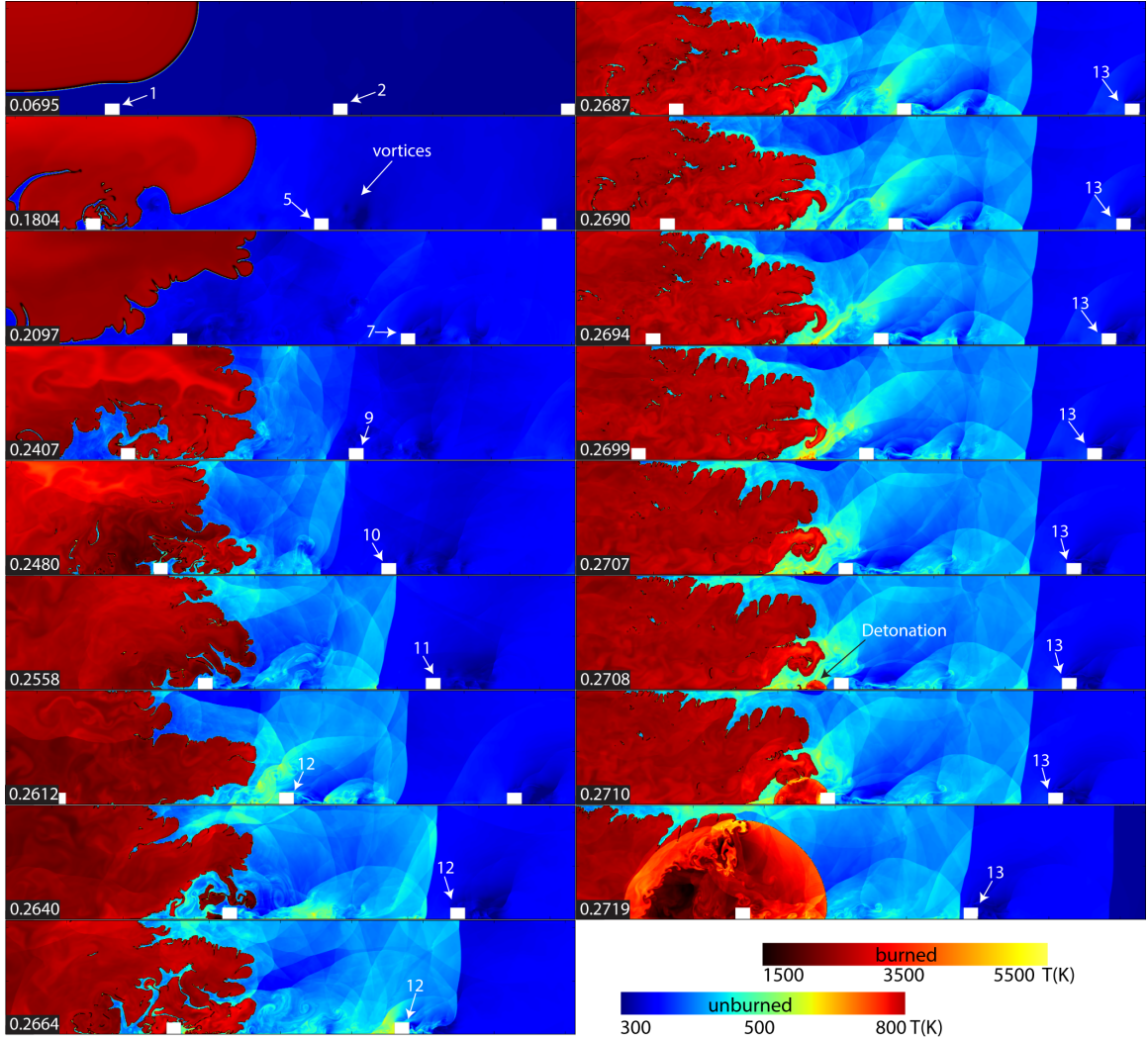
Fig. 15. Full simulation for blockage ratio of 0.10. Time in milliseconds is shown in the frame corners. Obstacles are numbered. Frame width is 1.6 cm.

immediately ahead of the flame, traveling to the right, and shock S2 is reflected from the downstream obstacle (shown in white in the lower right corner of each frame in Fig. 16) and travels to the left. A shock collision ignites two hot spots in the boundary layer, labeled H1 and H2. By 0.2707 ms, H1 evolves into a flame and shock, and H2 becomes a detonation. The analysis in Section 3.5.2 shows that the confluence of shocks causes transition to detonation in hot unburned gas in this intermdediate br regime through a detonation mechanism that has elements of both gradient ignition and direct initiation of detonation. This is also discussed in [28].
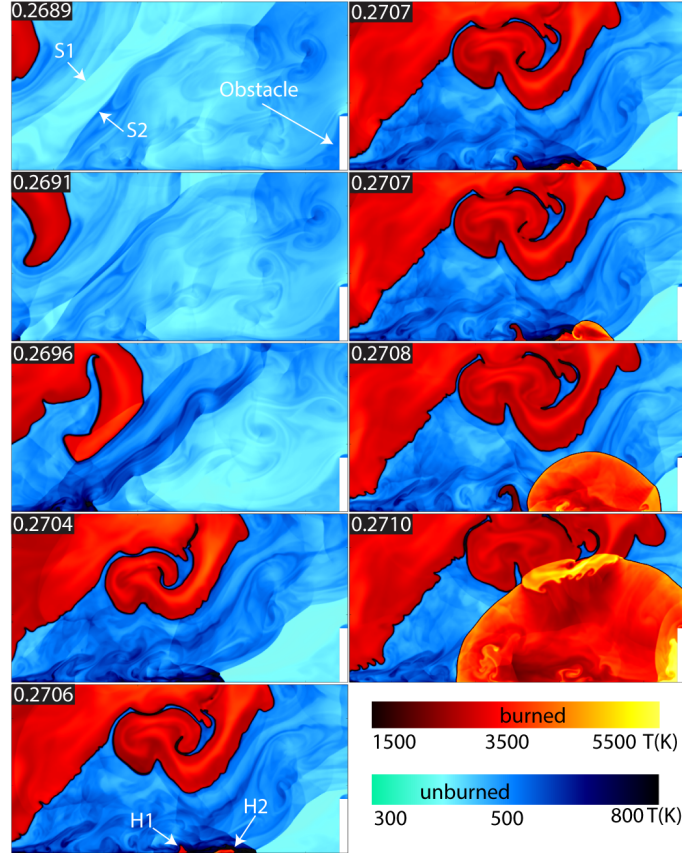
Fig. 16. Multiple shock collision and detonation for $br = 0.1$. Time in milliseconds is shown in the frame corners. Domain is x = [7.125,7.325] cm and y =[0,0.1] cm.

3.4.3 Low Blockage Ratio

In the low br regime, the flame accelerates very slowly. A relatively large, unburned, turbulent region filled with reflecting shocks and strong vortices forms between the flame and the leading shock. Figure 17 shows the complexity and dynamic structure in this shock-flame complex prior to DDT. Detonation, shown in Fig. 18, occurs at 0.5562 ms at 16.8 cm, after the flame passed 27 obstacles. A shock ahead of the flame, labeled S3, reflects against obstacle 28 and collides with shock S4, increasing the pressure and temperature of the gas subjected to the double shock collision. S4 then forms a Mach stem against the channel wall. A hot spot and subsequent detonation form when the Mach stem collides with obstacle 28.
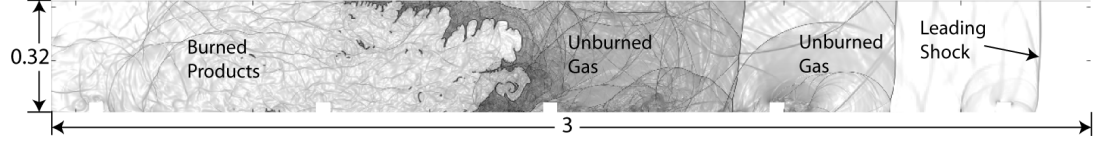
Fig. 17. Numerical schlieren, $|\nabla \rho|$, showing the turbulent region for $br = 0.05$. Dimensions are in cm.
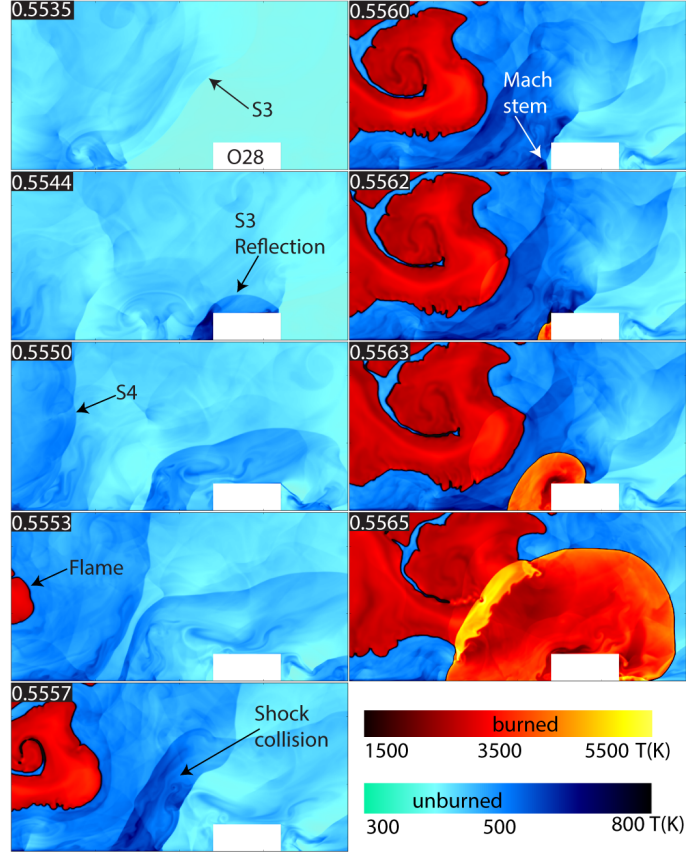
Fig. 18. Detonation with $br = 0.05$. Time in milliseconds is shown in the frame corners. Obstacle 28 is labeled. Domain is x = [16.8,17.0] cm and y =[0,0.1] cm.

3.4.4 Comparison of DDT in Two and Three Dimensions

Another set of simulations with a channel height of 0.16 cm and $br = 0.1$ was performed to compare 2D and 3D flame acceleration and DDT. The channel height was decreased from 0.32 cm to 0.16 cm to reduce computational expense in the 3D calculation. Figure 19 shows the computational setup, now for which $dx_{\min} = 6.67$ μm and $dx_{\max} = 53.33$ μm. Despite the difference in the two channel heights, the DDT mechanism is the same. The detonation in the 2D simulation with a reduced channel

height is shown in Fig. 20. Detonation occurs after the flame has passed 13 obstacles at 0.1472 ms, 4.11 cm into the channel. The accelerating flame creates pressures waves that coalesce into a shock and the shock reflects from the channel wall. The shock reflection passes through the turbulent flame front, causing the flame front to transition to a detonation, as it does in the case with $br = 0.8$ (see D3 in Fig. 12).
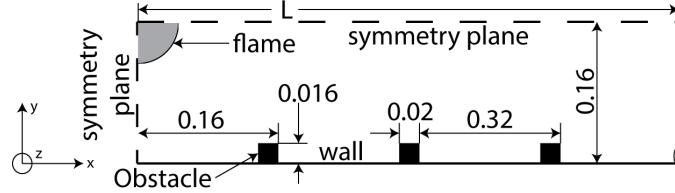
Fig. 19. Computational setup for 3D calculation in units of cm. Obstacles evenly spaced along channel length L. Radius of the initial burned region is 0.04 cm.
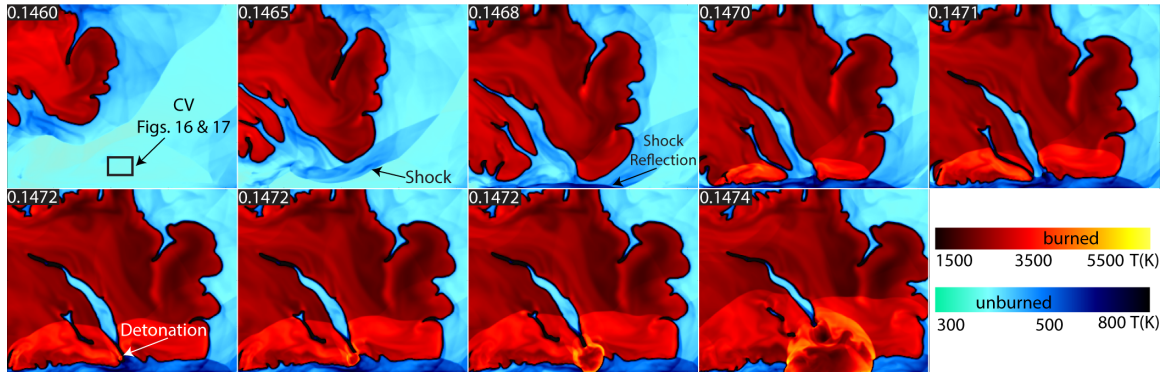
Fig. 20. Detonation with $br = 0.1$ and a channel height of 0.16 cm. Time in milliseconds is shown in the frame corners. Domain is x = [4.01,4.21] cm and y =[0,0.16] cm.

In the 3D case, the channel width is 0.16 cm with periodic boundary conditions in the z direction, with coordinate axes shown in Fig. 19. The turbulent flame acceleration and transition to detonation is shown in Fig. 21. The evolution of the flame and eventual DDT is similar to what is observed in a 2D channel with intermediate br. The initially laminar flame accelerates as it traverses the obstacles. A turbulent flame structure forms near the bottom wall after the flame has passed three obstacles, shown at 0.071 ms. After passing six obstacles, the entire flame front has become tur-

bulent. At 0.102 ms, the unburned mixture detonates near the bottom wall, 3.05 cm down the length of the channel, due to the same mechanism of energy deposition we see in the 2D simulations for intermediate br. The detonation begins near the center of the channel width and propagates down the length of the channel (x direction), forming cell structure as shown at 0.113 ms. The multidimensional turbulence in the 3D case leads to a faster rate of flame acceleration and earlier detonation than in the 2D case. Figure 22 shows the location of the tip of the reaction front as a function of time for the 2D and 3D cases.

3.5   Discussion

3.5.1   Effect of Blockage Ratio

A comparison of the simulations with high and low br shows that obstacle size plays a major role in flame acceleration, turbulence in the flame and unburned gas, shock formation, time or distance to detonation, and thus in the detonation mechanism. Figure 23 shows the position of the tip of the reaction front as a function of time for all blockage ratios studied. In the regime of high br, the time to detonation increases from 0.136 ms for $br = 0.8$ to 0.161 ms for $br = 0.35$. In the low br regime, it takes considerably longer for DDT to occur, here at 0.556 ms for $br = 0.05$. Figure 24 shows the number of obstacles traversed by the tip of the reaction front prior to DDT for each br. Higher obstacles cause the flow to become turbulent faster, as the higher obstacles perturb the flame more than smaller obstacles. A reverse relationship holds for the $br = 0.8$ case, where the reaction front traverses 7 obstacles before DDT, as opposed to the 6 obstacles before DDT in the $br = 0.5$ and 0.35 cases. The reaction front passes more obstacles before DDT when the $br = 0.8$ because the obstacles in this case are high enough to choke the initial laminar expansion of the flame, resulting in slower initial acceleration than in the $br = 0.5$ and 0.35 cases. In the $br = 0.05$ case, the obstacles take much longer to perturb the flame and create shocks of sufficient
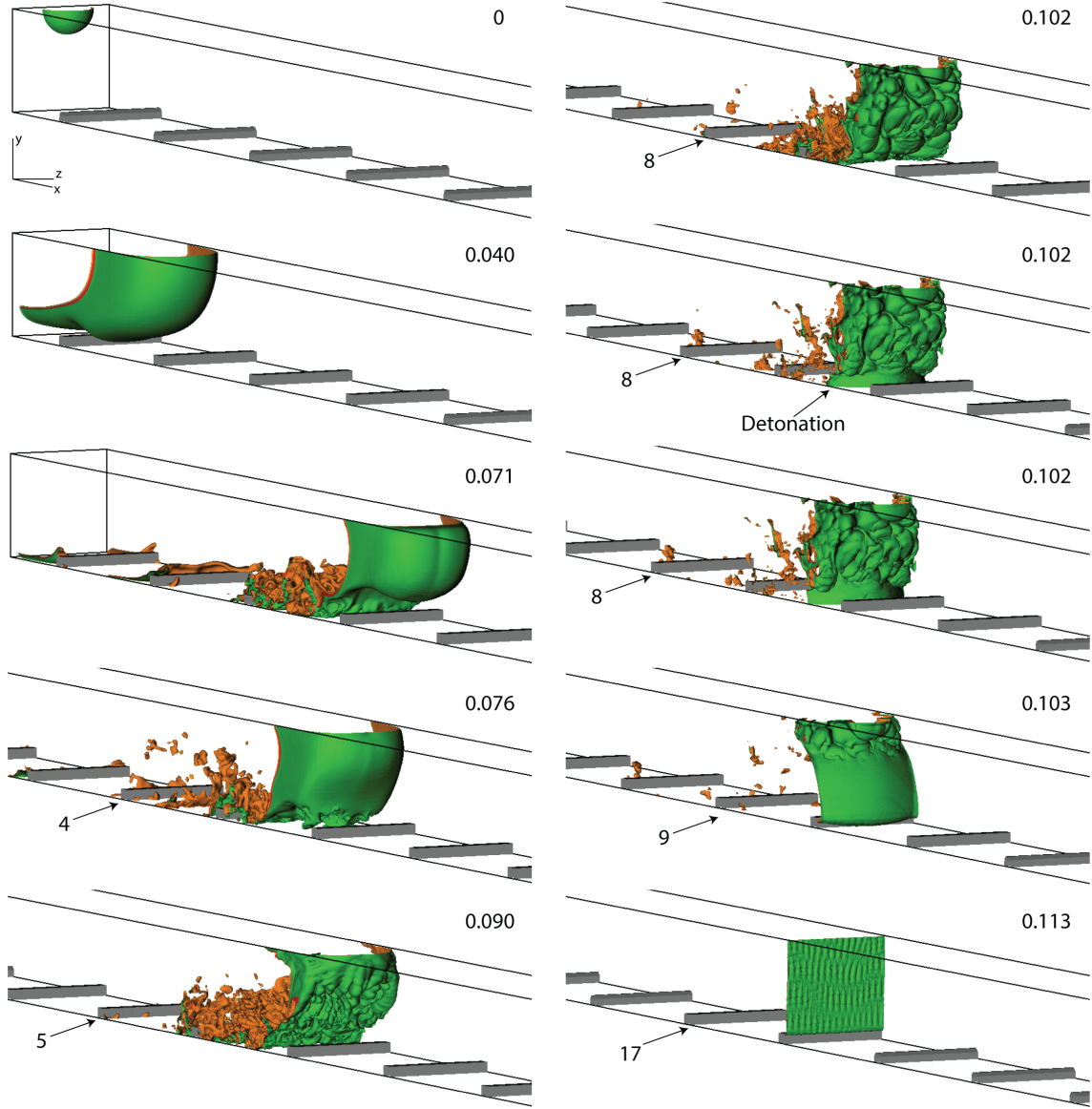
Fig. 21. Isosurfaces of reactant mass fractions, Y, of 0.2, 0.5, and 0.8 show flame acceleration and detonation in 3D channel with $br = 0.1$. Time in milliseconds is shown in the frame corners. Obstacles are numbered.

strength to detonate the unburned gas. When $br = 0.05$, the reaction front traverses 28 obstacles prior to detonation.

When br is in the intermediate range ($br = 0.1$ in Fig. 15), the flame accelerates more slowly and stays laminar further into the channel than it does for higher obstacles (such as $br = 0.5$, in Fig. 13). Higher values of br result in a more predictable flow

41
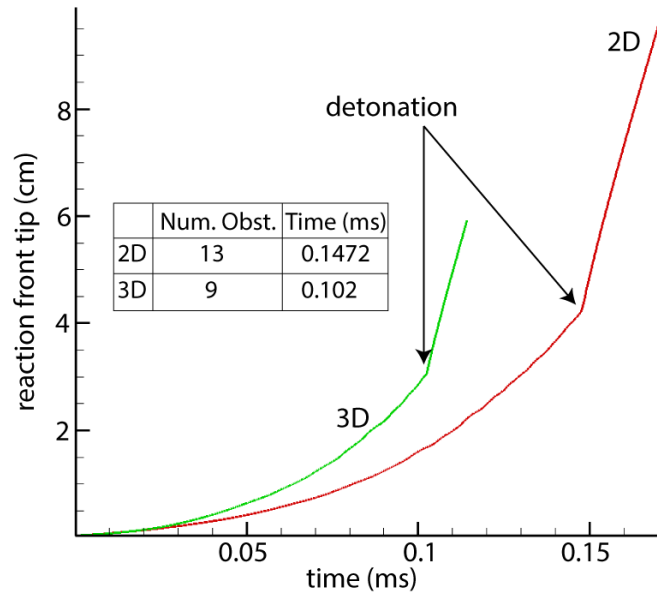
Fig. 22. Reaction front tip position vs. time for 2D and 3D simulations with a channel height of 0.16 cm and $br = 0.1$. The time and number of obstacles to detonation is shown.

	Num. Obst.	Time (ms)
2D	13	0.1472
3D	9	0.102
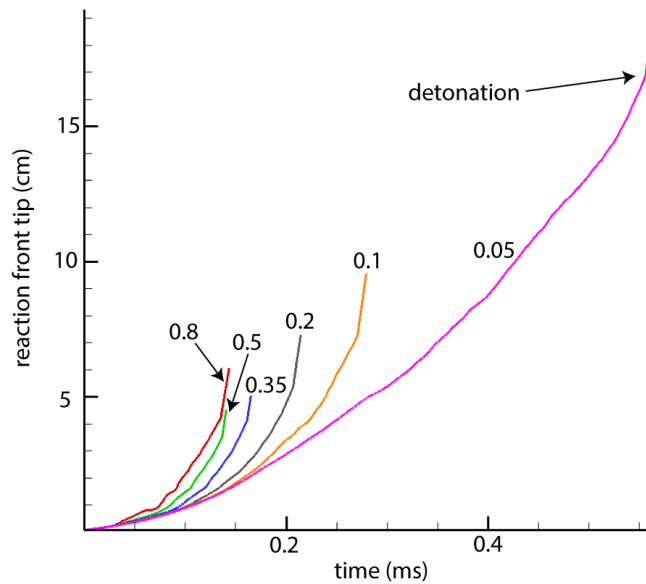
Fig. 23. Reaction front tip as a function of time for all blockage ratios in this series of simulations. Detonation occurs at the inflection point, as shown for $br = 0.05$.

as strong leading shocks form very close to the flame. These obstacles consistently produce Mach-stems and detonations that form behind Mach-stem reflections. For this stoichiometric ethylene-oxygen mixture, the flame never falls more than ~ 0.2
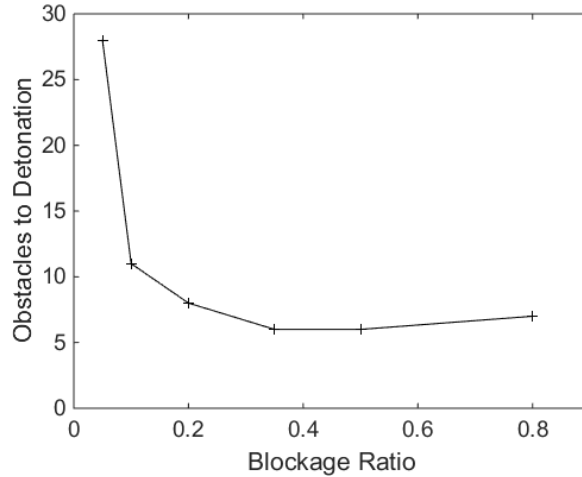
Fig. 24. Number of obstacles to detonation as a function of blockage ratio

cm behind the leading shock for $br = 0.5$. When br decreases to 0.1, the leading shocks form as far as 1.5 cm ahead of the flame tip, creating a large, unburned turbulent region ahead of the flame. Rather than a detonation always occurring in a Mach reflection against an obstacle, it may occur anywhere that energy is focused sufficiently to initiate the detonation. The actual detonation location is stochastic because the turbulent region is filled with shock collisions and reflections that may focus sufficient energy to detonate the unburned gas anywhere within the unburned, turbulent region ahead of the flame.

The case with $br = 0.8$ is particularly interesting because both DDT mechanisms arise. As shown in Fig. 11, detonation D2 occurs in a gradient of reactivity behind a Mach-stem reflection. Due to the height of the obstacles, there is insufficient reactant available between the burned gas and the obstacle for the D2 detonation front to traverse the obstacle and propagate through the channel. When the shock produced by D2 passes through the burned gas and the reaction front, it causes DDT through the SWACER mechanism. The shock couples with the flame and injects sufficient energy into the chemically reacting gas to cause the flame to transition to detonation D3. This process of shocks causing a flame front to transition to detonation is also

seen in the 2D, 0.16 cm channel height case, as shown in Fig. 20.

3.5.2   Shock Focusing and Rapid Energy Deposition

A control volume analysis was performed on a small, 33.3 μm x 33.3 μm region (marked in the first frame of Fig. 20) where the detonation emerges from the flame front at 0.1472 ms. The analysis tracked the change in pressure, temperature, density, and energy-release rate over a 0.45 μs period from 146.9 μs to 147.35 μs. This covers the time before the region is compressed by the shock reflection to a time after the detonation formed and propagated through the region. Figure 25 shows the trends of the state variables during this time period. Shock compression begins at 146.9 μs, and the material begins to react chemically at 147.15 μs. As the material is compressed by the shock reflection, the pressure and density increase dramatically. There is another spike when the mixture detonates. As the detonation propagates out of the region, the pressure and density decrease.
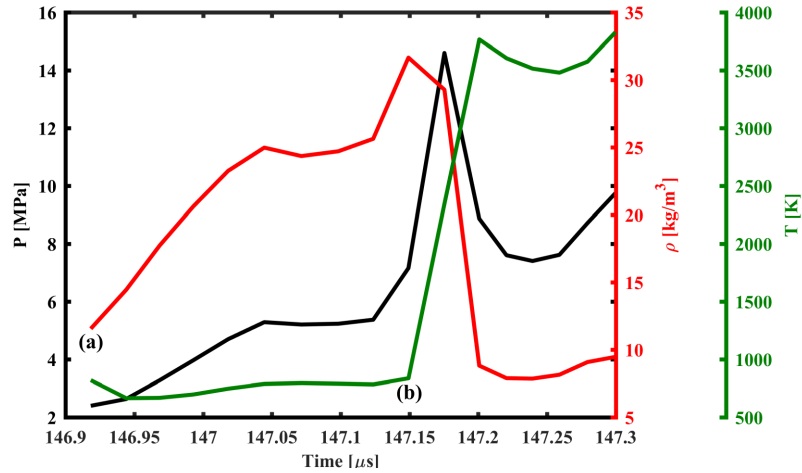
Fig. 25. State variables in the control volume from 146.9 μs to 147.35 μs. Shock compression begins at (a). Detonation occurs at (b). The gas begins to react chemically at 147.15 μs.

Figure 26 shows the rate of energy deposition into the control volume. Chemical energy release is defined as heat release per kg of reactant, q, and sensible internal
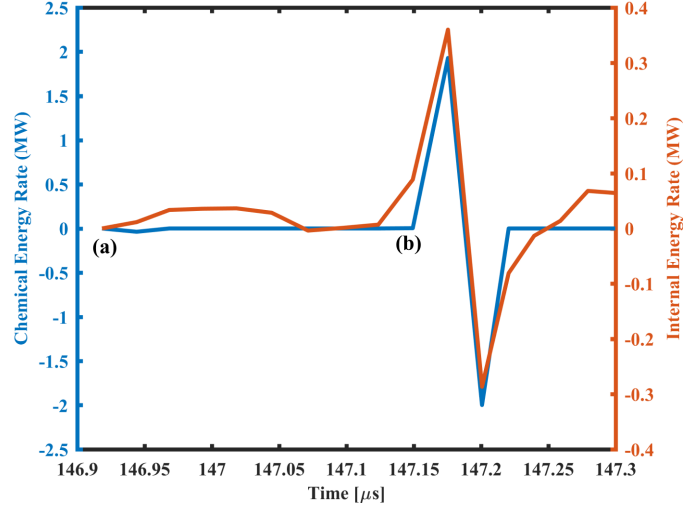
Fig. 26. Rate of energy deposition in control volume. Shock compression begins at (a). Detonation occurs at (b).

energy is $P/(\gamma-1)$. As the material in the region is compressed, the density, pressure, and internal energy increase. There is a second peak as the material detonates and chemical energy is released. The flow behind the detonation wave carries energy out of the region as the detonation propagates into the surrounding gas, resulting in the negative energy rates seen after 147.17 μs. The total energy content in the region, defined as the sum of chemical, internal, and kinetic energies, increases by a factor of 16 during shock compression. A similar analysis was performed in earlier work [28] for the case shown in Fig. 15 with $br = 0.1$ and a channel height of 0.32 cm. The analysis tracked the rate of energy deposition into a region of unburned gas subjected to multiple shock collisions resulting in a detonation, as shown in Fig. 16. The trends shown here in Figs. 25 and 26 are consistent with the earlier analysis. The shock compression causes a rapid increase in pressure, temperature, and density. The result is an increase in the rate of energy deposition, followed by direct initiation of a detonation in the unburned gas.

3.5.3 Stochastic Analysis

Prior work [18] has shown that for hydrogen and air mixtures in channels of different sizes, there were different regimes of DDT. The authors found that in some of these regimes, the detonation mechanism was more sensitive to the turbulence in the flow. The variations in br described in this paper reflect the same phenomenon, that is, that there are different regimes of DDT with varying sensitivity of the detonation mechanism to turbulence. In the $br = 0.1$ intermediate regime, the sensitivity of the solution to turbulence causes the detonation to occur at slightly different times and locations for cases with modified initial conditions. Following [18], we have now shown that simulations for cases in which the initial background temperature is varied within 298±0.01 K, the location and time of detonation change slightly, but the mechanism remains the same. Figure 27 shows the reaction-front tip position as a function of time for simulations with $br = 0.1$ and for slightly varied initial background temperature. The time to detonation differs within a range of 0.05 ms and the distance to detonation varies within a 2.4 cm range.
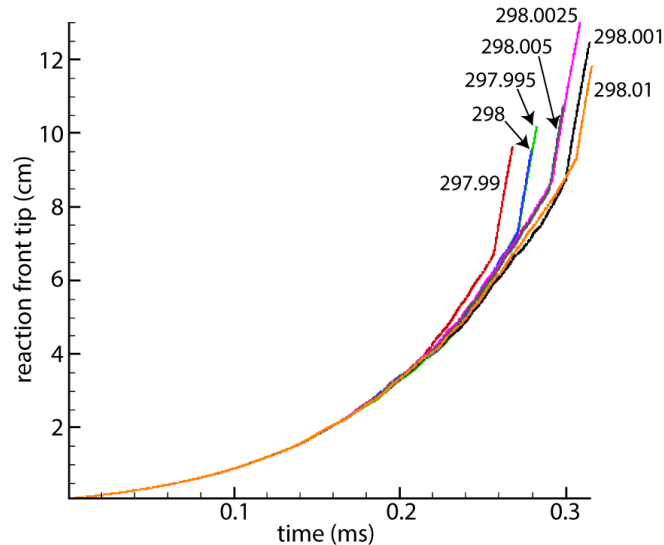
Fig. 27. Position of the reaction-front tip as a function of time for $br = 0.1$ for background temperatures (labeled in K) in the range 298±0.01 K. Range in time and distance to detonation are 0.05 ms and 2.4 cm, respectively.

Stochasticity in cases with $br = 0.1$ can also be seen when the grid size is varied. Figure 28 shows the detonation in another simulation with $br = 0.1$ with the same minimum grid size as in the original $br = 0.1$ case shown in Fig. 15, but with a finer coarse grid (26.7 μm instead of 53.3 μm). The location of the detonation is ~1.2 cm further along the channel boundary than the detonation that occurred in the original $br = 0.1$ case (shown in Fig. 16). Nevertheless, a detonation again appears where shock collisions and reflections are focused. The shock immediately ahead of the flame, labeled S5, reflects off the channel boundary and ignites a hot spot H3 in the boundary layer. The hot spot becomes a detonation while another shock ahead of the flame, labeled S6, reflects off the obstacle shown in the lower right corner of the figure. The reflection of S6 ignites another hot spot, labeled H4, that also becomes a detonation. The two detonations combine and propagate down the channel. Turbulence, an essentially stochastic process, dominates this region of fluid instabilities, shock collisions, and shock-boundary layer interactions.
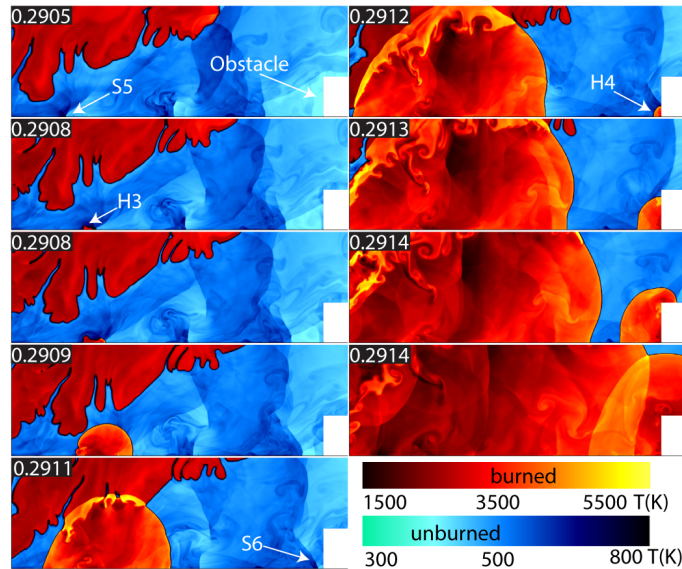
Fig. 28. Shock reflections and collisions result in initiation of two detonations. Time in milliseconds is shown in the frame corners. Domain is x = [8.35,8.65] cm and y =[0,0.2] cm.

3.6 Summary and Conclusions

The effect of the blockage ratio (br) on the mechanism of DDT was studied by analyzing a series of multidimensional, unsteady numerical simulations of an initially homogeneous mixture of ethylene and oxygen in partially blocked channels. This paper compared several cases taken from a series of simulations with $br = 0.05 - 0.8$, including a three-dimensional (3D) calculation.

For $br = 0.35 - 0.5$, detonation occurs due to the creation of a hot spot in a gradient of reactivity that forms behind a Mach reflection [18, 39, 40]. This was shown for different fuels than were used in prior work. In the case with $br = 0.05 - 0.2$, shock collisions increase the temperature, pressure, and density of the unburned material. These effects and interactions occur frequently due to the complexity of the shock structures and interactions in the unburned turbulent region between the flame and the leading shock. As the flame propagates down the channel, the strength of the shock collisions and reflections increases in this region. Multiple shocks collide and reflect against the channel boundary, focusing energy in a localized volume of unburned material and detonating the mixture. These results are consistent with direct initiation theory [10] and with detonations seen in experiments using similar blockage ratios ($br < 0.3$) [49]. Sufficient energy is deposited into a localized region on a timescale that is small relative to the acoustic timescale of the gas, thus initiating a detonation. DDT by rapid energy deposition into a localized region at a very small timescale was also seen in a 3D calculation with $br = 0.1$, validating two-dimensional (2D) results. Increased turbulence in the 3D calculation led to a faster flame acceleration and earlier DDT than in the comparable 2D case, although the detonation mechanism remained the same.

The case of high blockage ratio, $br = 0.8$, showed both mechanisms. A hot spot ignited in a gradient of reactivity formed behind a Mach reflection, but the detonation failed due to insufficient reactant for the detonation front to traverse the upstream

obstacles. The shock created by the second detonation propagated through the burned products, through the reaction front, and into the unburned gas. As the shock passed through the reaction front, the flame transitioned to detonation. The detonation mechanism here was shock focusing, as the reaction front was compressed by the shock and enough energy was deposited for transition to detonation. This same phenomenon is seen in the 2D, 0.16 cm channel height simulation with $br = 0.1$.

An additional series of simulations, with $br = 0.1$, investigated the sensitivity of the solution to initial conditions. Modifying the initial background temperature, within the range of 298±0.01 K resulted in a difference in detonation time and location, but the detonation mechanism was the same. This phenomenon was also seen in previous work with a different fuel mixture [18], where it was determined that some regimes of DDT are especially sensitive to turbulence in the flow.

3.7 Acknowledgments

3.8 Supplemental Material

3.8.1 Resolution & Stochasticity Considerations

The following work was not included in this chapter as originally published in [51], but is included here for additional discussion on the stochasticity of DDT. In addition to varying the initial background temperature of the unburned gas to examine the effect on time and distance to DDT, as discussed in Sec. 3.5.3, the grid resolution was varied for the $br = 0.1$ case to determine whether or not the solutions are grid independent. Five grid resolutions, including the original resolution used for the 2D calculation shown in Fig. 15, were used in the study.
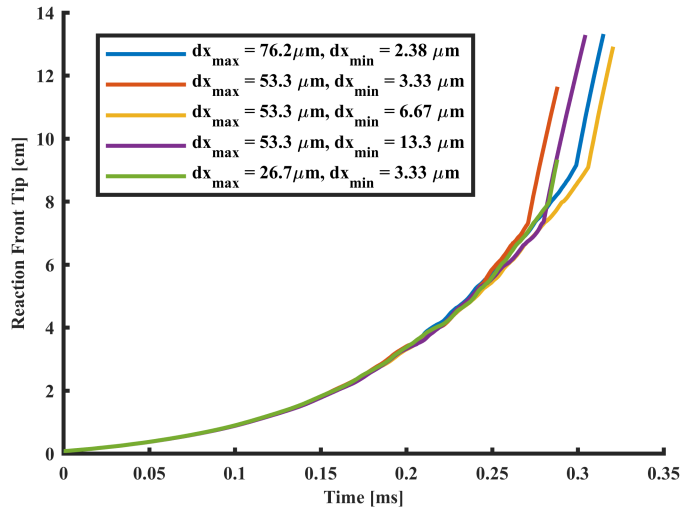
Fig. 29. Reaction front tip position as a function of time for the $br = 0.1$ case using five different grid resolutions.

Figure 29 shows reaction front tip position as a function of time for the five cases. The solution is initially grid independent during the laminar expansion phase of the flame's development (up to ~0.15 ms). Once the flame becomes turbulent through interaction with shocks, vorticity, and fluid instabilities, the solutions begin to diverge and the time and distance to detonation varies by 0.04 ms and 1 cm, respectively. The solutions do not begin to show better agreement as resolution increases, at least for the resolutions studied. Computational expense prohibited the testing of grids finer

than those considered here. Interestingly, the solution with the coarsest resolution for the fine mesh ($dx_{\min} = 13.3$ μm) agrees best with the solution with a significantly more refined mesh ($dx_{\min} = 3.33$ μm and $dx_{\max} = 26.7$ μm). This result is also apparent in Fig. 30, which shows reaction front speed as a function of time for the same five cases. The solutions show similar flame speed during the laminar portion of the flame's acceleration and begin to diverge as soon as the flow becomes turbulent due to the stochastic nature of turbulence in this system, as discussed in Sec. 3.5.3. For the five cases considered, there is no discernible causality between the time and distance to detonation and grid resolution.
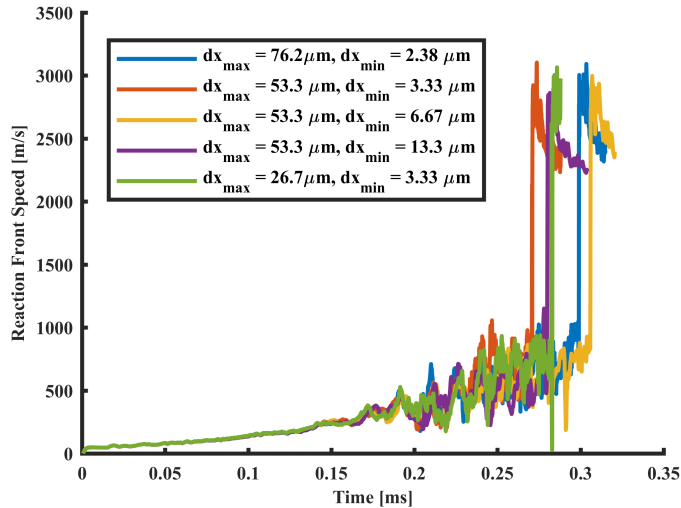
Fig. 30. Reaction front speed as a function of time for the $br = 0.1$ case using five different grid resolutions.

Inevitably, if computational resources were irrelevant and grid resolution were to be increased further and further, the solution would eventually converge and be grid independent. This is impractical from a computational perspective, but also unnecessary for the current study since the physics of interest are insensitive to initial conditions and grid resolution. Despite the variability in when and where detonation will occur, the same flame evolution process and DDT mechanism is observed in all cases. As such, the solutions can be considered qualitatively converged. If grid-independent, quantitative results are desired, such as where precisely a detonation will occur in a

51

given system, greater computational resources than those currently available will be required. However, as shown in Sec. 3.5.3, changes to the initial gas temperature that are small enough that they might be considered numerical error have the same effect on the time and distance to detonation as changes in grid resolution. This inherent stochasticity in turbulent flame development and DDT makes achieving truly, quantitatively converged solutions extremely challenging. Experiments are subject to the same challenges, as discussed in [18], where for the same experimental facility and conditions, the DDT location is observed to be variable due to minute differences in wall or gas temperature between runs, imperfections in the channel walls, etc., that are beyond the experimentalist's capabilities to control. Despite the inherent variability in quantitative results, resolution studies such as the one described here provide confidence in the qualitative convergence of the physics of interest.

3.8.2   Domain Geometry

A concern with simulation of detonation and DDT in thin channels is that the size of the computational domain may constrain or influence the solution if it is small relative to the chemical length scale of the fuel-oxidizer mixture. Since the channel considered in this work is only 0.32 cm in height, small relative to full-size detonation engines, some additional discussion on this subject is useful. There will inherently be interactions between the geometry and the flow that affect the solution, as has been shown here with varying blockage ratios. Regardless, it must be ensured that the domain size is sufficient to resolve all of the chemical scales of interest and is not limiting the detonation formation or propagation. A chemical length scale metric that can be used as a gauge for determining required domain size is the detonation cell height, λ, which is primarily a function of the chemical composition of the fuel-oxidizer mixture [52]. A detailed discussion of detonation cell structure can be found in previous work [53].
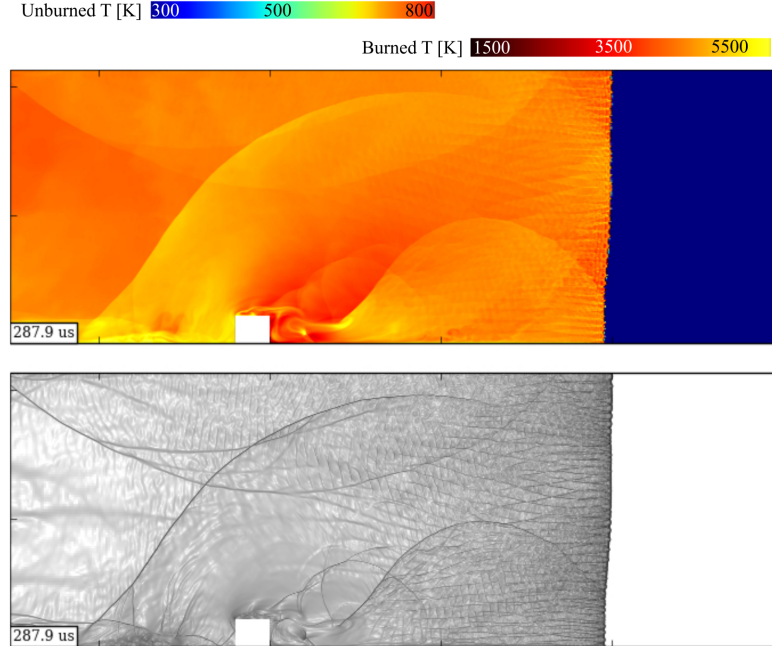
Fig. 31. Temperature and numerical schlieren contours showing a detonation wave propagating from left to right in the $br = 0.1$ simulation at 0.288 ms. Domain is x = [10.9,12.3] cm and y =[0,0.32] cm.

Detonation cell height is a preferred metric for sizing a computational domain in DDT simulations because the formation of detonation cells indicates that a detonation wave has reached a relatively steady-state solution. If many detonation cells are visible in the domain, it indicates that the domain is sufficiently sized and the grid is sufficiently resolved to accurately compute a detonation. Figure 31 shows a detonation wave propagating through the channel for $br = 0.1$ (same simulation as shown in Fig. 15). There are approximately 50 detonation cells spanning the channel height. This demonstrates that a 0.32 cm channel height is more than sufficient for resolving the chemical length scales required to accurately simulate DDT for a stoichiometric ethylene-oxygen mixture and the detonation's propagation is unhindered by the channel geometry. As discussed in Sec. 3.3, calculated cell heights of 0.1 mm were consistent with reported experimental results.

4   Flame Instability and Transition to Detonation in Supersonic Reactive Flows

Gabriel B. Goodwin, Elaine S. Oran

The problem examined in this paper uses the same channel height and fuel-oxidizer mixture as in Chaps. 2 and 3, but rather than igniting an initially laminar flame in a static flow, the mixture flows through an unobstructed channel at supersonic speeds. The purpose of this paper is to answer the following questions:

- Will the fuel-oxidizer mixture autoignite when flowing through a channel without obstacles at supersonic velocities? If so, does the flame remain stable or does it become turbulent?

- Will detonations occur and, if so, by what mechanism?

Two simulations are discussed, one in which the mixture fails to ignite and another in which the mixture ignites in the boundary layer. Flame evolution, instability, and detonations mechanism for this system are investigated in order to expand fundamental understanding of the behavior of supersonic premixed flames.

Abstract

Multidimensional numerical simulations of a homogeneous, chemically reactive gas were used to study ignition, flame stability, and deflagration-to-detonation transition (DDT) in a supersonic combustor. The configuration studied was a rectangular channel with a supersonic inflow of stoichiometric ethylene-oxygen and a transimissive outflow boundary. The calculation is initialized with a velocity in the computational domain equal to that of the inflow, which is held constant for the duration of the calculation. The compressible reactive Navier-Stokes equations were solved by

a high-order numerical algorithm on an adapting mesh. This paper describes two calculations, one with a Mach 3 inflow and one with Mach 5.25. In the Mach 3 case, the fuel-oxidizer mixture does not ignite and the flow reaches a steady-state oblique shock train structure. In the Mach 5.25 case, ignition occurs in the boundary layers and the flame front becomes unstable due to a Rayleigh-Taylor instability at the interface between the burned and unburned gas. Growth of the reaction front and expansion of the burned gas compress and preheat the unburned gas. DDT occurs in several locations, initiating both at the flame front and in the unburned gas, due to an energy-focusing mechanism. The growth of the flame instability that leads to DDT is analyzed using the Atwood number parameter. At the time this thesis was written, this paper was under review for presentation at the 37th International Symposium on Combustion and for publication in the *Proceedings of the Combustion Institute.*
Keywords: Turbulent flame; Hypersonics; DDT; Numerical simulations

4.1   Introduction

A comprehensive understanding of combustion in high-speed flows is necessary for the development of reliable hypersonic vehicles. Airbreathing engines that operate at high supersonic and hypersonic flight speeds will enable the next generation of extended-range, rapid response missile systems and low-cost space access due to significant gains in efficiency over traditional rocket engines [54, 55]. Maintaining flame stability across a wide range of inflow conditions in the combustor of an airbreathing hypersonic vehicle is a challenge [1, 2] due to the small timescales for mixing, ignition, and complete combustion. The fundamental physics underlying ignition and combustion in high-speed flows is complex due to the shocks, boundary layers, turbulence, and chemical reactions present in these systems. Experimental and computational studies exploring the interaction of these phenomena will enable the design of higher-performance hypersonic engines.

Combustion of premixed fuels and the influence of high-speed turbulence on flame development has been studied computationally [5, 56, 57], finding that under certain regimes, premixed turbulent flames are inherently unstable [6]. Detonation waves may be used instead of a flame or deflagration as a propulsion mechanism in a hypersonic engine [58, 59]. Detonation engines have been studied computationally [60–62] and experimentally [12, 63, 64] to characterize performance and detonation wave stability under a range of conditions. Prior work has examined the mechanisms for the deflagration-to-detonation transition (DDT) [17, 28, 39], which is required for ignition of a detonation engine. Hypersonic combustor test facilities are used to study the stabilization of detonation waves in premixed flows [65].

The purpose of this work is to characterize the effect of high supersonic and hypersonic flow speeds on premixed flames and identify the conditions that lead to flame instability and eventual DDT. As a background to this paper, a series of simulations was performed to investigate the effect of varying inflow Mach number, M_∞, of premixed fuel-oxidizer into a constant-area combustor on ignition, flame growth, formation of fluid instabilities, and DDT. The detailed results of these simulations, for $M_\infty = 3$ to 10, will be presented in a subsequent paper. The focus of this paper is on two of these cases, $M_\infty = 3$ and 5.25. In the $M_\infty = 3$ case, the temperature of the fuel-oxidizer mixture does not reach the threshold for autoignition. No combustion occurs and the flow reaches a steady-state repeating oblique shock structure. In the $M_\infty = 5.25$ case, autoignition occurs in the boundary layer. The flame front becomes turbulent and unstable through shock interactions and growth of fluid instabilities. Eventually, DDT occurs as shocks focus energy at the flame front resulting in the transition to detonation.

4.2 Numerical and Physical Model

The numerical model solves the full set of Navier-Stokes equations for an unsteady, fully compressible, chemically reacting gas, as described in [17]. The reaction of a stoichiometric mixture of ethylene and oxygen is modeled using a simplified, calibrated chemical-diffusive model of the form $dY/dt \equiv \dot{w} = -A\rho Y \exp(-E_\mathrm{a}/RT)$ where ρ, T, Y, and $\dot{w}$ are the mass density, temperature, mass fraction of reactant, and reaction rate, respectively. A is the pre-exponential factor and E_a is the activation energy. Input parameters for a stoichiometric ethylene-oxygen mixture initially at 298 K and 1 atm, as detailed in [29], were used. A genetic algorithm optimization procedure [66] was used to identify the input parameters that most accurately reproduce the flame and detonation properties for the fuel-oxidizer mixture. This reaction model quantitatively reproduces flame acceleration, onset of turbulence, and DDT mechanisms seen in experiments [7, 40, 67] and has recently been used to study DDT [28, 29, 68] and layered detonations [69]. A Godunov algorithm, fifth-order accurate in space and third-order accurate in time [19], is used to solve the equations on a dynamically adapting grid [47]. The simulations described below used grids with minimum size $dx_\mathrm{min} = 3.3\ \mu\mathrm{m}$ and coarsest size $dx_\mathrm{max} = 53.3\ \mu\mathrm{m}$. This choice of grids was tested and shown to resolve the shocks, boundary layers, flames, and other important flow and chemical structures.

The geometrical setup is shown in Fig. 32. A supersonic inflow condition is applied at the left boundary. For both $M_\infty = 3$ and 5.25, inflow temperature, pressure, and mass fraction of reactant are the same (298 K, 1 atm, 1, respectively) and are constant for the duration of the calculation. The calculation is initiated with velocity everywhere in the domain equal to the velocity at the inflow. The right boundary of the domain is a transmissive, non-reflecting outflow. The top and bottom walls are no-slip adiabatic boundaries. The channel height is 0.32 cm and the length is 3.2 cm. A height of 0.32 cm was determined to be sufficient for capturing the flame and

detonation physics of interest. The small scale flame and detonation properties of this fuel-oxidizer mixture, such as fast reactions and energy release, make ethylene-oxygen an ideal fuel-oxidizer mixture for studying ignition and flame development in high-speed premixed reactive flows.

4.3   Flame Growth and Transition to Detonation

The steady-state flowfield for the $M_\infty = 3$ case is shown in Fig. 32. The time required to reach steady-state is 50 μs. Boundary layers form quickly at the top and bottom walls. The inflow is deflected by the boundary layers, forming oblique shocks that reflect from the wall at a constant angle, a function of M_∞, repeating to the end of the domain. Following the first reflection, the shocks are trailed by expansion waves. Pressure increases as the flow passes through the oblique shock train, resulting in a 10% increase in average pressure from the inflow to outflow boundaries. Boundary layer temperature reaches a maximum of $\sim$500 K, below the threshold for ignition of the fuel-oxidizer mixture. No combustion occurs and the steady-state oblique shock train remains stationary in the lab reference frame.
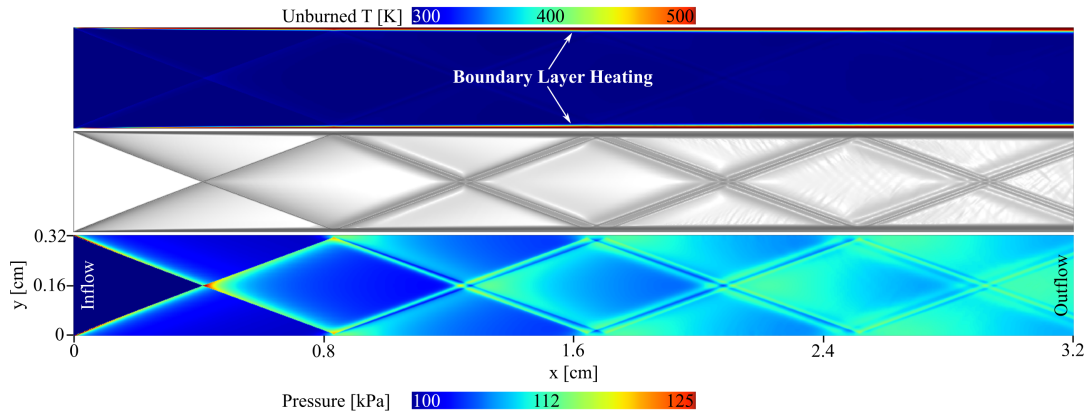
Fig. 32. Steady-state solution for Mach 3 inflow. Contours of (top) temperature (middle) numerical schlieren and (bottom) pressure.

Figure 33 shows temperature contours for the $M_\infty = 5.25$ case. At 14 μs the fuel-oxidizer mixture ignites in the boundary layer. The initial ignition location is

marked in Fig. 33 at 14.86 μs. The mixture ignites where the first oblique shock reflects from the channel wall. After ignition, the boundary layers are comprised of burned product that expands into the domain and upstream toward the inflow boundary. An oblique shock train, similar to what is observed for $M_\infty = 3$, forms in the channel of unburned gas between the reaction fronts. The interaction of the shocks with the reaction front results in perturbations to the flame that grow in time due to a Rayleigh-Taylor (RT) fluid instability (detailed in Sec. 4.4). Bubble and spike structures [70] form on the flame surface (labeled RT at 70.33 μs in Fig. 33). As time progresses, the burned gas expands and the reaction fronts extend further into the channel and closer to the inflow boundary. Intersection of oblique shocks with the flame front creates regions of high temperature and pressure that promote rapid flame expansion at several constriction points (labeled at 91 μs).

Temperature and pressure of the unburned gas increase dramatically as it flows through the constricted regions between reaction fronts. Eventually, a detonation is initiated (labeled D1 in Fig. 33) as a shock passes through the flame front and causes it to transition to a detonation front. The detonation front propagates upstream, consuming the unburned gas flowing between the flame fronts. A subsequent series of detonations is initiated (labeled D2 in Fig. 33) through the same mechanism as D1. The sequence in Fig. 34 is an enlargement of the events leading to D2. Shocks generated by D1 (labeled S1 and S2 in Fig. 34) travel upstream (toward the inflow boundary) ahead of D1 and pass through the flame fronts at D2. The shock amplifies energy release at the flame front, causing it to transition to detonation. The flame transitions to detonation through this mechanism in three locations (labeled D2A, D2B, and D2C in Fig. 34). Transition of a premixed flame to detonation as a result of energy addition of a passing shock has been observed in previous work [29].

Following the series of detonations at D2, the detonation front formed by D2C travels upstream toward the inflow boundary. Another series of detonations (labeled
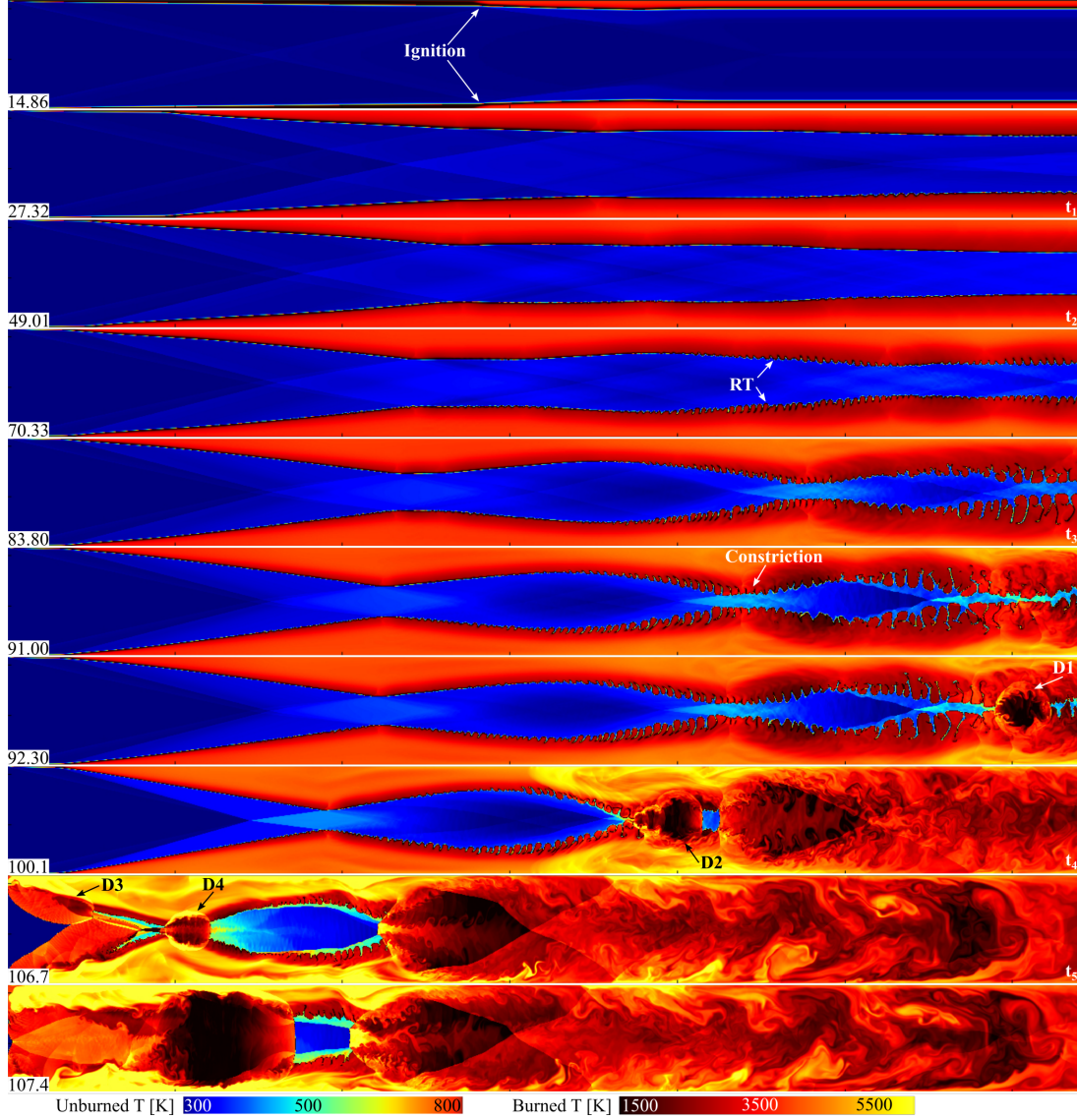
Fig. 33. Boundary layer ignition and expansion, growth of Rayleigh-Taylor instabilities (labeled RT), and detonation for Mach 5.25 inflow. Time in microseconds shown in frame lower left corners. Entire domain shown.

D3 in Fig. 33) occurs 5 μs following D2. The mechanism for D3 is the same as that of D2. Shocks generated by D2 pass through the reaction fronts near the inflow boundary and cause the flame to transition to detonation. Immediately following initiation of D3, a final series of detonations (labeled D4 in Fig. 33) is initiated in the unburned gas between the flame fronts. In D4, the unburned gas is compressed and heated by shocks generated by D2. As a result, the unburned gas detonates through

an energy focusing mechanism [28, 29] similar to the mechanism for D1-D3, but in D4 the detonation initiates in unburned gas rather than at a flame front.
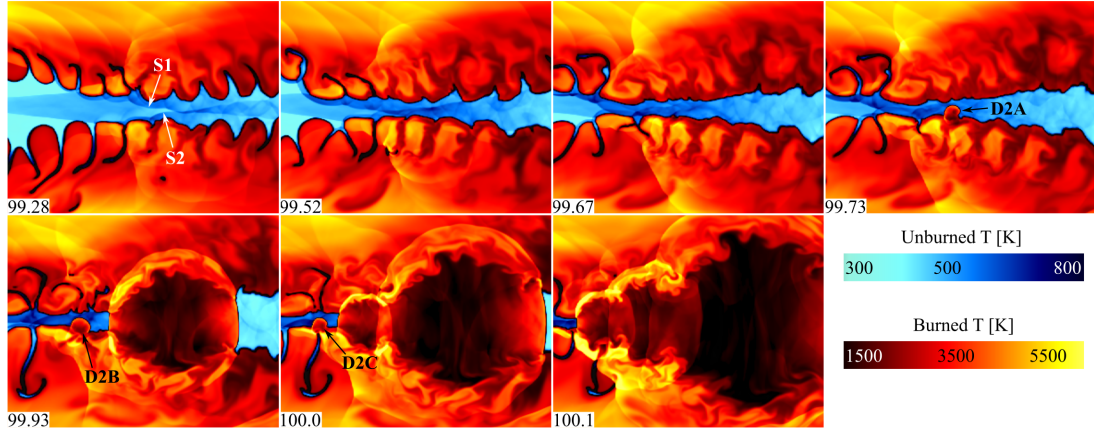
Fig. 34. Unstable flame front, shock collision, and detonation. Time in microseconds shown in frame corners. Domain is x = [1.85,2.10] cm and y = [0.075,0.225] cm.

Figure 35(a-c) shows profiles of Mach number, density, and pressure at a vertical slice across the channel height at x = 1.6 cm for five timesteps labeled t_1-t_5 correlating to 27.32, 49.01, 83.8, 100.1, and 106.7 μs, respectively. These timesteps are shown and labeled in Fig. 33. The slice location at x = 1.6 cm is labeled x_2 in Fig. 36. Figure 35d shows pressure at a horizontal slice across the channel length at y = 0.16 cm for the same timesteps.

Mach number is greater in the unburned gas than in the burned gas due to the significantly lower temperature and speed of sound. The flow in the burned gas is predominantly subsonic due to the higher speed of sound in this region. Density follows a similar trend. There is a sharp gradient across the flame; density in the burned gas is nearly an order of magnitude lower than density in the unburned gas. Pressure fluctuates in the burned and unburned gas as oblique shocks and expansion waves pass through slice x_2. Pressure increases to > 1 MPa at t_5 after detonation D2 passes through x_2. Figure 35(d) shows spikes in pressure through the oblique shock train followed by the pressure drops through the trailing expansion waves. The pressure spikes move closer to the inflow boundary at $x/H = 0$ as time progresses.
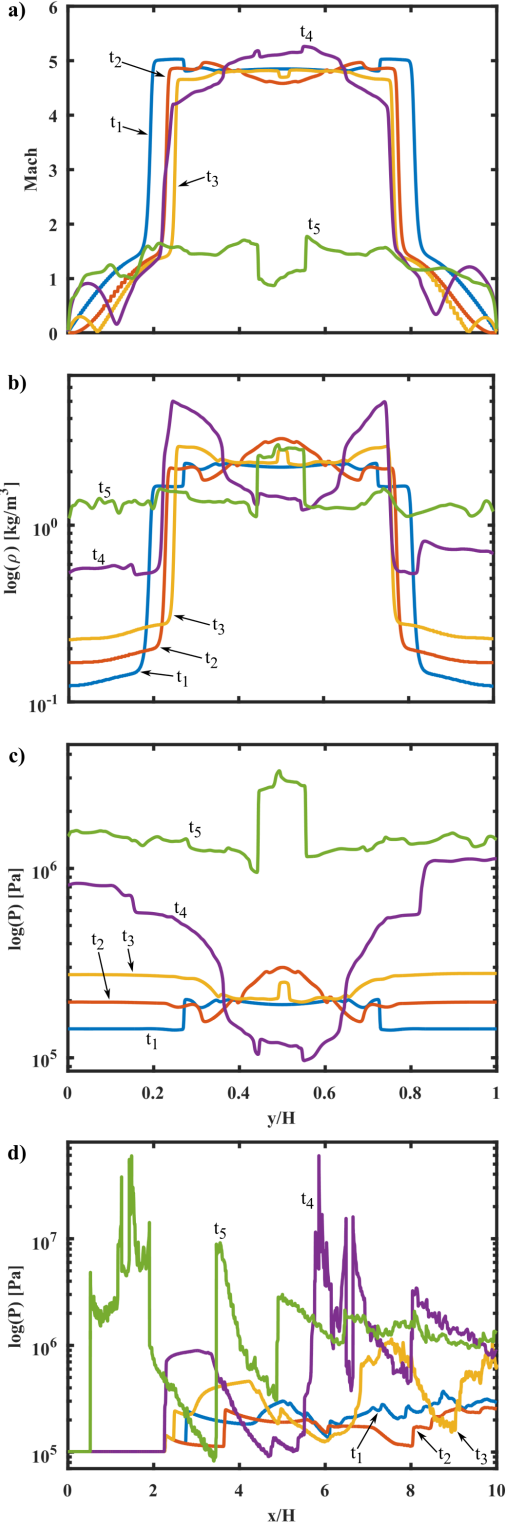
Fig. 35. (a) Mach number (b) density (c) pressure across vertical slice through domain at x = 1.6 cm. (d) Pressure across horizontal slice at y = 0.16 cm. Plots (a-c) share common x-axis.

62

4.4 Stability Analysis

For the $M_\infty = 5.25$ case, the flame front becomes increasingly unstable and turbulent with time. Figure 36 shows a numerical schlieren for the $M_\infty = 5.25$ calculation. At 27.32 μs, the fuel-oxidizer mixture has already ignited in the boundary layers and the flame fronts begin to expand into the center of the channel. An oblique shock train forms in the unburned gas. The oblique shocks pass through the burned gas and reflect from the channel walls generating bifurcated waves, or λ-shocks (labeled at 49.01 μs). These bifurcated waves remain anchored to the points at which the oblique shocks and flame front intersect. Ripples form on the flame surface at these locations. These ripples grow time due to a RT instability at the flame front. The RT instability forms at an interface between two fluids of different densities when the light fluid pushes the heavy fluid [8]. In this case, the low-density burned gas compresses the high-density unburned gas as the reaction front expands into the channel. The height of the ripples increases with time, forming bubble and spike structures (labeled RT in Figs. 33 and 36) typical to the RT instability [70]. Bubbles of low-density burned gas push into the high-density unburned gas and spikes of unburned gas form between the bubbles. At 83.8 μs, the bubbles have extended far into the center of the channel and nearly the entire channel cross section consists of burned gas. At 91 μs, compression of the unburned gas in the center of the channel increases its temperature to $\sim$750 K. Transition to detonation occurs shortly thereafter at D1 as described in Sec. 4.3.

One of the key parameters used to characterize the growth rate of a RT instability is the Atwood number, $At \equiv (\rho_H - \rho_L)/(\rho_H + \rho_L)$, where ρ_H is the density of the heavy fluid and ρ_L is the density of the light fluid. Bubble and spike structures are likely to develop at the fluid interface for flows with $At \simeq 1$ when the light fluid pushes the heavy fluid [70]. If $At \simeq 0$, a pattern of interpenetrating bubbles of heavy and light fluid is more likely to develop. Figure 37 shows At at three vertical slices through the domain (labeled x_1, x_2, and x_3 in Fig. 36) for the five timesteps shown in Fig. 36. The
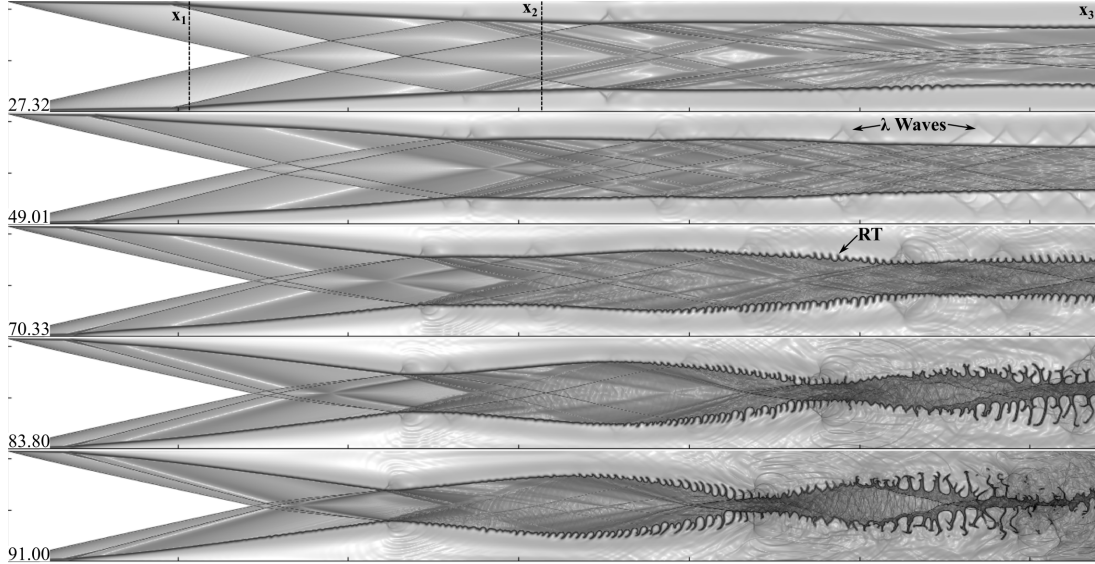
Fig. 36. Numerical schlieren for Mach 5.25 inflow. Time in microseconds shown in frame corners. Entire domain shown.

Atwood number was calculated by taking the average unburned gas density across the slice as ρ_H and the average burned gas density as ρ_L. The bubbles reach a maximum amplitude at x_3, where the lowest At is observed. Amplitude of the bubbles increases drastically from 27.32 μs to 91 μs, as shown in Fig. 36. Additionally, amplitude of the bubbles increases from the inflow to outflow indicating that the flame front becomes more unstable as distance downstream from the point of ignition increases. Structure develops on the spikes due to a Kelvin-Helmholtz instability, or gradient in velocity across the fluid interface, causing the spikes to deform and mushroom [70, 71]. This spike distortion effect is more pronounced at low At [70], particularly for compressible flows [72], and is most noticeable near x_3 at later timesteps where the lowest At is measured in this study. As seen in the evolution of the flame surface, the RT instability dominates the development of the reaction fronts and causes the formation of bubble-spike structure that compresses and preheats the unburned gas creating ideal conditions for a detonation to occur.
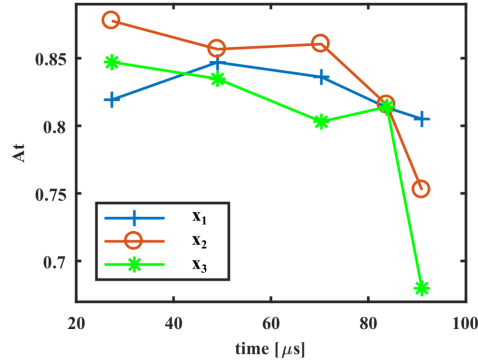
Fig. 37. Atwood number as a function of time at three vertical slices through domain.

4.5 Solution Sensitivity and Dimensionality

An additional simulation was performed for the $M_\infty = 5.25$ case with a coarser mesh resolution ($dx_{\min} = 13.3\ \mu m$) to investigate the effect of initial conditions on time and location of detonation, flame growth, fluid instabilities, and detonation mechanism. Time and location of the first detonation changed by 10 μs and 0.1 cm, respectively, when compared to the original simulation. Another simulation was performed using a shorter domain in the x direction (2.56 cm) with the same mesh resolution as in the original $M_\infty = 5.25$ simulation. The first detonation occurs in the same location as detonation D2 in the original simulation with a difference in time to detonation of 9 μs. For the shorter domain case, the D1 location in the original simulation would have been outside of the computational domain. In all cases, the same macroscopic flow features are observed: ignition of the fuel-oxidizer mixture in the boundary layer, growth of a RT instability at the flame front, and detonation of the unburned gas due to an energy-focusing mechanism after significant compression and preheating. Other than small deviations in time and location of detonation, the solution is insensitive to domain size or grid resolution. A three-dimensional (3D) simulation was performed to examine the effect of dimensionality on the growth of the flame instability and detonation. The results match what is seen in the 2D $M_\infty = 5.25$ case with respect to flame evolution and detonation mechanism. A detailed analysis of the 3D simulation

will be provided in a subsequent paper.

4.6 Conclusions

Multidimensional, unsteady numerical simulations of premixed ethylene and oxygen in a supersonic combustor were performed to characterize the effect of flow velocity on ignition, flame expansion and instability, and transition to detonation. This paper examined two cases, $M_\infty = 3$ and 5.25.

For $M_\infty = 3$, the fuel-oxidizer mixture does not reach sufficient temperature for ignition and no combustion occurs. In the case with $M_\infty = 5.25$, the temperature in the boundary layers at the channel walls is sufficient for ignition. The flames in the boundary layers expand and an oblique shock train forms between the reaction fronts. Interaction of the shock and the reaction front results in perturbations that are initially small ripples in the flame. These ripples grow in time due to a Rayleigh-Taylor fluid instability to form bubble and spike structures along the flame front as low-density burned gas compresses high-density unburned gas. Compression of the unburned gas increases its temperature and the fuel-oxidizer mixture detonates when a shock passes through the flame front through an energy-focusing mechanism. This detonation mechanism is consistent with previous work examining DDT in stoichiometric ethylene-oxygen mixtures [28, 29].

Additional simulations were performed to investigate the sensitivity of the solution to initial conditions. Modifying the domain size and mesh resolution resulted in small changes to the time and location of initial detonation, but ignition in the boundary layer, growth of a Rayleigh-Taylor instability at the flame front, and detonation through an energy-focusing mechanism were observed in all cases. Future work will catalog the effect of inflow Mach number and fuel-oxidizer mixture composition on time to ignition, flow structure, suppression of fluid instabilities, and transition to detonation.

4.7   Acknowledgments

5 Premixed Flame Stability and Transition to Detonation in a Supersonic Combustor

Gabriel B. Goodwin, Elaine S. Oran

This paper expands upon Chap. 4 by using the same geometry for a series of simulations with varying inflow speeds, from Mach 3 to 10, in order to investigate the following:

- Will the fuel-oxidizer mixture autoignite when flowing through a channel without obstacles at supersonic velocities? If so, does the flame remain stable or does it become turbulent? Will detonations occur and, if so, by what mechanism?

- What is the effect of Mach number on ignition, flame stability, and detonation initiation of the mixture flowing at supersonic speeds?

- How do fluid instabilities contribute to turbulence in the flame and detonation initiation?

Several simulations from the series are discussed, specifically addressing how the evolution of instability in the flame and transition to detonation is affected by the speed of the supersonic inflow. Detonations are initiated through the same energy-focusing mechanism discussed in prior chapters, though the manner in which the flames and shocks create the conditions for detonations to occur is considerably different. At the time this thesis was written, this paper was being prepared for submission to the *Journal of Combustion and Flame.*

Abstract

Inflow Mach number, M_∞, was varied in a supersonic combustor to investigate the effect of flow speed on ignition, flame stability, and transition to detonation of a pre-

mixed flame. The configuration studied was a rectangular channel with a supersonic inflow of stoichiometric ethylene-oxygen, a transmissive outflow boundary, and no-slip adiabatic walls. The compressible reactive Navier-Stokes equations were solved by a high-order numerical algorithm on an adapting mesh. Inflow Mach numbers of 3 to 10 were studied. For $M_\infty = 3$, the fuel-oxidizer mixture does not reach a sufficient temperature for autoignition. The incoming flow is deflected by boundary layers on the top and bottom walls resulting in the formation of a repeating oblique shock train. When M_∞ is increased to 5 or greater, the fuel-oxidizer mixture ignites in the boundary layers and the flame front expands into the channel. A shock-flame interaction causes a initial perturbation to the flame front that grows in time due to a Rayleigh-Taylor (RT) instability at the interface between the low-density burned gas and high-density unburned gas. Bubble and spike structure, characteristic of RT unstable interfaces with Atwood numbers less than 1, forms along the flame front. The unburned gas flowing between the flame fronts is compressed and preheated by the expanding flame and bubbles of burned gas. Detonation is initiated in several locations at the flame front and in the unburned gas through an energy-focusing mechanism. As M_∞ increases, the timescales for growth of the RT instability at the flame front and eventual detonation increase significantly. Despite the difference in timescales, the flame evolution process is, qualitatively, independent of M_∞: ignition in the boundary layer, laminar flame expansion, growth of an RT instability at the flame front, turbulent flame expansion, and deflagration-to-detonation transition.

5.1   Introduction

A comprehensive understanding of combustion in high-speed flows is required for the development of robust hypersonic vehicles. Airbreathing engines that operate at high supersonic and hypersonic flight speeds will enable more economical space

access and the next generation of extended-range, rapid response missile systems due to significant gains in efficiency over traditional rocket engines [54, 55]. Achieving flame stability across a wide range of inflow conditions in the engine of an airbreathing hypersonic vehicle is a challenge [1, 2] due to the small timescales for mixing, ignition, and complete combustion. The fundamental physics underlying ignition and combustion in high-speed flows is complex due to the chemical reactions, shocks, boundary layers, and turbulence present in these systems. Computational and experimental studies exploring the interaction of these phenomena will enable the design of higher-performing and more reliable hypersonic engines.

Combustion of premixed fuels and the effect of high-speed turbulence on flame development has been studied computationally [5, 56, 57], finding that under certain regimes, premixed flames are inherently unstable [6]. Detonation waves can be used instead of a flame or deflagration as a propulsion mechanism in a hypersonic engine [58, 59, 73]. Detonation engines have been studied experimentally [12, 63, 64] and computationally [60–62, 74] to characterize performance and detonation wave stability under a range of conditions. Prior work has examined the mechanisms for the deflagration-to-detonation transition (DDT) [17, 28, 39], which is required for ignition in rotating and pulse-detonation engines. Hypersonic combustor test facilities are used to study the stabilization of detonation waves in high-speed premixed flows [65, 75].

The purpose of this work is to characterize the effect of high supersonic and hypersonic flow speeds on premixed flames and identify the conditions that lead to flame instability and DDT. This paper presents a series of simulations performed to investigate the effect of varying inflow Mach number, M_∞, of an initially homogeneous fuel-oxidizer mixture into a constant-area combustor on ignition, flame growth, formation of fluid instabilities, and DDT. $M_\infty = 3$ to 10 are considered here. In the case of $M_\infty = 3$, the temperature of the fuel-oxidizer mixture does not reach the

threshold for autoignition. No combustion occurs and the flow reaches a steady-state repeating oblique shock structure. For $M_\infty \geq 5$, the fuel-oxidizer mixture ignites in the boundary layer and a flame front forms along the combustor walls. The flame front becomes turbulent and unstable through flame-shock interactions and growth of a Rayleigh-Taylor (RT) fluid instability along the flame surface. Eventually, DDT occurs as shocks focus energy at the flame front resulting in the transition to detonation. As M_∞ increases, the flame remains stable longer and time to detonation increases. Detonation is observed to initiate at the flame front as well as in a volume of unburned gas through an energy-focusing mechanism.

5.2 Background

Experimental and computational study of the fundamental physics underlying combustion, flame stability and acceleration, turbulence, and DDT has been substantial due to the need to understand these phenomena and their complex interactions as they are present in many physical systems, from aircraft engines to supernovae. Recent emphasis on achieving economical and reliable hypersonic flight for defense and space access applications has directed significant research effort into these subjects. A brief overview of some of the previous work in these areas is provided here to contextualize the work discussed in this paper.

Turbulence plays a key role in flame instability and, as such, turbulence-flame interactions are one of the most intensively studied phenomenon in combustion. Poludnenko et al. studied the dynamics of unconfined premixed flames in the presence of homogeneous, isotropic high-speed subsonic turbulence [5], where high-speed refers to turbulent velocities greater than the mixture's laminar flame speed. When the time-averaged internal structure of the many convolved flamelets comprising the turbulent flame was examined, it was discovered to be very close to that of the planar laminar flame, however, there was significant broadening of the preheat zone. The

71

effect of turbulence at scales smaller than the laminar flame thickness was found to be limited to progressively finer wrinkling of the flame surface, on the fuel side of the flame, as the turbulent energy cascade failed to penetrate the internal structure of the flame. It was determined that the evolution of the turbulent flame was completely determined by fluid motions at or greater than the laminar flame speed. In following work [57], frequent flame collisions in the presence of high-speed turbulence led to the formation of highly curved flame cusps, which was identified as a crucial process in turbulent flame evolution. Turbulence also resulted in unstable burning, which created pressure build-up around the flame and the formation of shocks [6]. Coupling of pressure gradients with density gradients across the flame led to amplification of turbulence within the flame, flame acceleration, and, in some cases, detonations.

The response of premixed flames to oscillatory pressure waves was investigated by Teerling et al. [76]. They determined that pressure waves magnify wrinkling in the flame surface due to a RT instability, which increases the overall burning rate of the flame. The effect of pressure waves on premixed flame stability in channels was studied by Xiao et al. [77]. The acoustic properties of the channels into which the premixed flames propagated played an important role in the formation of the pressure waves that affected flame evolution. They observed that the wrinkling and perturbations to the flame shape were due to the growth of a RT instability at the flame surface. The interaction of pressure waves with curved flame fronts was found to have a destabilizing effect that triggered the RT instability, resulting in deformation of a smooth, laminar flame to a distorted tulip flame [7].

In supersonic flow, shocks generated by deflection of the flow or by flame expansion have a significant effect on flame evolution. Shock-flame interactions were studied experimentally by Thomas et al. [78]. They found that perturbation of an initially laminar flame by shocks induced turbulence in the flame causing it to accelerate and often couple closely to the shock. If the shock increased local gas pressure and temper-

ature sufficiently, transition to detonation occurred in the immediate vicinity of the reaction front. Similar results were observed computationally [79] in the collisions of shocks and expanding flame fronts. The shock-flame interaction, primarily through the Richtmyer-Meshkov fluid instability, created a highly turbulent flame brush as funnels of unburned gas propagated into the burned gas. Repeated shock-flame interactions, and coalescence of shocks in the unburned gas, resulted in the development of high-speed shocks that moved in and out of the turbulent flame, creating conditions under which DDT might occur. Interaction of the flame with strong shocks also generated high levels of vorticity in the flame brush, which can lead to direct initiation of a detonation [9].

The process for flame acceleration and the mechanism of DDT in smooth and obstructed channels has been studied experimentally; much of this work is summarized by Ciccarelli et al. in their review paper [80]. Acceleration of the flame compresses, heats, and induces turbulence in the unburned reactants and creates the ideal conditions for the initiation of a detonation. Detonation initiation has been observed to occur through a variety of processes, such as through shock focusing, instabilities near the flame front, flame interactions with pressure waves, or pressure and temperature fluctuations in the boundary layer. Numerical simulations have also been used to investigate the mechanisms for DDT [17]. Shock-flame interactions were once again found to be important in creating the conditions in which DDT can occur. As shocks passed through turbulent flames, the shock strength was enhanced and the shock-flame collision drove the turbulence in the flame. The intense pressure fluctuations caused by passing shocks in the region of the turbulent flame brush created hot spots, or localized ignition centers, in the unburned gas. The hot spot produced a detonation through an ignition-gradient mechanism [14, 15] if the gradient of reactivity was sufficient to support propagation of the spontaneous reaction wave. If the gradient could not support the propagation of a detonation wave, a decoupled shock and flame

front would form. Gamezo et al. observed DDT through the ignition-gradient mechanism in obstructed channels when the reflection of Mach stems against obstacles ignited hot spots that transitioned to spontaneous waves and detonations [18].

More recent computations have shown that, when the blockage ratio in an obstructed channel is reduced, detonations primarily occur through an energy-focusing mechanism [51]. The collision of shocks deposited significant energy into the turbulent unburned gas at a timescale smaller than the acoustic timescale of the gas, resulting in the direct initiation of a detonation. The passage of a strong shock through a turbulent flame was also observed to increase energy release at the flame front and, in some cases, cause it to transition to a detonation. When the channel is unobstructed, the detonation initiates in the boundary layer of unburned gas formed against the wall, between the leading shock and the expanding flame [68]. Preheating by the leading shock and viscous dissipation in the boundary layer ignited the unburned gas, producing a spontaneous wave that transitioned to detonation. Regardless of blockage ratio or channel geometry, flame stability and the processes of flame growth and detonation initiation are primarily dependent upon the complex interactions between the flame, shocks, boundary layers, and turbulence. This paper explores the interplay between these phenomena in the context of high-Mach flow of a fuel-oxidizer mixture through an unobstructed combustor of uniform cross-sectional area.

5.3 Numerical and Physical Model

The numerical model solves the full set of Navier-Stokes equations for an unsteady, fully compressible, chemically reacting gas,

$$\frac{\partial \rho}{\partial t} + \nabla \cdot (\rho \mathbf{U}) = 0 \tag{11}$$

$$\frac{\partial (\rho \mathbf{U})}{\partial t} + \nabla \cdot (\rho \mathbf{U}\mathbf{U}) + \nabla P = \nabla \cdot \hat{\tau} \tag{12}$$

$$\frac{\partial E}{\partial t} + \nabla \cdot ((E + P)\mathbf{U}) = \nabla \cdot (\mathbf{U} \cdot \hat{\tau}) + \nabla \cdot (K\nabla T) - \rho q \dot{w} \qquad (13)$$

$$\frac{\partial(\rho Y)}{\partial t} + \nabla \cdot (\rho Y \mathbf{U}) + \nabla \cdot (\rho D \nabla Y) - \rho \dot{w} = 0 \qquad (14)$$

$$P = \frac{\rho R T}{M} \qquad (15)$$

where ρ is the mass density, $\mathbf{U}$ is the velocity, E is the energy density, P is the pressure, T is the temperature, Y is the mass fraction of reactant, $\dot{w}$ is the reaction rate, q is the total chemical energy release, K is the thermal conduction coefficient, D is the mass diffusion coefficient, R is the universal gas constant, and M is the molecular weight. The reaction of a stoichiometric mixture of ethylene and oxygen is modeled using a simplified, calibrated chemical-diffusive model,

$$dY/dt \equiv \dot{w} = -A\rho Y \exp(-E_{\mathrm{a}}/RT) \qquad (16)$$

where A is the pre-exponential factor and E_{a} is the activation energy. The effects of viscosity, diffusion, and heat conduction are dependent upon temperature and density,

$$\nu = \nu_0 \frac{T^n}{\rho}, D = D_0 \frac{T^n}{\rho}, \frac{K}{\rho C_p} = \kappa_0 \frac{T^n}{\rho}, \qquad (17)$$

where ν_0, D_0, and κ_0 are constants, $C_p = \gamma R/M(\gamma - 1)$ is the specific heat at constant pressure, and $n = 0.7$ emulates the typical temperature dependence for the system. To solve Eqns. (11)–(17), the input parameters shown in Table 3 were chosen to reproduce the flame and detonation properties for a stoichiometric ethylene-oxygen mixture initially at 298 K and 1 atm. A genetic algorithm optimization procedure was used to identify the input parameters that most accurately reproduce the flame and detonation properties, calculated using detailed chemistry, for the fuel-oxidizer mixture [66]. This reaction model quantitatively reproduces flame acceleration, onset of turbulence, and DDT mechanisms seen in experiments [7, 40, 67] and has recently been used to study DDT [28, 29, 68] and layered detonations [69].

Table 3. Input model parameters and output combustion wave properties for stoichiometric ethylene and oxygen initially at 1 atm and 298 K.

	Input	
P_o	1 atm	Initial Pressure
T_o	298 K	Initial Temperature
ρ_o	1.27×10^{-3} g/cm^3	Initial Density
γ	1.2195	Adiabatic Index
M	31 g/mol	Molecular Weight
A	1.05×10^{12} cm^3/(g s)	Pre-Exponential Factor
E_a	$39.2RT_\mathrm{o}$	Activation Energy
q	$59.7RT_\mathrm{o}/\mathrm{M}$	Chemical Energy Release
ν_o	7.0×10^{-6} g/s-cm-K$^{0.7}$	Viscosity
$\kappa_\mathrm{o} = D_\mathrm{o}$	1.0×10^{-5} g/s-cm-K$^{0.7}$	Transport Constants
	Output	
S_L	413 cm/s	Laminar Flame Speed
T_b	$11.7T_\mathrm{o}$	Post-Flame Temperature
ρ_b	$0.085\rho_\mathrm{o}$	Post-Flame Density
x_l	8.88×10^{-3} cm	Laminar Flame Thickness
D_CJ	2.20×10^5 cm/s	CJ Detonation Velocity
P_ZND	$54.5P_\mathrm{o}$	Post-Shock Pressure
P_CJ	$27.8P_\mathrm{o}$	Pressure at CJ Point
T_ZND	$6T_\mathrm{o}$	Post-Shock Temperature
T_CJ	$15.5T_\mathrm{o}$	Temperature at CJ Point
ρ_ZND	$9.8\rho_\mathrm{o}$	Post-Shock Density
ρ_CJ	$2\rho_\mathrm{o}$	Density at CJ Point
x_d	3.2×10^{-4} cm	Half-Reaction Thickness
λ	~ 0.02 cm	Detonation Cell Size

A Godunov algorithm, fifth-order accurate in space and third-order accurate in time [19], is used to solve the equations on a dynamically adapting grid [47]. The simulations described below used grids with minimum size $dx_\mathrm{min} = 3.3$ μm and coarsest size $dx_\mathrm{max} = 53.3$ μm, unless otherwise stated. This choice of grids was tested and shown to resolve the shocks, boundary layers, flames, and other important flow and chemical structures. Grid resolution is discussed in detail in Secs. 5.4.1 and 5.5.3.

The geometrical setup is shown in Fig. 38. A supersonic inflow condition is applied at the left boundary. For all M_∞ cases, inflow temperature, pressure, and mass fraction of reactant are the same (298 K, 1 atm, 1, respectively) and are constant for

the duration of the calculation. The calculation is initiated with velocity everywhere in the domain equal to the velocity at the inflow. The right boundary of the domain is a transmissive, non-reflecting outflow. The top and bottom walls are no-slip adiabatic boundaries. The channel height is 0.32 cm and the length is 3.2 cm. A height of 0.32 cm, also used in prior work [28, 29] investigating flame acceleration and DDT mechanisms using ethylene-oxygen, was determined to be sufficient for capturing the flame and detonation physics of interest. The small scale flame and detonation properties of this fuel-oxidizer mixture, such as fast reactions and energy release, make ethylene-oxygen an ideal fuel-oxidizer mixture for studying ignition and flame evolution in high-speed premixed reactive flows.

5.4   Results

5.4.1   Mach 3 Inflow
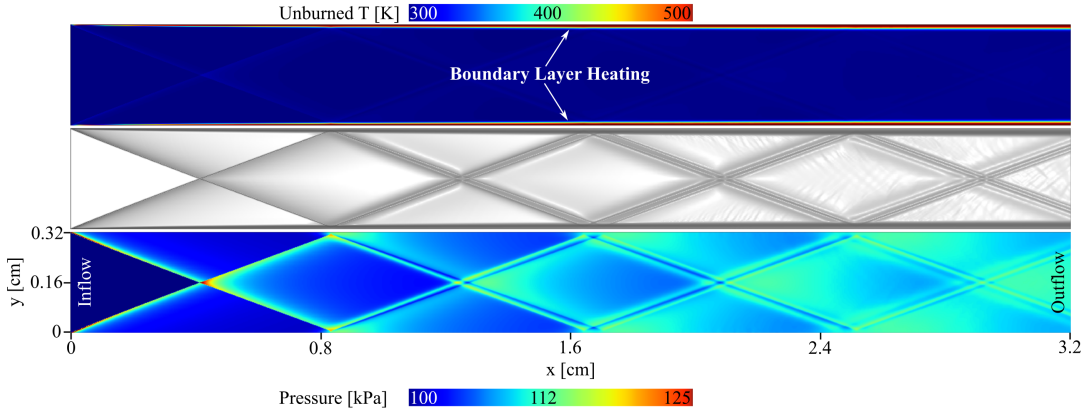
Fig. 38. Steady-state solution for Mach 3 inflow. Contours of (top) temperature (middle) numerical schlieren and (bottom) pressure.

The steady-state flowfield for the $M_\infty = 3$ case is shown in Fig. 38. The time required to reach steady-state is 50 μs. Boundary layers form quickly at the top and bottom walls. The inflow is deflected by the boundary layers, forming oblique shocks that reflect from the wall at a constant angle, a function of M_∞, repeating to the end of the domain. Following the first reflection, the shocks are trailed by
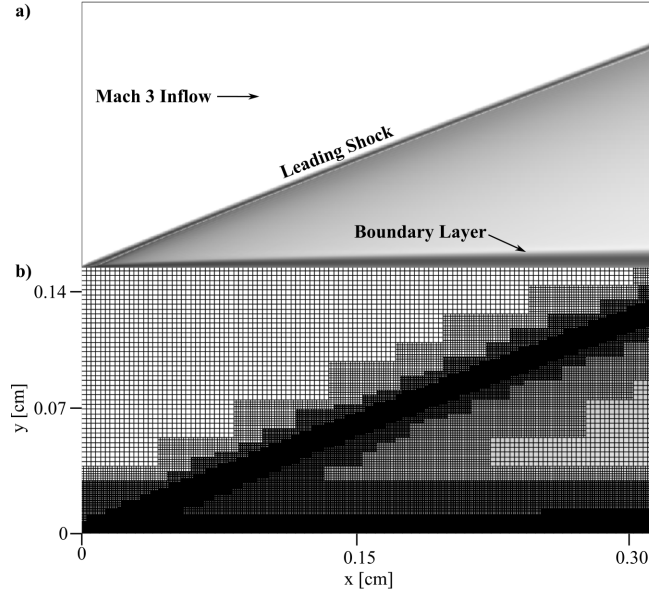
Fig. 39. (a) Numerical schlieren for $M_\infty = 3$ showing the leading oblique shock formed by deflection of the inflow by the boundary layer and (b) the same image as in (a) overlaid with the computational grid showing refinement across the shock and through the boundary layer.

expansion waves. Pressure increases as the flow passes through the oblique shock train, resulting in a 10% increase in average pressure from the inflow to outflow boundaries. Boundary layer temperature reaches a maximum of ~550 K, below the threshold for ignition of the fuel-oxidizer mixture. No combustion occurs and the steady-state oblique shock train remains stationary. Figure 39(a) shows the leading shock and the boundary layer near the inflow boundary and Fig. 39(b) shows the same image with the computational mesh overlaid. The adaptive meshing provides increased resolution across the shock and in the boundary layer. Dimensionless wall distance, $y+ \equiv u_* y / \nu$, is often used to characterize the near-wall mesh resolution, where u_* is the friction velocity at the wall, y is the distance to the wall, and ν is the local kinematic viscosity. In the $M_\infty = 3$ case, a $y+ < 3$ is achieved throughout the boundary layer.
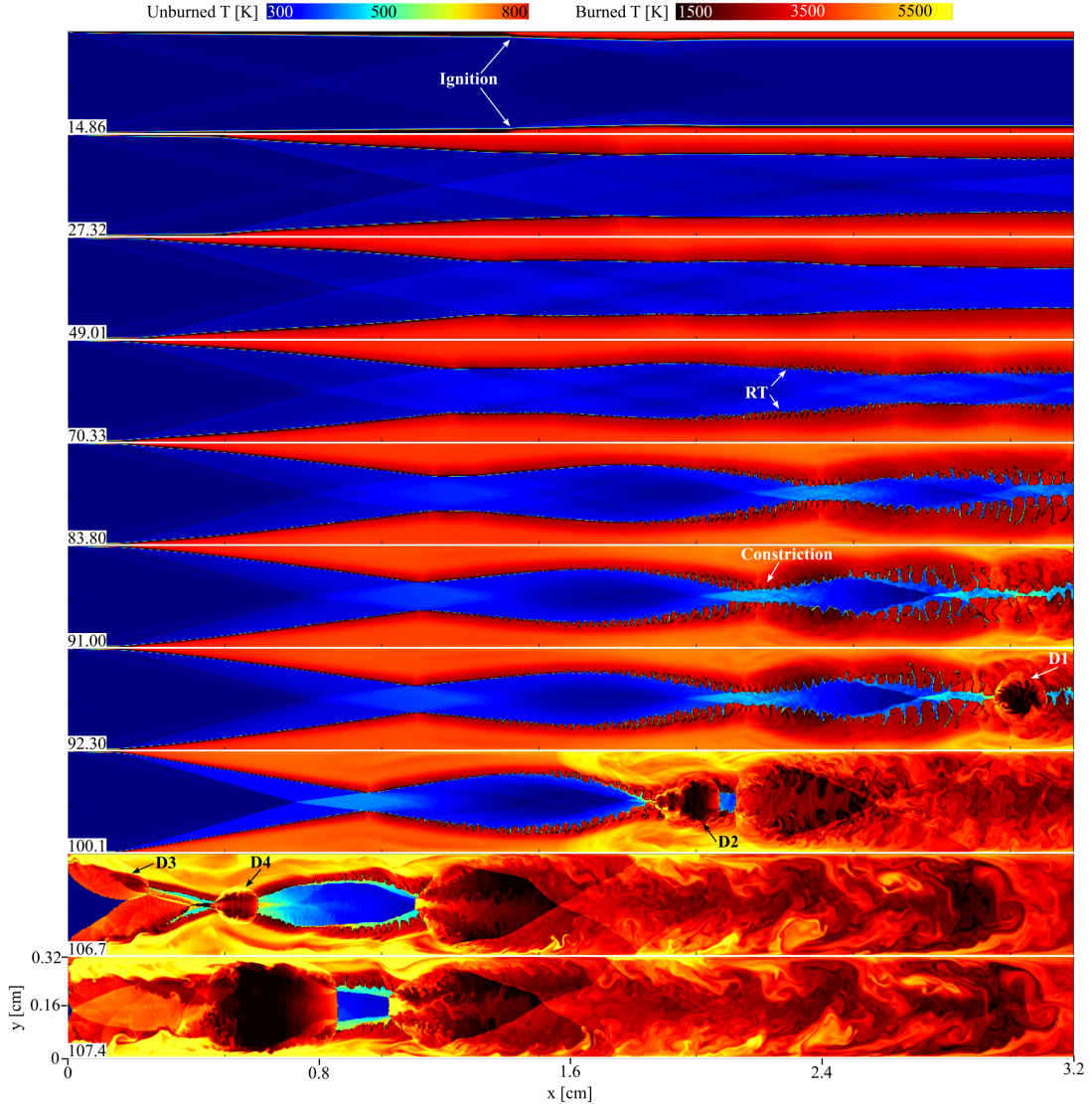
Fig. 40. Boundary layer ignition, flame expansion, growth of Rayleigh-Taylor instabilities (labeled RT), and detonation for $M_\infty = 5.25$. Time in μs shown in frame lower left corners.

5.4.2 Mach 5.25 Inflow

Figure 40 shows temperature contours for the $M_\infty = 5.25$ case. At 14 μs the fuel-oxidizer mixture ignites in the boundary layer. The initial ignition location is marked in Fig. 40 at 14.86 μs. The mixture ignites where the first oblique shock reflects from the channel wall. After ignition, the boundary layers are comprised of burned product that expands into the channel and upstream toward the inflow boundary. An

oblique shock train, similar to what is observed for $M_\infty = 3$, forms in the channel of unburned gas between the flame fronts.

Ripples form on the flame surface as it expands into the channel. These ripples grow in time due to a RT instability at the flame front (discussed in greater detail in Sec. 5.5.2). The RT instability forms at an interface between two fluids of different densities when the light fluid pushes the heavy fluid [8]. In this case, the low-density burned gas compresses the high-density unburned gas as the reaction front expands into the channel. The height of the ripples increases with time, forming bubble and spike structures (labeled RT in Figs. 40) typical to the RT instability [70]. Bubbles of low-density burned gas push into the high-density unburned gas and spikes of unburned gas form between the bubbles. At 83.8 μs, the bubbles have extended far into the center of the channel and nearly the entire channel cross section consists of burned gas. At 91 μs, compression of the unburned gas in the center of the channel increases its temperature to $\sim$750 K. The compression is most pronounced at several constriction points (labeled at 91 μs) that form at the locations where the oblique shocks and the flame front intersect.

Eventually, a detonation is initiated (labeled D1 in Fig. 40) when a shock passes through the flame front and causes it to transition to a detonation front. The detonation front propagates upstream, consuming the unburned gas flowing between the flame fronts. A subsequent series of detonations is initiated (labeled D2 in Fig. 40) through the same mechanism as D1. The sequence in Fig. 41 is an enlargement of the events leading to D2. Shocks generated by D1 (labeled S1 and S2 in Fig. 41) travel upstream (toward the inflow boundary) ahead of D1 and pass through the flame fronts at D2. The shock amplifies energy release at the flame front, causing it to transition to detonation. The flame transitions to detonation through this mechanism in three locations (labeled D2A, D2B, and D2C in Fig. 41) nearly simultaneously. Transition of a premixed flame to detonation as a result of the energy addition of a passing shock
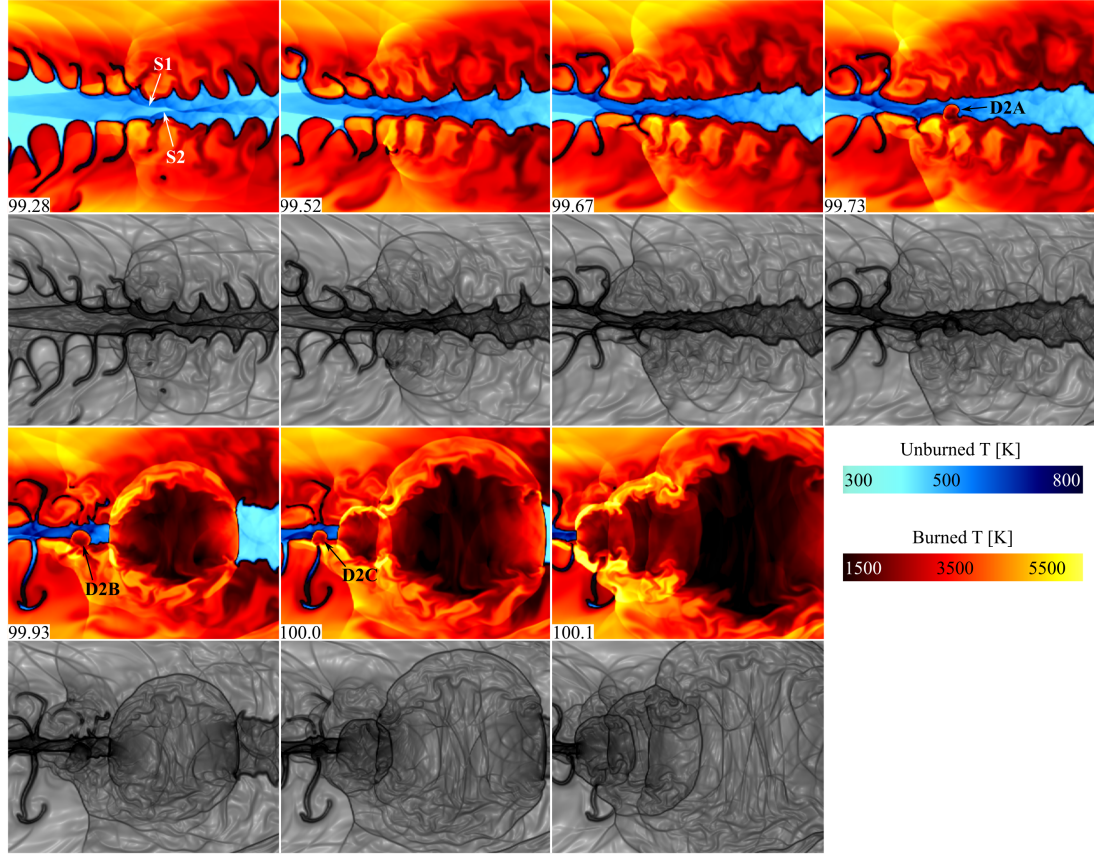
Fig. 41. Unstable flame front, shock collision, and detonation D2. Temperature and numerical schlieren shown for each time step. Time in μs shown in frame corners. Domain is x = [1.85,2.10] cm and y = [0.075,0.225] cm.

has been observed in previous work [29].

Following the series of detonations at D2, the detonation front formed by D2C travels upstream toward the inflow boundary. Shocks generated by D2 coalesce with shocks S1 and S2 to form stronger shocks, S3 and S4. Another series of detonations (labeled D3 in Fig. 40) occurs 5 μs following D2. An enlargement of D3 is shown in Fig. 42. The mechanism for D3 is the same as that of D2. Shocks S3 and S4, generated by D1 and D2, pass through the reaction fronts near the inflow boundary and cause the flame to transition to detonation in several locations, labeled D3A-D3C in Fig. 42. Detonation cell structure forms immediately after initiation of D3A-C and the detonation waves quickly consume the unburned reactant entering the domain through the inflow boundary.
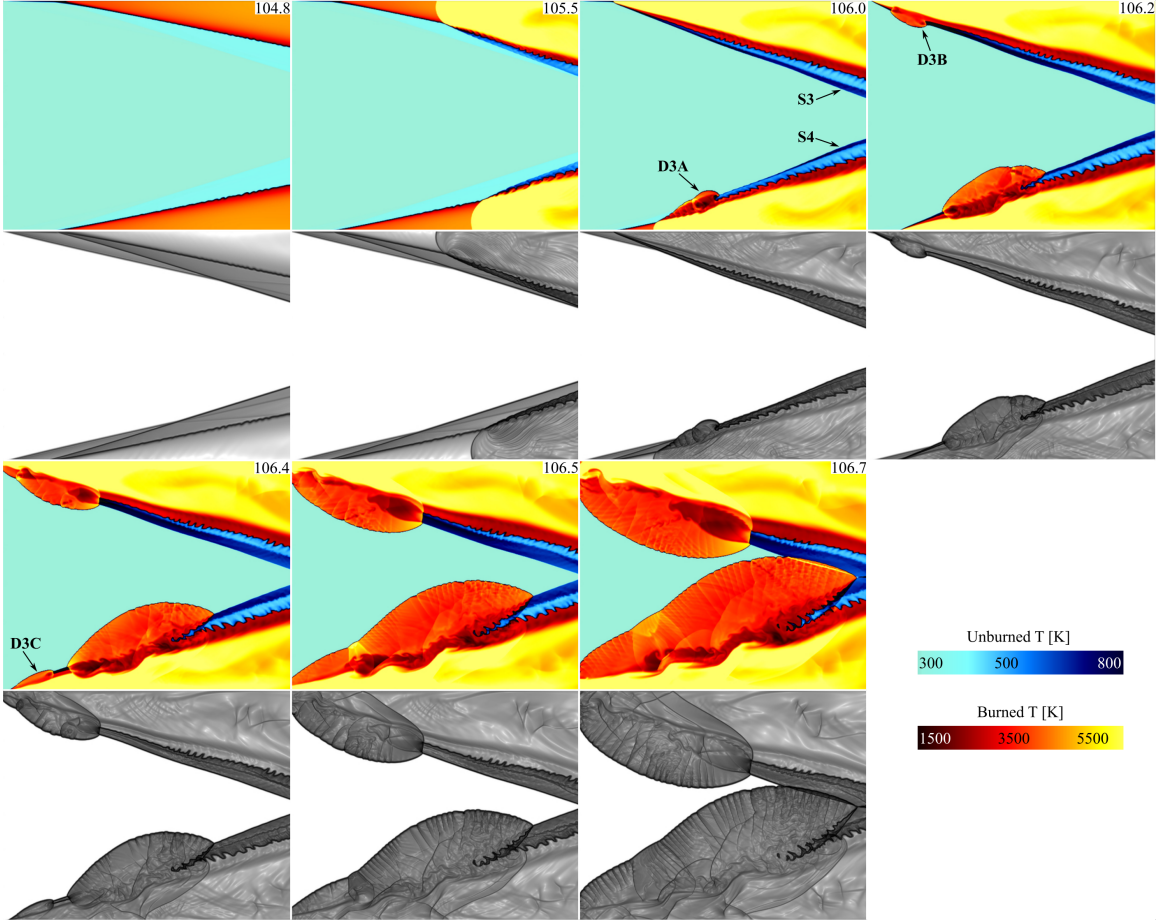
Fig. 42. Initiation of detonation D3 near inflow boundary following passage of shocks through flame front. Temperature and numerical schlieren shown for each time step. Time in μs shown in frame corners. Domain is x = [0,0.4] cm and y = [0,0.32] cm.

Following detonation D3, a final series of detonations (labeled D4 in Fig. 40) is initiated in the unburned gas between the flame fronts. An enlargement of D4 is shown in Fig. 43. The unburned gas is compressed and heated as it flows through a constriction point between the flame fronts where D4 will occur. Shocks S3 and S4 pass through the flame fronts and collide in the preheated unburned gas. As S3 and S4 collide, the unburned gas ignites and detonations are initiated in several locations simultaneously, labeled D4A-D4C in Fig. 43. The collision of S3 and S4 deposits sufficient energy into the compressed and preheated unburned gas to cause it to detonate, similar to the detonation initiation following shock collision observed in obstacle-laden channels with low blockage ratios [28, 29]. This energy focusing det-
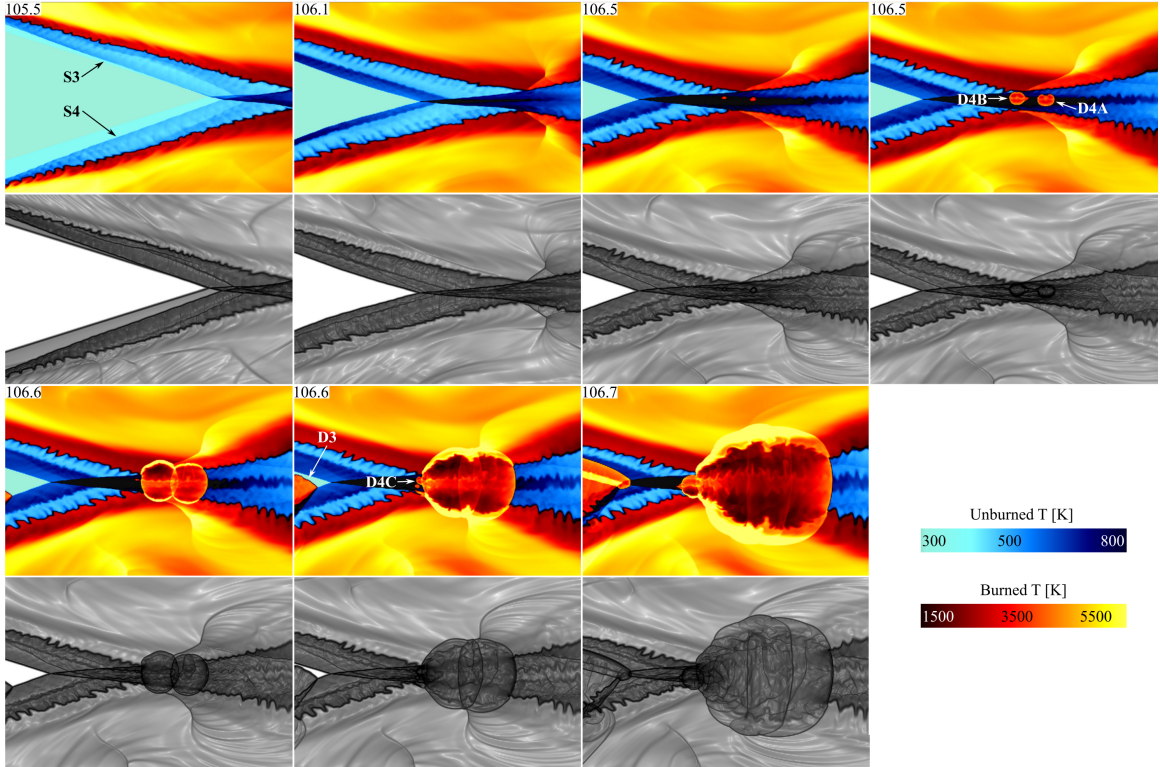
Fig. 43. Shock collision and initiation of detonation D4 in the unburned gas between flame fronts. Temperature and numerical schlieren shown for each time step. Time in μs shown in frame corners. Domain is x = [0.45,0.60] cm and y = [0.1,0.2] cm.

onation mechanism is similar to what is observed for D1-D3, but in D4 the detonation initiates in unburned gas rather than at a flame front.

Figure 44(a) shows the trend of flame surface length as a function of time for the $M_\infty = 5.25$ case. The flame surface is defined as the isosurface where $Y = 0.5$. Following ignition at 14 μs, the flame surface grows rapidly, extending downstream from the point of ignition to the outflow boundary along both walls. Increase in flame surface length is gradual during the laminar flame expansion portion of the flame growth, from $15 - 60$ μs. Once the bubble and spike structure is observed on the flame front due to growth of the RT instability, the flame surface length begins to increase much more rapidly as bubbles of burned gas extend far into the unburned gas flowing between reaction fronts. This period of rapid flame expansion, characterized by increasing turbulence in the flame front, continues until the first detonation, D1,
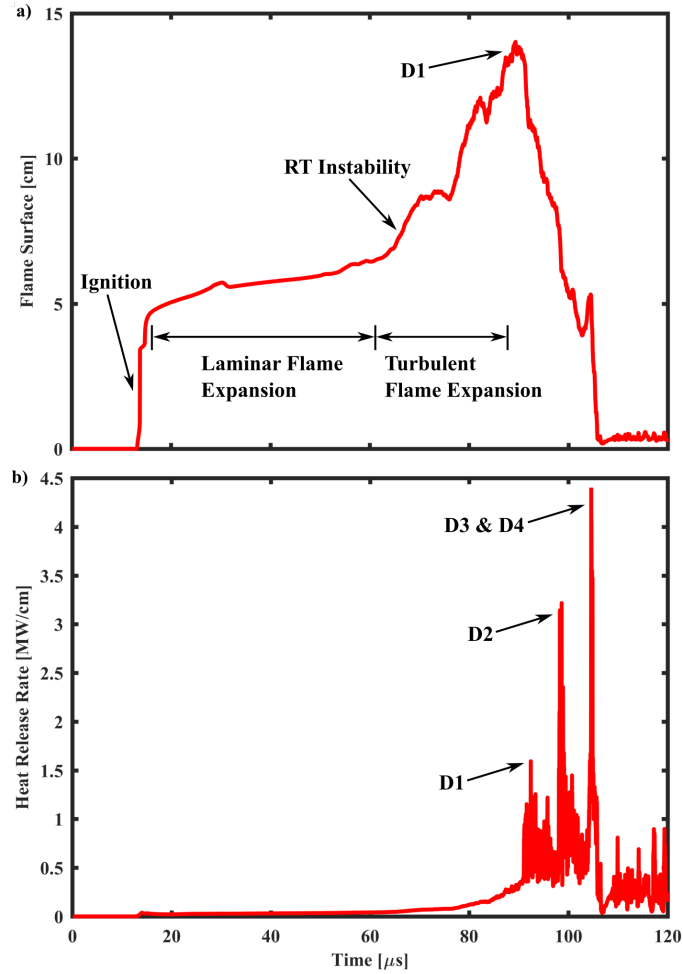
Fig. 44. (a) Flame surface length and (b) heat release rate per unit cm for the M_∞ = 5.25 case shown in Fig. 5.4.2.

occurs at 91 μs. Flame surface length then decreases steadily as the detonation waves consume the unburned gas in the channel.

Figure 44(b) shows heat release rate in the domain by combustion, per unit cm in the third dimension, as a function of time for $M_\infty = 5.25$. Heat release is minimal during laminar flame expansion, but it begins to rise steadily as the RT instability becomes more dominant and turbulence in the flame increases. There is a spike in heat release during detonation D1 of 1.5 MW/cm, followed by subsequent spikes to 3.25 MW/cm and 4.4 MW/cm during detonations D2 – D4. Following detonations D3 and D4, heat release oscillates about a value of ~0.25 MW/cm as the detonation

84

waves consume the reactant flowing into the domain.

A three-dimensional (3D) simulation was performed for $M_\infty = 5.25$, shown in Fig. 45. The domain height in the 3D case is reduced to 0.16 cm and $dx_{\min}$ is increased to 13.3 μm to reduce the computational expense of the simulation. The boundary conditions are labeled in Fig. 45. Symmetry planes are used to model a quarter channel, with no-slip, adiabatic walls at the x-z and x-y planes. Temperature at the walls and the $Y = 0.5$ isosurface are plotted as a function of time. The fuel-oxidizer mixture ignites at 11 μs in the boundary layer where the two walls meet. The flame front propagates along the walls and ripples appear at the flame surface very shortly after ignition, visible first at 14.19 μs. The flame front continues to propagate further along the walls toward the inflow boundary as it also expands toward the center of the channel. RT bubble and spike structure appears at $\sim$20 μs. The bubbles emerge very close to the ignition point. Bubble size increases with distance from the ignition point until the bubble passes through the constriction point, labeled at 45.12 μs, where the reaction front extends far into the channel and compresses the unburned gas. As in the 2D case, the constriction points develop where the leading oblique shocks intersect the flame. While passing through this point, the bubbles are flattened, then they continue to grow once again as they propagate further downstream toward the outflow boundary.

The flame continues to expand into the channel and compress the unburned gas until nearly the entire cross-sectional area at the outflow consists of burned product. Detonations D5 and D6, labeled at 55.50 μs, initiate simultaneously as shocks collide with the flame front in a region of significant compression and heating of the unburned gas. The flame front transitions to a detonation front following the shock collision, as it does in the 2D $M_\infty = 5.25$ case. The impact of the D5 and D6 detonation waves against the walls is visible in the wall temperature contours at 56.61 μs. Two subsequent detonations occur, labeled D7 and D8 at 61.71 μs and 64.41 μs, respectively,
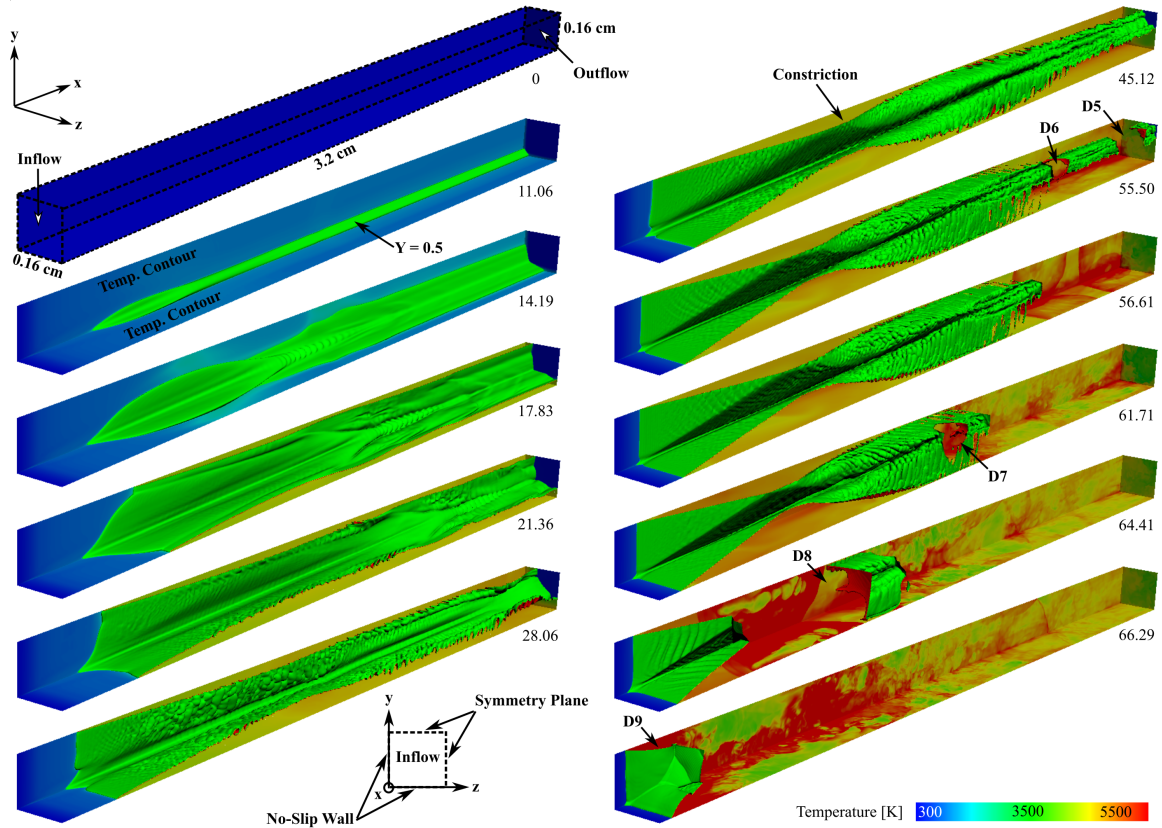
Fig. 45. Three-dimensional simulation for $M_\infty = 5.25$. Flame contour ($Y = 0.5$ isosurface) and temperature at the walls and outflow plotted as a function of time.

through the same initiation mechanism as D5 and D6. The final detonations, labeled D9 at 66.29 μs, originate at the flame front close to the inflow as shocks pass through the flame and cause the transition to detonation, similar to detonation D3 depicted in Fig. 42. The multidimensional turbulence in the 3D $M_\infty = 5.25$ case leads to a faster rate of flame expansion and earlier detonation than in the 2D case, but growth of the RT instability, turbulence in the flame compressing the unburned gas, and DDT through an energy focusing mechanism are observed in both cases.

5.4.3   Mach 8 & 10 Inflow

Additional 2D simulations were performed with $M_\infty = 5.5, 5.75, 6, 7, 8$ and 10. All inflow conditions other than velocity are the same for these simulations as those used
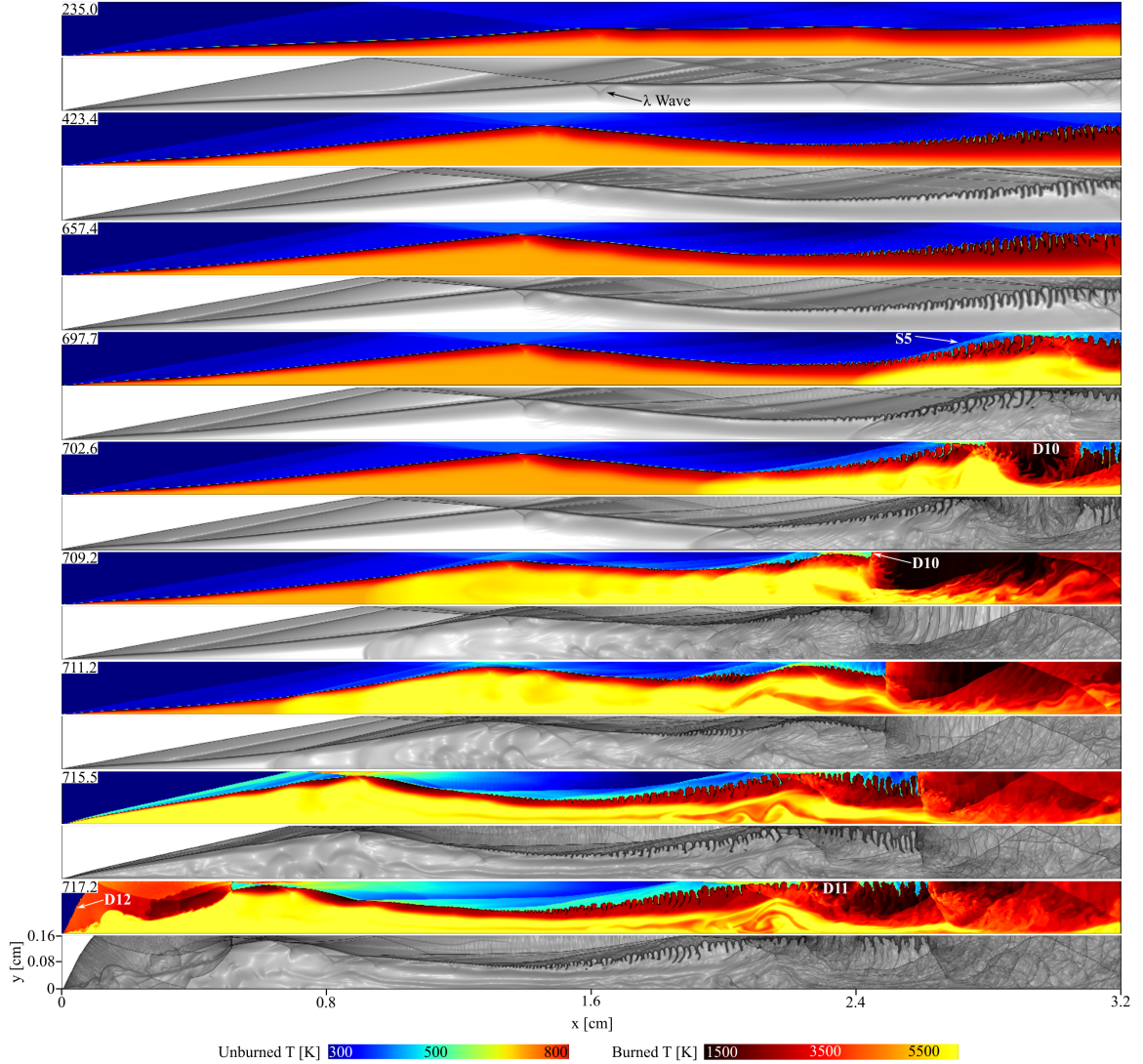
Fig. 46. Evolution of flame and DDT for $M_\infty = 8$. Temperature and numerical schlieren shown for each time step. Time in μs shown in frame corners.

in the $M_\infty = 3$ and 5.25 cases. A domain height of 0.16 cm with a symmetry plane at the top boundary was used for the $M_\infty = 8$ and 10 cases to reduce computational expense. Runtime for the $M_\infty = 8$ and 10 simulations was greater than that required for lower Mach inflow due to the larger timescales for flame expansion and DDT. Figure 46 shows the $M_\infty = 8$ case. The flame remains stable with no noticeable perturbations to the flame surface until $\sim$280 μs when bubble and spike structure begins to emerge. The bubbles grow in amplitude as they propagate toward the outflow boundary. Bubbles also begin to emerge farther upstream, closer to the

ignition point, as time progresses. Compression of the unburned gas increases its temperature to 600 K as the bubbles of burned gas expand to occupy nearly the entire cross-sectional area of the channel, as shown at 697.7 μs. A shock, labeled S5, forms upstream of the burned gas bubbles, due to the deflection of the inflow of Mach 8 unburned gas by the expanding reaction front. Shock S5 reflects from the symmetry plane and passes through the flame front, causing it to transition to a detonation, labeled D10.

The D10 detonation wave begins to propagate upstream, as shown at 709.2 μs. As the flowrate of unburned gas toward the D10 detonation front increases (the cross-sectional area of unburned gas upstream of D10 increases, visible from 709.2 to 711.2 μs), the detonation front is unable to consume the reactant quickly enough to continue to propagate upstream. Detonation D10 continues to move downstream while the bubble and spike structure immediately upstream of D10 increases in amplitude, resulting in compression of the unburned gas and the initiation of another detonation, labeled D11. Almost simultaneously, detonation D12 initiates near the inflow as shock S5 passes through the flame front and causes the transition to detonation. An enlargement of the events leading to D12 is shown in Fig. 47.
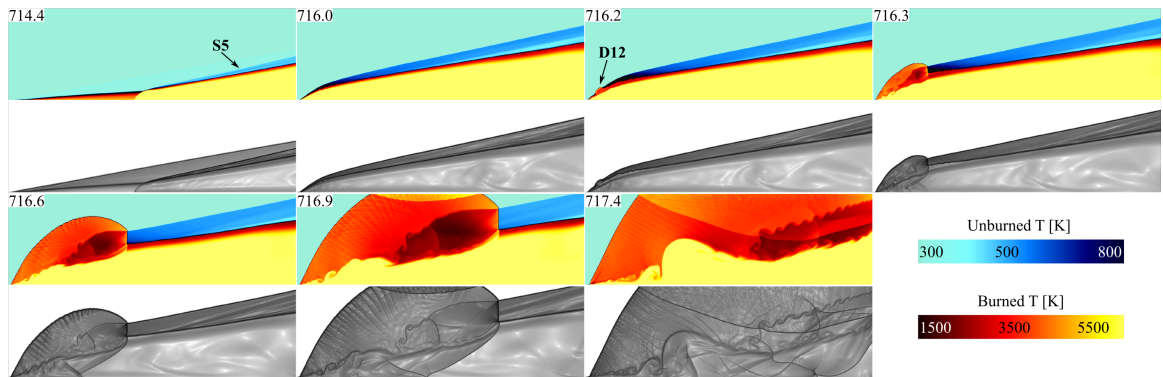
Fig. 47. Transition of flame front near inflow boundary to detonation D12 in $M_\infty = 8$ case. Temperature and numerical schlieren shown for each time step. Time in μs shown in frame corners. Domain is x = [0,0.5] cm and y = [0,0.16] cm.

Figure 48 shows the temperature and pressure across the top boundary of the

domain (y = 0.16 cm) for the first five time steps shown in Fig. 46. Pressure and temperature are greatest at the constriction points, where the burned gas has expanded furthest into the channel, at x = 1.5 cm and x = 3 cm. At x = 1.5 cm, the unburned gas is compressed to 7 atm and 425 K prior to initiation of the first detonation, D10. The unburned gas is compressed significantly more at x = 3 cm, where detonation D10 initiates, reaching a pressure of 37 atm and temperature of 600 K just prior to detonation.
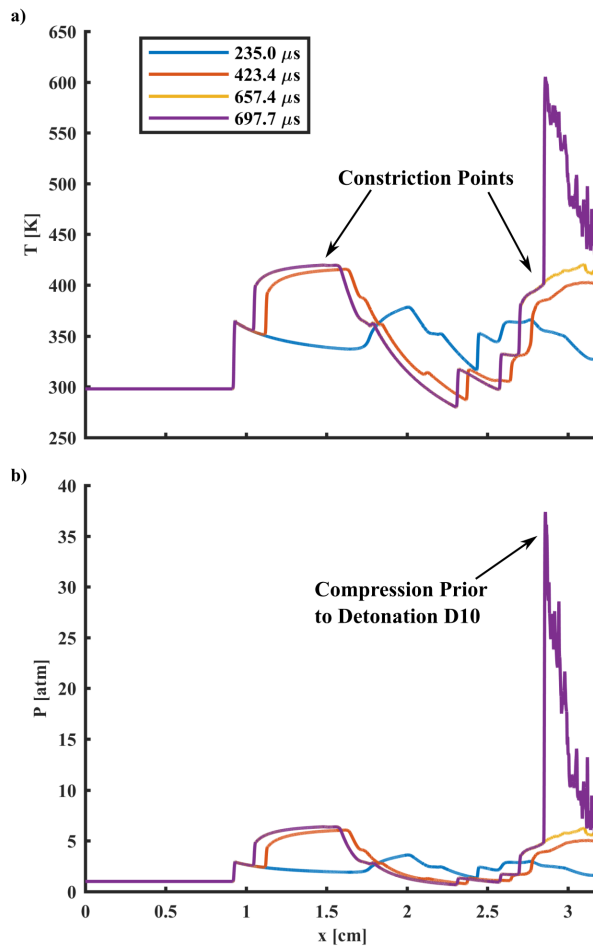
Fig. 48. (a) Temperature and (b) pressure for the first five time steps of the $M_\infty = 8$ case shown in Fig. 46. Values measured at a horizontal slice through the domain at y = 0.16 cm

The $M_\infty = 10$ case was performed using a domain with same dimensions as the $M_\infty = 8$ case. Contours of temperature, numerical schlieren, and pressure for the final
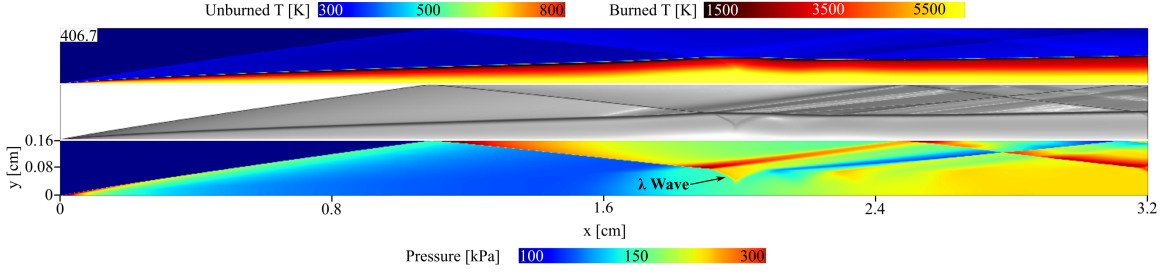
Fig. 49. (top) Temperature, (middle) numerical schlieren, and (bottom) pressure for $M_\infty = 10$ case at 406.7 μs.

time step calculated in the $M_\infty = 10$ case are shown in Fig. 49. The calculation was stopped at 406.7 μs due to computational expense. At this time, the flame expansion is still laminar with an occasional ripple emerging at the flame front. The flame front expands gradually, propagating toward the upper boundary of the domain at a rate of $\sim$2 cm/s. The oblique shock train, formed between the flame front and upper boundary, is stationary. A lambda shock, labeled in Fig. 49, remains anchored to the location where the first shock reflection and the flame intersect. Temperature in the burned gas is considerably greater than in the lower M_∞ cases due to the higher near-wall velocity.

5.5   Discussion

5.5.1   Effect of Inflow Mach Number

Time from initialization of the calculation to ignition in the boundary layer, t_{ign}, is shown in Fig. 50 for $M_\infty = 5 - 8$. Time to ignition decreases with increasing M_∞ and for $M_\infty \geq 8$, the boundary layer ignites almost immediately after the calculation begins. Rapid ignition at higher M_∞ is due to the stagnation temperature of the inflow, and consequently the temperature at the wall, increasing with M_∞. An inverse relationship is observed with time to detonation, t_{det}, which increases with increasing M_∞. Figure 49 shows t_{det} as a function of M_∞. Fitting a quadratic function to the calculated values of t_{det} allows the prediction t_{det} for the $M_\infty = 10$ case, with
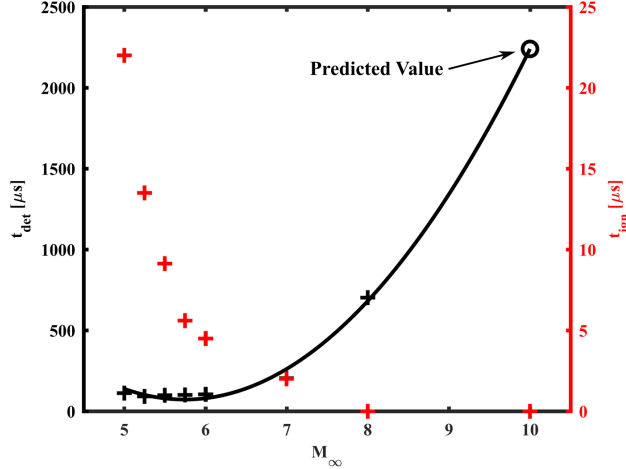
Fig. 50. Time to ignition and detonation as a function of M_∞. A quadratic function is fit to the $t_{\det}$ data points and is used to predict $t_{\det}$ for the $M_\infty = 10$ case.

a predicted value of 2240 μs. The time to detonation increases with M_∞ due to the longer period of laminar flame expansion prior to bubble and spike structure developing on the flame front. The expanding bubbles of burned gas compress the unburned gas and create the ideal conditions for a detonation to occur. In the $M_\infty = 5.25$ case, ripples are visible on flame surface at ~20 μs. For $M_\infty = 8$, no perturbations to the flame surface are visible until ~200 μs. Despite the difference in timescales for the flame to become unstable, the same qualitative features are observed from $M_\infty = 5$ to 8: laminar flame expansion, growth of the RT instability, turbulent flame expansion, and DDT.

Figure 51 shows density, pressure, velocity magnitude in the x-direction, and mass fraction of reactant across the outflow boundary for the $M_\infty = 5.25$ and 10 cases. The $M_\infty = 10$ plots are taken at 406.7 μs, as shown in Fig. 49, and the $M_\infty = 5.25$ plots are taken at 70.33 μs, as shown in Fig. 40. These two time steps were chosen to illustrate the difference in unburned and burned gas states across the channel between a relatively stable, high-Mach case ($M_\infty = 10$) and an unstable, lower-Mach case ($M_\infty = 5.25$). The $M_\infty = 10$ plots were reflected about the symmetry plane at the top boundary (y = 0.16 cm) for a more direct comparison to the $M_\infty = 5.25$ case. Each
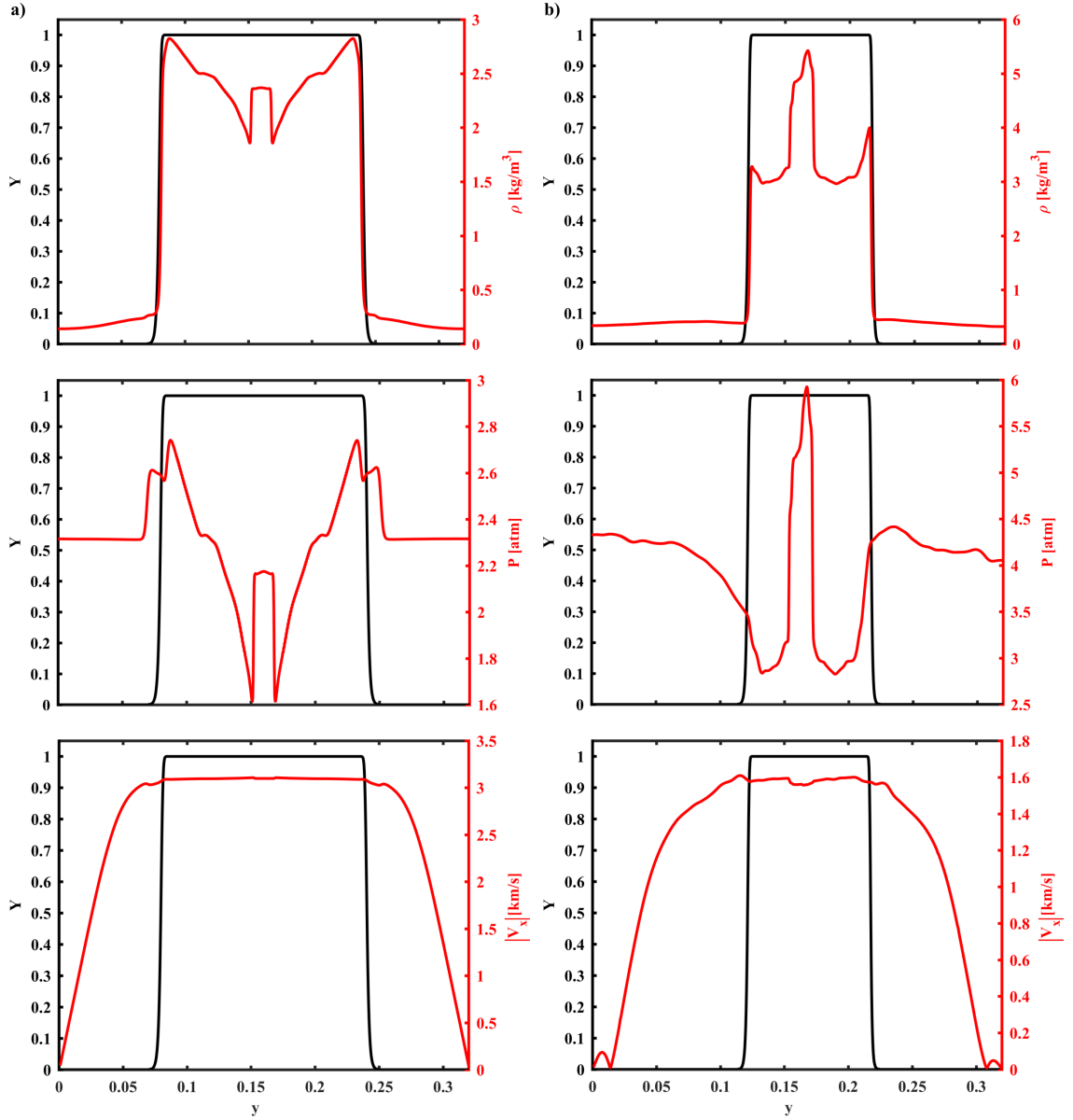
Fig. 51. Density, pressure, and magnitude of velocity in the x-direction plotted over mass fraction of reactant across the outflow boundary for (a) $M_\infty = 10$ at 406.7 μs and (b) $M_\infty = 5.25$ at 70.33 μs.

plot shows ρ, P, and velocity magnitude in the x-direction, $|V_x|$, plotted over Y to illustrate the change in state across the flame, where the flame is defined as the region over which Y changes from one (entirely reactant) to zero (entirely product). The thinner region where $Y = 1$ in the $M_\infty = 5.25$ case indicates greater flame expansion for the lower Mach flow. In both cases, there is a sharp gradient in density across

the flame, though the difference in density between the burned and unburned gas in the $M_\infty = 5.25$ case is greater, indicating greater compression of the unburned gas. There is also a pressure gradient across the flame in both cases, inverse to the direction of the density gradient. This misalignment between pressure and density gradients contributes to the growth of a RT instability across a flame [77]. Velocity in the x-direction of the unburned gas is more uniform in the $M_\infty = 10$ case. For $M_\infty = 5.25$, greater turbulence in the unburned gas results in variability in $|V_x|$. Velocity drops steeply through the burned gas near the walls. There is some recirculation in the $M_\infty = 5.25$ case, shown in the local $|V_x|$ maxima in the near-wall regions.
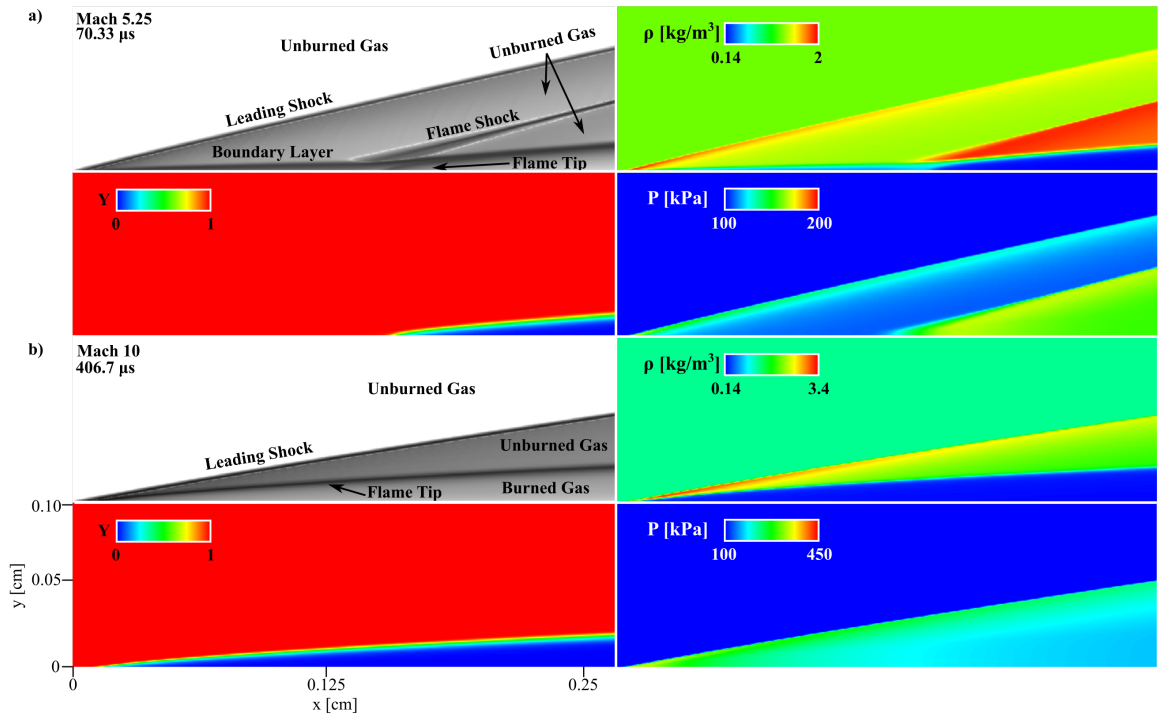
Fig. 52. Numerical schlieren, Y, ρ, and P showing the interaction of the leading shock and flame for (a) $M_\infty = 5.25$ at 70.33 μs and (b) $M_\infty = 10$ at 406.7 μs for the domain x = [0,0.26] cm and y = [0,0.1] cm.

The reaction front propagates closer to the inflow boundary for higher M_∞. Figure 52 shows a numerical schlieren image and contours of Y, ρ, and P for a portion of the domain at the inflow for the $M_\infty = 5.25$ and 10 cases at 70.33 μs and 406.7 μs, respectively. The deflection of the inflow by the boundary layer results in the

93

formation of the leading shock. The fuel-oxidizer mixture ignites in the boundary layer, with the tip of the reaction front, labeled "Flame Tip" in Fig. 52(a), at x = 0.15 cm. Following ignition, the reaction front propagates downstream, extending further from the wall with distance from the ignition point. The flame tip moves upstream toward the inflow boundary at a rate of 2970 cm/s. A secondary shock, labeled "Flame Shock" in Fig. 52(a), forms upstream of the reaction front due to the deflection of the unburned gas by the reaction front. The formation of the flame shock upstream of the reaction front causes inverse pressure and density gradients across the flame tip, as shown in the ρ and P plots. In the $M_\infty = 10$ case, shown in Fig. 52(b), the flame tip is closer to the inflow boundary than in the $M_\infty = 5.25$ case; after ignition, the position of the flame tip is constant at x = 0.015 cm. The reaction front deflects the inflow to form the leading shock, rather than a boundary layer upstream of the flame tip causing the inflow deflection, as is the case for $M_\infty = 5.25$. An inverse gradient in pressure and density is also observed across the flame tip for $M_\infty = 10$.

5.5.2 Stability Analysis

For the $M_\infty = 5 - 8$ cases, the flame becomes increasingly turbulent with time due to the RT instability at the interface between the high-density unburned gas and the low-density burned gas. In the case of $M_\infty = 10$, ripples were beginning to emerge at the flame surface at the time the calculation was stopped (406.7 μs). The schlieren images for the $M_\infty = 8$ case in Fig. 46 show the flame evolution process. At 235 μs there are several ripples in the flame surface, just upstream of the outflow boundary where the lambda waves have formed in the burned gas. At 423.4 μs the ripples have grown to form the bubble-spike structure typical to the RT instability [70].

The Atwood number, $At \equiv (\rho_H - \rho_L)/(\rho_H + \rho_L)$, is one of the key parameters used to characterize the development of a RT instability, where ρ_H is the density of
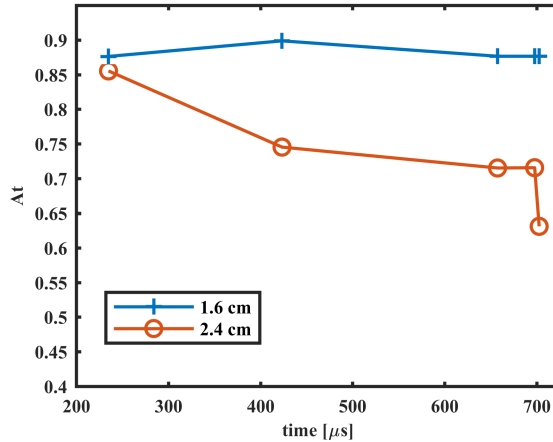
Fig. 53. Atwood number as a function of time, measured at vertical slices x = 1.6 and 2.4 cm for the first five time steps in the $M_\infty = 8$ case shown in Fig. 46.

the heavy fluid and ρ_L is the density of the light fluid. Bubble and spike structures are likely to develop at the fluid interface for flows with $At \simeq 1$ when the light fluid pushes the heavy fluid [70]. If $At \simeq 0$, a pattern of interpenetrating bubbles of heavy and light fluid is more likely to develop. Figure 53 shows At at two vertical slices through the domain for the first five time steps shown in Fig. 46. The vertical slices were taken at x = 1.6 and 2.4 cm. The Atwood number was calculated by taking the average burned gas density across the slice as ρ_L and the average unburned gas density as ρ_H. At x = 1.6 cm, At stays relatively constant with a value of $\sim$0.9. No bubbles are visible on the flame front at x = 1.6 for the five time steps considered in this analysis. At x = 2.4 cm, At decreases with time as the amplitude of the bubbles at this location increases. The lowest At is observed immediately prior to the initiation of detonation D10. Increase in amplitude of the bubbles from the inflow to outflow indicates that the flame front becomes more unstable as distance downstream from the point of ignition increases. Atwood numbers approaching unity were measured across the flame in earlier time steps and At decreased with time and distance from the point of ignition as the flame surface became more turbulent.

In addition to the amplitude of the bubbles increasing, the bubble-spike structure
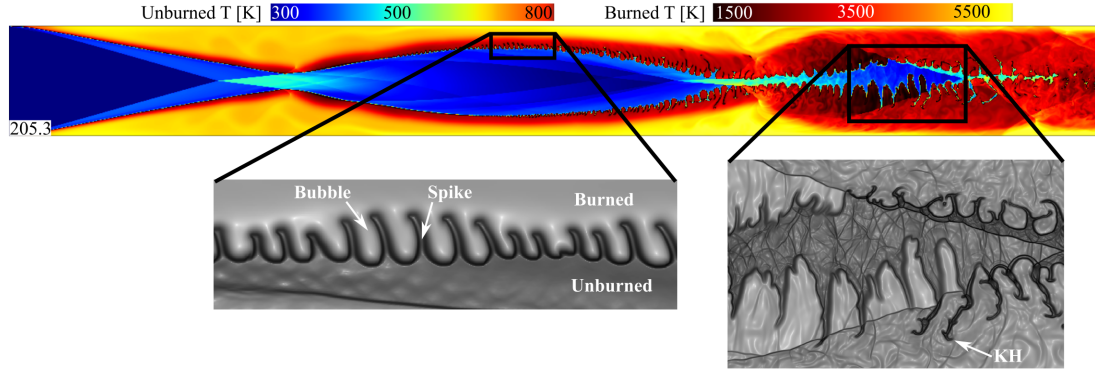
Fig. 54. Temperature for $M_\infty = 7$ case at 205.3 μs and schlieren enlargements of regions showing typical Rayleigh-Taylor bubble-spike structure and distorted bubble-spike structure with secondary Kelvin-Helmholtz instabilities.

becomes more distorted as distance from the point of ignition increases. Structure develops on the spikes due to a Kelvin-Helmholtz instability, or velocity gradient across the fluid interface, causing the spikes to deform and mushroom [70, 71]. The spike distortion effect is most pronounced for low At [70], particularly for compressible flows [72]. This matches what is seen for $M_\infty = 8$, where lower At values are measured as the bubbles and spikes are distorted. The distortion process is observed for the other M_∞ cases as well. Figure 54 shows a time step from the $M_\infty = 7$ case shortly before the first detonation occurs. Closer to the point of ignition, the bubbles and spikes are relatively uniform. Near the outflow boundary, the amplitude and shape of the bubbles varies considerably and the secondary Kelvin-Helmholtz instability causes many of the spikes to mushroom and deform. As the unburned gas is compressed by the RT bubbles, strong shocks form and the passage of the shocks through the flame causes further flame distortion through the Richtmyer-Meshkov instability as channels of unburned gas are driven into the burned gas. Despite the presence of secondary fluid instabilities, the RT instability is dominant in the early evolution of the flame fronts and causes the formation of bubble-spike structure that compresses and preheats the unburned gas creating ideal conditions for a detonation to occur.

5.5.3   Solution Sensitivity
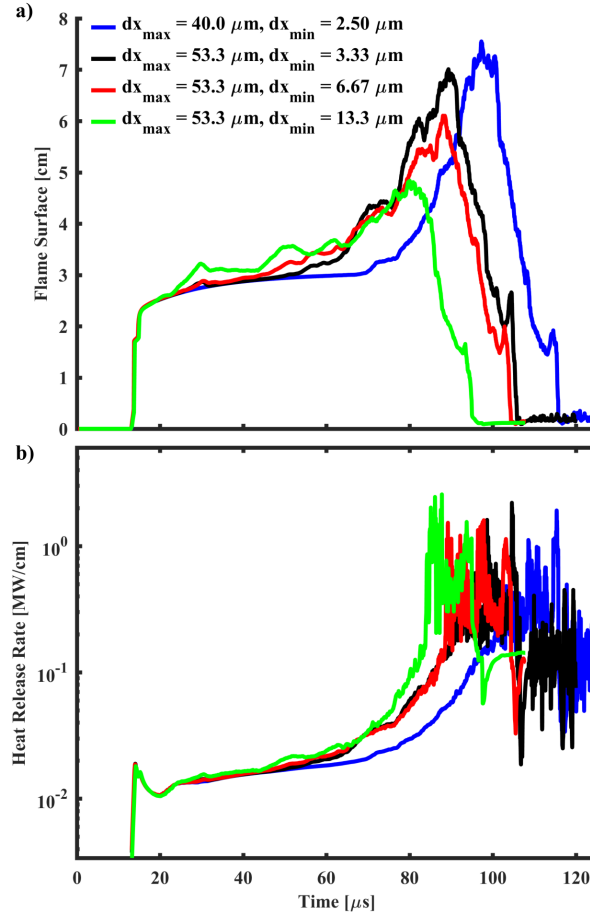
Fig. 55. (a) Flame surface length and (b) heat release rate for $M_\infty = 5.25$ simulations with four different grid resolutions.

A resolution study was performed to investigate the sensitivity of the solution to the computational grid spacing. Four 2D simulations were run with a domain height of 0.16 cm, a symmetry plane at the top wall (same geometry as shown in Figs. 46 and 49), and an inflow condition of $M_\infty = 5.25$. The number of grid points per laminar flame thickness varied from 35.5 to 6.7 from the finest to coarsest grid resolutions, respectively. Figure 55 shows flame surface and heat release rate as a function of time for the four cases. Flame surface increases steadily until the first detonation occurs, then it decreases rapidly as the detonation waves consume the reactant in the domain. Similarly, heat release rate increases as the flame expands into the channel,

with a sharp increase following detonation. As grid resolution increases, so does the time to onset of turbulence in the flame and DDT, where oscillations in the flame surface over time indicate turbulence in the flame. The difference in time to the first detonation between the coarsest and finest cases is 18 μs. The slower rate of flame expansion for finer grid resolution is also evident in the heat release rate over time. Ignition occurs at approximately the same time for all four cases, but the heat release rate takes longer to increase for the cases with finer grid resolution. Maximum heat release rate is on the order of 1 MW/cm for all four cases.

The maximum flame surface length increases with finer grid resolution due to the greater refinement in the RT bubble-spike structure achieved with more computational cells across the flame surface. The bubble-spike structure emerges on the flame surface in all four cases, but the width of the bubbles increases as the mesh is coarsened, resulting in lower values for flame surface length. This is evident in Fig. 56, which shows the flame evolution and DDT for a $M_\infty = 5.25$ case with a channel height of 0.32 cm where the coarsest grid resolution was used ($dx_{\max} = 53.3$ μm, $dx_{\min} = 13.3$ μm). The RT bubbles are noticeably wider than in the higher resolution $M_\infty = 5.25$ case shown in Fig. 40. This is due to increased numerical diffusion with a coarser mesh, resulting from larger $dx_{\min}$, which can smooth out finer detail at the flame front.

Despite the differences in time to DDT and flame expansion rate, the same macroscopic flow features are observed in all cases and are independent of grid resolution: ignition of the fuel-oxidizer mixture in the boundary layer, growth of a RT instability at the flame front, increasing turbulence in the flame, and detonation of the unburned gas due to an energy-focusing mechanism after significant compression and preheating. These features are also independent of calculation dimensionality and domain size, as they are observed in the 3D $M_\infty = 5.25$ case shown in Fig. 45 and in cases with channel heights of both 0.16 and 0.32 cm.
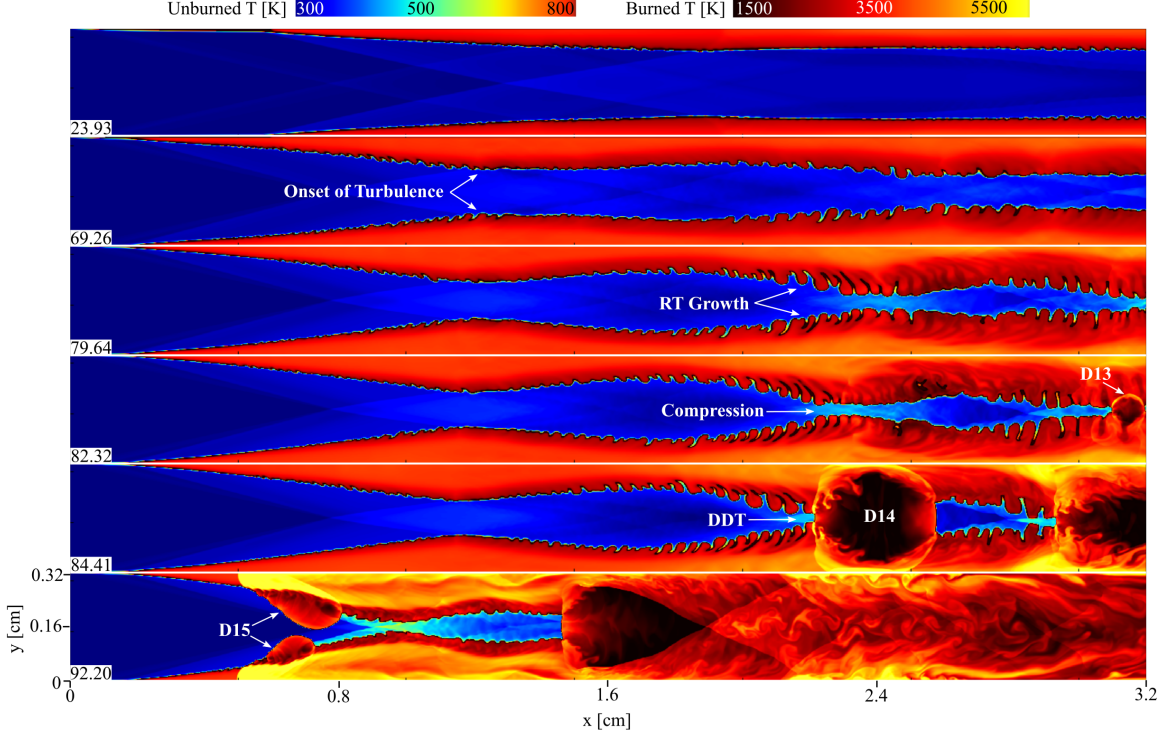
Fig. 56. Evolution of flame and DDT for $M_\infty = 5.25$ with $dx_{\max} = 53.3$ μm and $dx_{\min} = 13.3$ μm. Time in μs shown in frame corners.

5.6   Summary & Conclusions

The effect of inflow Mach number, M_∞, on ignition, flame expansion and instability, and transition to detonation of an initially homogeneous mixture of ethylene and oxygen in a supersonic combustor was studied using multidimensional, unsteady numerical simulations. This paper compared several cases taken from a series of simulations with $M_\infty = 3 - 10$. Both two and three-dimensional calculations were performed.

For the lowest inflow Mach number studied, $M_\infty = 3$, the fuel-oxidizer mixture does not reach a sufficient temperature to ignite and combustion does not occur. Deflection of the inflow by the boundary layers at the combustor walls forms an oblique shock train and the flow reaches a steady-state solution. When $M_\infty \geq 5$, the fuel-oxidizer mixture ignites in the boundary layers. The flames in the boundary layers expand into the channel and an oblique shock train, similar to that observed

for $M_\infty = 3$, forms between the reaction fronts. Interaction of the leading shock and the tip of the reaction front causes perturbations that are initially small ripples in the flame. The ripples grow in time, as well as in distance from the point of ignition, due to a Rayleigh-Taylor (RT) fluid instability at the flame front. Bubble and spike structures develop along the flame and the expanding bubbles of low-density burned gas compress and preheat the high-density unburned gas flowing between the flame fronts. Shocks form as the bubbles extend further into the channel, increasing pressure and temperature in the unburned gas. Detonation occurs when a shock passes through the flame front through an energy-focusing mechanism that is consistent with previous work investigating deflagration-to-detonation transition in ethylene-oxygen mixtures [28, 29].

The timescales for growth of instability in the flame and detonation initiation increase with M_∞. The detonations occur in slightly different locations as M_∞ is varied, but in all cases the mechanism for DDT is energy focusing. A RT instability at the flame surface, resulting from inverse gradients in pressure and density, causes small ripples in the flame to grow to large bubble-spike structures that compress and preheat the unburned gas and create the ideal conditions for a detonation to occur. Although this process was observed to be qualitatively independent of M_∞, the time to initiation of the first detonation increased quadratically with M_∞.

A resolution study was performed to examine the sensitivity of the solution to computational grid spacing. The macroscopic flow features, ignition in the boundary layer, growth of the RT instability, and DDT through an energy-focusing mechanism, were found to be grid-independent despite small variations in flame surface length and time to detonation. These flow features were also observed to be independent of dimensionality and domain size. Future work will investigate the effect of fuel-oxidizer mixture, variable equivalence ratio, and combustor geometry on ignition, flame growth and stability, and detonation mechanism.

5.7 Acknowledgments

6 Conclusions

6.1 Summary of Research Findings

Multidimensional numerical simulations of unsteady, compressible, chemically reacting flows were performed to study the mechanisms for deflagration-to-detonation transition (DDT) in obstructed channels and the effect of supersonic flow speeds on premixed flame stability. Previous work had investigated DDT in channels filled with a hydrogen-air mixture [18, 39], finding that detonations always initiated in the unburned gas behind a Mach stem reflection through an ignition-gradient mechanism [14, 15]. Using channel geometries differing from those used in previous work, particularly with respect to the obstacle blockage ratio, was found to significantly affect flame evolution, turbulence in the unburned gas, and DDT. Detonation transition occurred by a mechanism not previously observed, which led to the following questions that this work sought to answer:

- Can detonation occur in the unburned gas through a mechanism other than the ignition-gradient mechanism previously observed?

- Does detonation initiation always occur in the unburned gas, or can shock-flame interactions cause the flame front to transition to a detonation?

- How does varying the blockage-ratio in the canonical obstacle-laden channel affect flame evolution, development of turbulence, and detonation initiation? Will the mixture detonate for very low blockage ratios?

- Will the fuel-oxidizer mixture autoignite when flowing through a channel without obstacles at supersonic velocities? If so, does the flame remain stable or does it become turbulent? Will detonations occur and, if so, by what mechanism?

- What is the effect of Mach number on ignition, flame stability, and detonation initiation of the mixture flowing at supersonic speeds?

- How do fluid instabilities contribute to turbulence in the flame and detonation initiation?

These questions were investigated using two different computational geometries. The first geometry was a thin channel, 0.32 cm in height and 21 cm in length, with regularly spaced obstacles along the bottom wall. The channel was filled with an initially homogeneous mixture of stoichiometric ethylene and oxygen that was ignited by initializing a region of hot, burned gas in the channel corner. Obstacle blockage ratio (br) was varied from 0.05 to 0.8. Several regimes of flame evolution and DDT were observed when br was varied. In the intermediate regime of $0.35 \leq br \leq 0.5$, the flame expanded and compressed the unburned gas upstream, forming a leading shock that remained closely coupled to the flame. As the leading shock diffracted over the obstacles, it reflected from the channel wall forming a Mach stem. The Mach stem reflected from the next obstacle, dramatically increasing the pressure, temperature, and density of the unburned gas in the region behind the Mach stem reflection. Hot spots ignited in this preheated region, which transitioned to detonations through the ignition-gradient mechanism. This result was consistent with previous work using larger channels filled with stoichiometric hydrogen-air [18, 39].

DDT became far less predictable for br outside of the intermediate regime. For $br < 0.35$, the rate of flame acceleration is slower and the leading shock traveled further upstream, creating a highly turbulent, dynamic region of unburned gas between the leading shock and the turbulent flame front. This region was characterized by shock-shock and shock-flame collisions, shock-boundary layer interactions, shock reflections from the obstacles and the walls, and strong vortical motion. The strength of the shocks increased as they propagated further down the channel and, eventually, a shock collision focused energy in a localized volume of unburned gas causing it to detonate instantaneously. This energy-focusing detonation mechanism, observed in both two and three-dimensional calculations, is consistent with direct initiation

103

theory [10] and detonations seen in experiments using similar blockage ratios [46]. The time and location of DDT in this regime was found to be stochastic due to the strong dependency on turbulence, which is heavily dependent on initial conditions, but the energy-focusing mechanism was robust and insensitive to changes in grid resolution, initial conditions, channel height, and dimensionality. These simulations provided an answer to the first question posed above: detonations are likely to occur in the unburned gas through an energy-focusing mechanism if the unburned gas is turbulent and characterized by shock-shock, shock-flame, and shock-boundary layer interactions.

When br was increased to 0.8, the flame accelerated at a higher rate than in lower br cases and detonation was initiated through two different mechanisms, in both the unburned gas and at the flame front. DDT occurred through the ignition-gradient mechanism in the region behind a Mach stem reflection in the unburned gas, but this detonation did not survive and propagate out of the end of the channel. However, a shock generated by this detonation passed through the turbulent flame front and caused the flame front to transition to a detonation. The mechanism for this detonation was energy-focusing, in that the passage of the shock through the flame compressed the reaction front and deposited sufficient energy to cause its transition to a detonation. This result provided an answer to the second question: a flame front can transition to a detonation front and DDT does not occur solely in the unburned gas. A shock-flame interaction, with a shock of sufficient strength, can cause a flame front to transition to a detonation.

The third question was addressed through examining the change in flame evolution and detonation initiation mechanisms as a function of blockage ratio for a series of simulations spanning $0.05 \leq br \leq 0.8$. When br decreased, the flame remained laminar further into the channel as lower obstacles did not significantly obstruct flame expansion. The longer phase of laminar expansion also resulted in a slower rate of

flame acceleration and longer durations from ignition to the formation of shocks and DDT. Despite these larger timescales to shock formation and turbulence in the unburned gas, the unburned gas eventually becomes significantly more turbulent in the cases with lower br. Increased turbulence was accompanied by stochasticity in the exact time and location of detonation. Despite this variation, the mechanism for the detonation in the lower br regime was consistently found to be energy-focusing through shock collisions in the unburned gas or shock collisions with the turbulent flame. The lowest br examined for this computational geometry was 0.05 and detonation did occur, but the time to detonation was over four times greater than for the $br = 0.5$ case.

The latter three questions were investigated using a canonical supersonic combustor. The computational geometry was a constant-area channel, 0.32 cm in height and 3.2 cm in length, with a supersonic inflow of stoichiometric ethylene and oxygen. A series of simulations was performed with inflow Mach numbers, M_∞, from 3 to 10. The flow reached a steady-state oblique shock train structure when $M_\infty = 3$. The mixture did not reach a sufficient temperature for autoignition and no combustion occurred. When $M_\infty > 5$ the mixture ignited in the boundary layer and flame fronts formed along the channel walls that gradually expanded into the center of the channel. The flame surface was perturbed by oblique shocks at the reaction front tip, forming ripples on the flame surface that grew in time due to a Rayleigh-Taylor (RT) instability at the interface between the unburned and burned gas. As the flame fronts expanded, the low-density burned gas compressed the high-density unburned gas and bubble and spike structures developed along the flame surface, typical to the RT instability. As the inflow of unburned gas was deflected by the expanding bubbles of burned gas, shocks formed that increased the pressure, temperature, and density of the unburned gas. Eventually, the flame front transitioned to detonation as a shock passed through the flame front and caused it to transition to a detonation. The se-

quence of events leading to DDT here is similar to that observed in the obstacle-laden channel with $br = 0.8$; a strong shock passes through a flame, compresses the reaction front, and deposits sufficient energy to cause the flame to transition to detonation through the energy-focusing mechanism. Subsequent detonations occur throughout the channel, originating at the flame front as well as in the unburned gas.

Simulating supersonic flow of premixed fuel and oxidizer through the combustor provided insight into the stability of premixed flames in high-speed flows. With sufficiently high M_∞, the mixture ignited in the boundary layer and the flame became unstable and turbulent soon after ignition. The mechanism for DDT in this flow was the same as in the obstructed channel for $br < 0.35$ as well as $br = 0.8$. This result agrees with the observation that turbulent, shock-heated fuel-oxidizer mixtures are likely to detonate through the energy-focusing mechanism, either at the flame front or in the unburned gas.

Flame evolution and detonation initiation mechanism were found to be qualitatively independent of M_∞, as long as M_∞ was sufficiently high for the mixture to ignite in the boundary layer. In all cases for $M_\infty > 3$, there are several distinct phases of flame evolution: laminar flame expansion, growth of RT instability, turbulent flame expansion, and transition to detonation. Quantitatively, the timescales for growth of instability in the flame and detonation initiation increased with M_∞. This indicates that the growth rate of the RT instability is small relative to the characteristic flow speed for higher M_∞. An inverse relationship was observed between M_∞ and time to ignition, where the boundary layer ignites almost immediately for $M_\infty > 8$.

To address the final question regarding the effect of fluid instabilities on turbulence in the flame and detonation initiation, the Atwood number, At, was used to characterize the growth rate of the RT instability at the flame front for the $M_\infty = 5.25$ and 8 cases. An $At < 1$ was calculated at all points where sampled for both M_∞ cases, indicating that a RT instability was likely to grow at the flame surface.

Lower values of At were calculated at later times in locations along the flame furthest from the point of ignition, indicating increasing instability with time and distance from the inflow. This result agrees with the qualitative changes seen in the flame, where the bubble-spike structure became more distorted and the amplitude of the bubbles increased with time and distance from the inflow. Distortion of the bubbles caused turbulence in the flame front to increase and shocks to form as the bubbles deflected the flow of the incoming unburned gas. Secondary Kelvin-Helmholtz (KH) and Richtmyer-Meshkov (RM) instabilities developed as the shocks passed through the flame front, which further distorted the flame and drove turbulence in both the burned and unburned gas. This sequence of events preheated the unburned gas and increaseed turbulence in the flame, creating the ideal conditions for detonation to occur through the energy-focusing mechanism.

6.2   Future Work

There are many opportunities for expanding the work presented here, particularly through the use of different fuel-oxidizer mixtures, chemical models, geometries, and boundary conditions. All of the simulations discussed in this work used a stoichiometric ethylene-oxygen mixture. Future work will incorporate a variable fuel equivalence ratio chemical model which calculates input parameters, such as heat release and activation energy, as a function of equivalence ratio. This will allow simulation of fuel-rich or lean premixed combustion and accurate modeling of diffusion flames in high-speed flows. Stoichiometric ethylene-oxygen is a highly reactive mixture and the effect of the mixture's composition on DDT through energy focusing is a topic that requires further investigation. Using higher hydrocarbon fuels, such as JP-8 or kerosene, will likely influence the effect of fluid instabilities on generating turbulence in the flame and may delay detonation initiation or cause DDT to occur through a different mechanism than the energy-focusing mechanism detailed in this work.

The walls for the channels and combustor geometries used in these simulations were modeled as adiabatic; no energy from the computational domain was lost to the surroundings. This constraint is useful for studying the physics of flame stability and DDT, as isothermal walls can hinder processes such as ignition and detonation initiation if the walls are cold, or near room temperature. In an actual experimental facility, the walls are neither adiabatic nor held constant at room temperature. Reality falls somewhere in between these two limits and could best be simulated with a wall model that accounts for transient heating as a function of heat release inside the domain. This type of wall treatment will be critical for applying the numerical methodology used for the simulations in this work to more applied problems.

Using detonations to generate thrust in a system such as the supersonic combustor studied here is a topic that warrants further exploration. Recent interest in pulse and rotating detonation engines has shown that detonations are gaining traction as a reliable means of propulsion of air and spacecraft. If a detonation wave could be stabilized within a planar combustor, such as the one studied in this work, considerable thrust would be produced. This concept has been introduced to the propulsion community as a standing detonation wave engine [58], but it has not received as much attention as pulse or rotating detonation engines. A first step to a proof-of-concept of this engine design would be an investigation into changes in the geometry, inflow conditions, and mixture composition that promote stabilization of the detonation wave within the combustor. It is likely that when flowing lean fuel-air mixtures into the combustor at a velocity equal to or greater than the detonation's Chapman-Jouget velocity, a detonation wave could be stabilized and the thrust generated by such an engine could be quantified. Active control of the inflow conditions as a function of wall pressure changes in the combustor, indicating movement of the detonation wave, would be a viable method for detonation wave stabilization across a range of flight conditions.

In the cases of supersonic flow through the constant-area combustor, it was clear that the RT instability was the dominant mechanism for transformation of the laminar flame fronts to turbulent flames. Secondary KH and RM instabilities further distorted the flame in the later stages of the calculations, creating a highly turbulent, shock-laden flow in the microseconds prior to detonation initiation. Similarly, in the case of the obstructed channel, the flow prior to detonation is characterized by many shock collisions and repeated shock-flame interactions at the flame front. In both situations, the flow is incredibly turbulent prior to DDT occurring with repeated shock-shock and shock-flame interactions on all scales, from the scale of the physical system to the flame thickness. It is unlikely that in flow dominated by repeated shock collisions that the turbulence is isotropic or homogeneous and has an equilibrium spectrum in accordance with typical Kolmogorov turbulence that has been a subject of considerable research emphasis over the past several decades. Future work to investigate the nature of the turbulence in these flows and the cascade of energy from the large to small scales would greatly enhance our understanding of the flow conditions where detonations are likely to occur through the energy-focusing mechanism.

Finally, the monotone-integrated large eddy simulation (MILES) method for computing turbulent, high-speed, chemically reacting flows has historically been used for fundamental research problems much more often than for applied work, such as investigating flame stability in a scramjet engine of realistic scale. Simulations using the MILES method, when coupled with a simplified chemical-diffusive model of the type used in this work, have been shown to agree quite well with experimental data for a variety of problems (several of these are referenced in Chap. 1.5) and quantitatively reproduce features such as flame speed, thickness, acceleration, and heat release. Additionally, this numerical method is computationally efficient, especially when coupled with adaptive mesh refinement, allowing the calculation of flows spanning many orders of magnitude in scale. A natural progression in the utility of MILES

is to apply the method to simulating flow through realistic propulsive geometries, such as an experimental scramjet combustor, for which there is qualitative and quantitative data for comparison. Once agreement between simulation and experiment has been obtained for this type of problem, the MILES method has the potential to be an incredibly useful tool for engine design and analysis.

6.3   Closing Remarks

This work has been an exploration into the fundamental physics underlying flame acceleration, flame stability in supersonic flows, and detonation initiation mechanisms. Research to provide definitive answers to the questions posed here is ongoing, but considerable insight has been gained into the complex interplay between flames, high-speed flow, shocks, and turbulence. It is our hope that this work established a foundation for theory, computation, and experimentation to bridge the gaps still remaining in our knowledge such that detonations and high-speed, turbulent combustion can be reliably and safely used for next generation propulsion concepts.

References

[1] C. C. Rasmussen, J. F. Driscoll, K.-Y. Hsu, J. M. Donbar, M. R. Gruber, C. D. Carter, Stability limits of cavity-stabilized flames in supersonic flow, Proc. Combust. Inst. 30 (2005) 2825–2833.

[2] A. Ben-Yakar, R. K. Hanson, Cavity flame-holders for ignition and flame stabilization in scramjets: an overview, Journal of Propulsion and Power 17 (2001) 869–877.

[3] M. Berglund, C. Fureby, Les of supersonic combustion in a scramjet engine model, Proceedings of the Combustion Institute 31 (2007) 2497–2504.

[4] J. Larsson, S. Laurence, I. Bermejo-Moreno, J. Bodart, S. Karl, R. Vicquelin, Incipient thermal choking and stable shock-train formation in the heat-release region of a scramjet combustor. part ii: Large eddy simulations, Combustion and Flame 162 (2015) 907–920.

[5] A. Y. Poludnenko, E. S. Oran, The interaction of high-speed turbulence with flames: Global properties and internal flame structure, Combust. Flame 157 (2010) 995–1011.

[6] A. Y. Poludnenko, Pulsating instability and self-acceleration of fast turbulent flames, Physics of Fluids 27 (2015) 014106.

[7] H. Xiao, R. W. Houim, E. S. Oran, Formation and evolution of distorted tulip flames, Combust. Flame 162 (2015) 4084–4101.

[8] G. Taylor, The instability of liquid surfaces when accelerated in a direction perpendicular to their planes, The instability of liquid surfaces when accelerated in a direction perpendicular to their planes, Proceedings of the Royal Society of London A: Mathematical, Physical and Engineering Sciences 201 (1950) 192–196.

[9] A. M. Khokhlov, E. S. Oran, A. Y. Chtchelkanova, J. C. Wheeler, Interaction of a shock with a sinusoidally perturbed flame, Combustion and flame 117 (1999) 99–116.

[10] A. D. Kiverin, D. R. Kassoy, M. F. Ivanov, M. A. Liberman, Mechanisms of ignition by transient energy deposition: Regimes of combustion wave propagation, Phys. Rev. E 87 (2013) 033015.

[11] K. Hirose, 2011 fukushima dai-ichi nuclear power plant accident: summary of regional radioactive deposition monitoring results, Journal of environmental radioactivity 111 (2012) 13–17.

[12] D. Allgood, E. Gutmark, J. Hoke, R. Bradley, F. Schauer, Performance measurements of multicycle pulse-detonation-engine exhaust nozzles, Journal of Propulsion and Power 22 (2006) 70.

[13] F. Schauer, J. Stutrud, R. Bradley, Detonation initiation studies and performance results for pulsed detonation engine applications, in: 39th Aerospace Sciences Meeting and Exhibit, 2001, p. 1129.

[14] Y. Zeldovich, V. Librovich, G. Makhviladze, G. Sivashinsky, On the development of detonation in a non-uniformly preheated gas, Astronautica Acta 15 (1970) 313–321.

[15] J. Lee, R. Knystautas, N. Yoshikawa, Photochemical initiation of gaseous detonations, Acta Astronautica 5 (1978) 971–982.

[16] E. S. Oran, J. P. Boris, Detailed modelling of combustion systems, Progress in Energy and Combustion Science 7 (1981) 1–72.

[17] E. S. Oran, V. N. Gamezo, Origins of the deflagration-to-detonation transition in gas-phase combustion, Combust. Flame 148 (2007) 4–47.

[18] V. N. Gamezo, T. Ogawa, E. S. Oran, Flame acceleration and ddt in channels with obstacles: Effect of obstacle spacing, Combust. Flame 155 (2008) 302–315.

[19] R. W. Houim, K. K. Kuo, A low-dissipation and time-accurate method for compressible multi-component flow with variable specific heat ratios, J. Comput. Phys. 230 (2011) 8527–8553.

[20] E. S. Oran, J. P. Boris, Numerical simulation of reactive flow, Cambridge University Press, 2005.

[21] J. P. Boris, On large eddy simulation using subgrid turbulence models comment 1, in: Whither turbulence? Turbulence at the crossroads, Springer, 1990, pp. 344–353.

[22] C. Fureby, S.-I. Möller, Large eddy simulation of reacting flows applied to bluff body stabilized flames, AIAA journal 33 (1995) 2339–2347.

[23] F. Grinstein, E. Gutmark, T. Parr, D. Hanson-Parr, U. Obeysekare, Streamwise and spanwise vortex interaction in an axisymmetric jet. a computational and experimental study, Physics of Fluids 8 (1996) 1515–1524.

[24] D. Knight, G. Zhou, N. Okong'o, V. Shukla, Compressible large eddy simulation using unstructured grids, in: 36th AIAA Aerospace Sciences Meeting and Exhibit, 1998, p. 535.

[25] D. Kessler, V. Gamezo, E. Oran, Simulations of flame acceleration and deflagration-to-detonation transitions in methane–air systems, Combustion and Flame 157 (2010) 2063–2077.

[26] C. Fureby, F. Grinstein, Monotonically integrated large eddy simulation of free shear flows, AIAA journal 37 (1999) 544–556.

[27] C. Fureby, G. Tabor, H. Weller, A. Gosman, A comparative study of subgrid scale models in homogeneous isotropic turbulence, Physics of fluids 9 (1997) 1416–1429.

[28] G. Goodwin, R. Houim, E. Oran, Shock transition to detonation in channels with obstacles, Proc. Combust. Inst. 36 (2017) 2717–2724.

[29] G. B. Goodwin, R. W. Houim, E. S. Oran, Effect of decreasing blockage ratio on ddt in small channels with obstacles, Combust. Flame 173 (2016) 16–26.

[30] P. Middha, O. Hansen, Predicting deflagration to detonation transitions in hydrogen explosions, Process Safety Progress 27 (2008) 192–204.

[31] P. Thibault, L. Britton, F. Zhang, Deflagration and detonation of ethylene oxide vapor in pipelines, Process Safety Progress 19 (2000) 125–139.

[32] R. Sorin, R. Zitoun, D. Desbordes, Optimization of the deflagration to detonation transition: reduction of length and time of transition, Shock Waves 15 (2006) 137–145.

[33] R. Smirnov, R. Zitoun, D. Desbordes, Deflagration-to-detonation transition in gases in tubes with cavities, Journal of Engineering Physics and Thermophysics 83 (2010) 1287–1316.

[34] Y. Huang, H. Tang, J. Li, J. Wang, Deflagration-to-detonation transition of keroseneair mixtures in a small-scale pulse detonation engine, Journal of Aerospace Engineering 225 (2011) 441–448.

[35] R. Zipf, V. Gamezo, M. Sapko, W. Marchewka, K. Mohamed, E. Oran, D. Kessler, E. Weiss, J. Addis, F. Karnack, D. Sellers, Methane-air detonation experiments at niosh lake lynn laboratory, Journal of Loss Prevention in the Process Industries 26 (2013) 295–301.

[36] J. Lee, A. Higgins, Comments on criteria for direct initiation of detonation, Phil. Trans. R. Soc. Lond. 357 (1999) 3503–3521.

[37] B. Zhang, H. Ng, J. Lee, Measurement and relationship between critical tube diameter and critical energy for direct blast initiation of gaseous detonations, Journal of Loss Prevention in the Process Industries 26 (2013) 1293–1299.

[38] J. Lee, The Detonation Phenomenon, 1 ed., Cambridge University Press, New York, NY, 2008.

[39] V. N. Gamezo, T. Ogawa, E. S. Oran, Numerical simulations of flame propagation and ddt in obstructed channels filled with hydrogen?air mixture, Proc. Combust. Inst. 31 (2007) 2463–2471.

[40] D. A. Kessler, V. N. Gamezo, E. S. Oran, Simulations of flame acceleration and deflagration-to-detonation transitions in methane-air systems, Combust. Flame 157 (2010) 2063–2077.

[41] G. Ciccarelli, C. Fowler, M. Bardon, Effect of obstacle size and spacing on the initial stage of flame acceleration in a rough tube, Shock Waves 14 (2005) 161–166.

[42] A. Na'inna, H. Phylaktou, G. Andrews, Effects of obstacle separation distance on gas explosions: the influence of obstacle blockage ratio, International Symposium on Safety Science and Technology 84 (2014) 306–319.

[43] D. Kassoy, The response of a compressible gas to extremely rapid transient, spatially resolved energy addition: an asymptotic formulation, Journal of Engineering Mathematics 68 (2010) 249–262.

[44] G. Ciccarelli, S. Dorofeev, Flame acceleration and transition to detonation in ducts, Progress in Energy and Combustion Science 34 (2008) 499 – 550.

[45] V. N. Gamezo, T. Ogawa, E. S. Oran, Deflagration-to-detonation transition in h2-air mixtures: Effect of blockage ratio, AIAA Paper 2009-440 (2009).

[46] S. Maeda, S. Minami, D. Okamoto, T. Obara, Visualization of Deflagration-to-detonation Transitions in a Channel with Repeated Obstacles, Proc. of the 25th Int. Colloquium on the Dynamics of Explosions and Reactive Systems, 2015.

[47] Center for Computational Sciences and Engineering, University of California, Berkeley, available at https://ccse.lbl.gov/BoxLib (Retrieved 03-2015).

[48] M. Wu, W. Kuo, Accelerative expansion and ddt of stoichiometric ethylene/oxygen flame rings in micro-gaps, Proc. of the Combust. Inst. 34 (2013) 2017–2024.

[49] S. Maeda, S. Minami, D. Okamoto, T. Obara, Visualization of deflagration-to-detonation transitions in a channel with repeated obstacles, in: Proceedings of the 25th International Colloquium on the Dynamics of Explosions and Reactive Systems, 2015.

[50] A. Chaudhuri, A. Hadjadj, A. Chinnayya, On the use of immersed boundary methods for shock/obstacle interactions, J. Comput. Phys. 230 (2011) 1731 – 1748.

[51] G. B. Goodwin, E. S. Oran, Flame instability and transition to detonation in supersonic reactive flows, arXiv preprint arXiv:1711.05160 (2017).

[52] C. Engel, R. Strehlow, Transverse waves in detonations. ii-structure and spacing in h sub 2-o sub 2, c sub 2 h sub 4-o sub 2, and ch sub 4-o sub 2 systems., AIAA journal 7 (1969) 492–496.

[53] R. A. Strehlow, Nature of transverse waves in detonations, Astronautica Acta 14 (1969) 539.

[54] P. Waltrup, M. White, F. Zarlingo, E. Gravlin, History of us navy ramjet, scramjet, and mixed-cycle propulsion development, Journal of Propulsion and Power 18 (2002) 14–27.

[55] R. Daines, C. Segal, Combined rocket and airbreathing propulsion systems for space-launch applications, Journal of Propulsion and Power 14 (1998).

[56] P. E. Hamlington, A. Y. Poludnenko, E. S. Oran, Interactions between turbulence and flames in premixed reacting flows, Physics of Fluids 23 (2011) 125111.

[57] A. Y. Poludnenko, E. S. Oran, The interaction of high-speed turbulence with flames: Turbulent flame speed, Combust. Flame 158 (2011) 301–326.

[58] K. Kailasanath, Review of propulsion applications of detonation waves, AIAA Journal 38 (2000) 1698–1708.

[59] K. Kailasanath, G. Patnaik, Performance estimates of pulsed detonation engines, Proc. Combust. Inst. 28 (2000) 595–601.

[60] D. Schwer, K. Kailasanath, Numerical investigation of the physics of rotating-detonation-engines, Proc. Combust. Inst. 33 (2011) 2195–2202.

[61] D. Schwer, K. Kailasanath, Fluid dynamics of rotating detonation engines with hydrogen and hydrocarbon fuels, Proc. Combust. Inst. 34 (2013) 1991–1998.

[62] N. Tsuboi, Y. Watanabe, T. Kojima, A. K. Hayashi, Numerical estimation of the thrust performance on a rotating detonation engine for a hydrogen–oxygen mixture, Proc. Combust. Inst. 35 (2015) 2005–2013.

[63] R. Dyer, A. Naples, T. Kaemming, J. Hoke, F. Schauer, Parametric testing of a unique rotating detonation engine design, Parametric testing of a unique rotating detonation engine design, 50th AIAA Aerospace Sciences Meeting, AIAA (2012).

[64] J. K. Lefkowitz, P. Guo, T. Ombrello, S. H. Won, C. A. Stevens, J. L. Hoke, F. Schauer, Y. Ju, Schlieren imaging and pulsed detonation engine testing of ignition by a nanosecond repetitively pulsed discharge, Combust. Flame 162 (2015) 2496–2507.

[65] J. Sosa, M. Hoban, K. Ahmed, Advances on the stabilization of standing continuous detonation for pressure gain propulsion, Advances on the Stabilization of Standing Continuous Detonation for Pressure Gain Propulsion, 53rd AIAA/SAE/ASEE Joint Propulsion Conference, AIAA (2017).

[66] C. R. Kaplan, A. Ozgen, E. S. Oran, Chemical-diffusive models for flame acceleration and transition to detonation: Genetic algorithm and optimization procedure, arXiv preprint arXiv:1709.00096 (2017).

[67] H. Xiao, R. W. Houim, E. S. Oran, Visualization of deflagration-to-detonation transitions in a channel with repeated obstacles, Visualization of Deflagration-to-detonation Transitions in a Channel with Repeated Obstacles, Proceedings of the 26th International Colloquium on the Dynamics of Explosions and Reactive Systems, WIT Press (2017).

[68] R. W. Houim, A. Ozgen, E. S. Oran, The role of spontaneous waves in the deflagration-to-detonation transition in submillimetre channels, Combustion Theory and Modelling 20 (2016) 1068–1087.

[69] R. W. Houim, R. T. Fievisohn, The influence of acoustic impedance on gaseous layered detonations bounded by an inert gas, Combust. Flame 179 (2017) 185–198.

[70] D. H. Sharp, An overview of rayleigh-taylor instability, Physica D: Nonlinear Phenomena 12 (1984) 3IN111–10IN1018.

[71] A. Banerjee, W. N. Kraft, M. J. Andrews, Detailed measurements of a statistically steady rayleigh–taylor mixing layer from small to high atwood numbers, Journal of Fluid Mechanics 659 (2010) 127–190.

[72] J. Glimm, X. L. Li, R. Menikoff, D. Sharp, Q. Zhang, A numerical study of bubble interactions in rayleigh–taylor instability for compressible fluids, Physics of Fluids A: Fluid Dynamics 2 (1990) 2046–2054.

[73] G. P. Menees, H. G. Adelman, J.-L. Cambier, J. V. Bowles, Wave combustors for trans-atmospheric vehicles, Journal of Propulsion and Power 8 (1992) 709–713.

[74] S. Ashford, G. Emanuel, Oblique detonation wave engine performance prediction, Journal of propulsion and power 12 (1996) 322–327.

[75] J. Sosa, K. Ahmed, J. Hoke, F. R. Schauer, Experimental investigation of detonation wave propagation in a supersonic crossflow, in: 2018 AIAA Aerospace Sciences Meeting, 2018, p. 0156.

[76] O. Teerling, A. McIntosh, J. Brindley, V. Tam, Premixed flame response to oscillatory pressure waves, Proceedings of the Combustion Institute 30 (2005) 1733–1740.

[77] H. Xiao, R. W. Houim, E. S. Oran, Effects of pressure waves on the stability of flames propagating in tubes, Proceedings of the Combustion Institute 36 (2017) 1577–1583.

[78] G. Thomas, R. Bambrey, C. Brown, Experimental observations of flame acceleration and transition to detonation following shock-flame interaction, Combustion Theory and Modelling 5 (2001) 573–594.

[79] A. Khokhlov, E. Oran, G. Thomas, Numerical simulation of deflagration-to-

detonation transition: the role of shock–flame interactions in turbulent flames, Combustion and Flame 117 (1999) 323–339.

[80] S. B. Ciccarelli, G. Dorofeev, Flame acceleration and transition to detonation in ducts, Prog. Energy Combust. Sci. 34 (2008) 499–550.